The production of synthetic kerosene by combined DAC with water electrolysis and biomass gasification for Rotterdam-The Hague Airport along with intermittent electricity supply

A techno-economic assessment

Maurice R. J. Rijs

The production of synthetic kerosene by combined DAC with water electrolysis and biomass gasification for Rotterdam-The Hague Airport along with intermittent electricity supply

A techno-economic assessment

by

Maurice R.J. Rijs

to obtain the degree of

Master of Science
in Mechanical Engineering

at the Delft University of Technology,
to be defended publicly on Monday August 23, 2021 at 10:00 AM.

Student number:	4389573	
Supervisor:	Prof. dr. ir. W. de Jong	
Thesis committee:	Prof. dr. ir. W. de Jong,	TU Delft
	Dr. ir. R.M. Stikkelman,	TU Delft
	M. Ramdin Msc.,	TU Delft

TU Delft

Preface and Acknowledgement

About two years ago when I flew from Valencia back to Amsterdam, I read through an airline magazine. At the very last page, a short introduction to synthetic kerosene was given. A topic I never heard of, but it caught my interest ever since. By chance, when I was looking for a master thesis topic, a proposal to do research on synthetic kerosene came across. I immediately accepted the proposal and it didn't bore or disappoint me throughout the year I worked on it. It fascinated me that I could explain people how sustainable aviation can become in the future.

Throughout my studies and writing my thesis I received support from many people, but there are a few that deserve special attention.

At first, I would highly thank my supervisor Professor Wiebren de Jong for his time, dedication and support during this project and giving me the opportunity to work on this topic. I am grateful for the experience and knowledge you provided me with. Without this help the graduation project would have been more difficult en less pleasant, especially because the Covid-19 crisis made studying more difficult and less interactive. Secondly, I would also thank Dr. Rob Stikkelman and Msc. Mahinder Ramdin for their help when I had questions and being part of my thesis committee.

Next, my gratitude goes to my fellow students and roommates for their help and support throughout my studies. But more important, they made my time as a student much more enjoyable. In particular the daily 'Mario Kart' sessions with my roommates during this thesis were perfect to relax and clear my mind.

Finally, I would like to thank my family who supported, motivated and encouraged me throughout my studies and beyond.

Maurice Rijs
Delft, August 2021

Abstract

Replacing conventional kerosene has gained interest in an effort to make aviation more sustainable. In 2018 a total of 895 million tonnes of CO_2 was emitted, equivalent to 2% of global CO_2 emissions. For normal passenger and cargo planes synthetic kerosene is most feasible to replace conventional kerosene, hydrogen powered or electricity driven airplanes face problems and may only be feasible for small airplanes. Increased interest in electrolysis, direct air capture (DAC) and production pathways for synthetic kerosene has encouraged development and reduced the price gap with conventional kerosene. Although small pilot plants are realized last decade, little research has been done on large-scale studies. And most research is focused on one method, while an integrated system can be promising either. This thesis focused on both topics, taking Rotterdam-The Hague Airport as reference airport. Syngas will be obtained from biomass gasification and water electrolysis with a proton exchange membrane (PEM) electrolyzer. CO_2 to form CO is retrieved from a DAC plant. The syngas is converted into fuel by Fischer-Tropsch (FT) technology.

Several gasification technologies were studied and the direct heated steam/oxygen fluidized bed gasifier was found to be the best option. This gasifier was built and validated according to the Institute of Gas Technology (IGT) gasifier located in Hawaii. In order to accurately estimate the behavior of the process, a steady state model is developed using Aspen Plus. Two scenarios are defined and represent the intermittent behavior of renewable electricity. The first scenario simulates high renewable electricity production, while the second scenario is driven by low supply of electricity. Biomass gasification is integrated to remain a constant syngas flow for the FT reactor and subsequent kerosene production.

To reach the intended annual kerosene production of 50.000 ton, it was found that a gasifier with a maximum capacity of 100 ton/h is required. Thermal efficiencies of 35% and 33% are achieved for scenario 1 and 2 respectively, taking gasoline, diesel and waxes into account as useful side-products. Total land-area required to fulfill electricity demand equals $0.9km^2$ of solar panels together with a wind farm covering $3.6km^2$ assuming turbines of $10MW$.

A cost analysis has been conducted to investigate the economical feasibility of the project. The average fuel price obtained in this project reached 1.74-2.87€/kg, exceeding conventional fuel prices. But estimated price reductions and technical improvements for wind/solar power, PEM electrolysis and DAC decrease the fuel price to 1.49-2.78€/kg by 2050. In addition, carbon taxes are expected to increase hence reducing the gap between conventional and synthetic kerosene even more.

Future research and development must focus on extending and improving the model to acquire more precise results. Furthermore, improvements have to be made for electrolysis and DAC plants before they are economically competitive and suitable for large scale.

In conclusion, the models in this thesis have shown promising results in terms of future feasibility of large scale synthetic kerosene production in an integrated system. It has proved that when future developments are realised and DAC and PEM electrolysis have become more mature, the price gap between conventional and synthetic kerosene can be overcome and large scale projects become feasible.

Contents

List of Figures

List of Tables

List of Abbreviations

AEC	Alkaline electrolysis
AEM	Anion exchange membrane
ASF	Anderson-Schulz-Flory
ASTM	The American Society for Testing and Materials
ATR	Autothermal reforming
BFB	Bubbling fluidized bed
CAPEX	Capital expenditures
CEPCI	Chemical Engineering Plant Cost Index
CFB	Circulating fluidized bed
CORSIA	Carbon Offsetting and Reduction Scheme for International Aviation
DAC	Direct air capture
DEF STAN	Defence Standard UK
DME	Dimethyl ether
EoS	Equation of State
ER	Equivalence ratio
ECN	Energieonderzoek centrum Nederland (Energy research Centre of the Netherlands
FAME	Fatty acid methyl ester
FICFB	Fast Internally Circulating Fluidized Bed
FT	Fischer-Tropsch
HHV	Higher heating value
ICAO	International Civil Aviation Organization
IGT	Institute of Gas Technology
KPI	Key Performance Indicator
LHV	Lower heating value
LOX	Liquid oxygen
MSA	Moisture swing adsorption
MSW	Municipal Solid Waste
NIMBY	Not in my backyard
NRTL	Non-random-two-liquid
NTP	Non thermal plasma
OPEX	Operational expenditures
PBP	Payback period
PEM	Proton exchange membrane
PSI	Peak Sun Insolation
PV	Photovoltaic
RFS	Renewable Fuel Standard
RHIA	Rotterdam The Hague Innovation Airport
RWGS	Reverse water gas shift
SAF	Sustainable aviation fuel
SBR	Steam to biomass ratio
SOEC	Solid oxide electrolysis
SMR	Steam (methane) reforming
SWRO	Seawater reverse osmosis
SPK	Synthetic paraffinic kerosene
TES	Thermal energy storage
TSA	Temperature swing adsorption
UNIFAC	UNIQUAC functional-group activity coefficients

1

Introduction

Aviation contributes to 2% of the total carbon dioxide emissions worldwide, which was equivalent to 895 million tonnes of CO_2 in 2018 [61] [84]. Boeing estimates that the aviation sector will grow with an annual rate of 4.2% and 4.7% for number of passengers respectively cargo-air traffic. The aviation sector will be doubled in 2040 compared to 2018. To note, these numbers were published before the Covid-19 pandemic and might change future aviation growth. Inactive fleets across the world, delays in production activities for sustainable aviation fuel (SAF) in multiple industries and less efficient airplanes that do not return to service are some examples of how Covid-19 impacted the aviation. But it is inevitable that the carbon footprint of aviation will increase if the sector does not invest in sustainability. Alternative fuels will play a primary role in the coming years motivated by numerous climate agreements, such as the Carbon Offsetting and Reduction Scheme for International Aviation (CORSIA) and the Paris Climate Agreement (2015). CORSIA is an initiative from the UN's International Civil Aviation Organization (ICAO) where they agreed on to reduce CO_2 emissions from international aviation. According to a study done by MarketDigits [8], the SAF market is expected to grow from 66 million USD in 2020 to 15.307 million USD by 2030. The biggest progress can be made at large (>100) passenger airplanes. They contribute to 90% of the total emitted CO_2 emissions from the commercial aviation sector [30] [84].

Rotterdam-The Hague Airport is the third biggest airport of The Netherlands and received 2.1 million passengers in 2019. They launched the 'Rotterdam The Hague Innovation Airport' (RHIA) in 2019 along with the municipality of Rotterdam [9]. Which covers several initiatives to become more environmentally friendly by innovating economical and technical aspects of the airport. One of these initiatives is replacing the conventional kerosene by synthetic kerosene. Other initiatives are more silent airplanes and better mobility of the airport. This research will discuss the feasibility of synthetic kerosene, economically and practically.

Several methods have passed by the last years to reach a more sustainable aviation fuel. SAF can reduce the carbon dioxide emissions by up to 80% compared to fossil fuel over the lifecycle [8]. It will depend on the feedstock used, supply chain to the airport and the production method. Flying on electricity, hydrogen, synthetic kerosene and bio-fuel are suggested alternatives.

At first, electricity for transportation is gaining more interest. The share and availability of electric cars has increased the last years. Rapid improvements in price and performance have made it possible to replace the conventional cars that run on diesel or gasoline. Using electricity, and thus batteries, for aviation transport is more difficult. It might be an option for small airplanes, but the batteries are too heavy for normal passenger airplanes and cargo. Compared to kerosene, a battery does not lose weight during the flight while a kerosene tank gets lighter. Besides the weight of the battery, it must also function at high altitudes and therefore at low temperatures. At last, the energy density of kerosene is much higher than the best batteries available now.

Secondly, hydrogen is also a new type of fuel which might have potential in future transport. At several places in the world hydrogen is already in use for trains, busses, cars and even boats. The energy mass density of hydrogen is 2.5 times bigger than kerosene, but hydrogen storage tanks are too heavy for airplanes and for this reason not an achievable option at the moment. If hydrogen will be used, the design of the aircraft needs to be modified (Figure 1.1) which takes years and a new infrastructure for the airports is needed to transport the hydrogen [16].

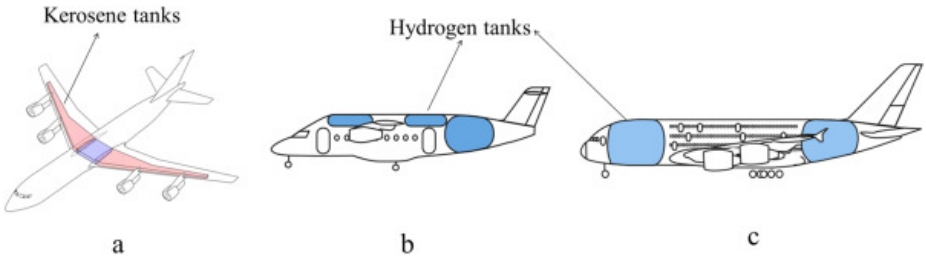

Figure 1.1: Fuel tank locations a) traditional b) medium range hydrogen-powered airplanes c) long range hydrogen-powered airplanes [16]

Thirdly, kerosene can also be produced by the use of water electrolysis and carbon monoxide (CO). Synthesis gas is a mixture of hydrogen (H_2), the product of water electrolysis, and carbon mono-oxide (CO). It can be produced via fossil fuels or in a more sustainable way. Sasol, a company in South Africa, produces synfuel from coal. Syntroleum from the United States and Shell in Malaysia use gas to produce synfuel [75].

But the more sustainable method is by capturing carbon dioxide from the air or straight out of the industry, point source carbon capture [45]. If the electricity for the electrolysis process is generated by renewable sources, solar and/or wind, then this method can be more sustainable than bio-fuel.

One significant advantage of this synthetic kerosene over hydrogen or electricity driven airplanes is that it can function as a so called drop-in fuel. This means that the vehicle, in this case airplane, does not require technical modifications to make use of the new fuel. Another advantage of synthetic kerosene in airplanes is that it does not emit sulphur and aromatics [70].

At last, bio-fuel can be an alternative to replace the conventional way of kerosene production. Some examples of biomass for bio-fuels are algea, wood, crops, cooking oil and animal fats. But not all types of bio-fuel are certified to be blended with 50% conventional kerosene, currently the maximum fraction of alternative kerosene allowed in an airplane is 50% [89]. Two types are certified, 1) the Fischer-Tropsch hydroprocessed synthesized paraffinic kerosene (SPK) and 2) the SPK from hydroprocessed esters and fatty acids (FA) [14]. All around the world there have been flights on bio-fuels the last decade. Air New Zealand used jatropha plants in 2009 and Virgin Atlantic used fatty acid methyl ester (FAME) in 2008. While KLM Royal Dutch Airlines performed the very first commercial biofuel flight in 2011 with synthetic paraffinic kerosene (SPK) [30]. Japan Airline performed a test flight in 2009 with camelina oil derived biodiesel and in Germany, at Leipzig/Halle airport, research was done on four multiblends that can be used for aviation (2020) [82]. No performance problems were recorded during aforementioned flights [97].

The sustainability of biomass strongly depends on the source. Growing biomass can have a potential effect on land-use change, food security and deforestation. If these parameters are taken into account, multiple forms of biomass are less sustainable than expected [105]. So for this reason it is preferred to use waste biomass to produce kerosene. But there are three reasons why using solely biomass to produce synthetic kerosene is not a good option. First, 1.000 times more water is required to produce kerosene from biomass grown in The Netherlands than from synthetic kerosene. Which can cause scarcity of fresh water in regions where limited water is available [121].

Secondly, kerosene production from biomass requires 1.000 times more land area compared to synthetic kerosene production. This means that the growth of biomass feedstock for fuels needs to compete with growing food and other industries. Third, bio-fuel is not necessarily carbon neutral. Gasification, creating farmlands and biomass drying all require additional process steps that emit CO_2 which will later on not be used in the kerosene. But kerosene from biomass can be helpful to absorb fluctuations of renewable energy at the production of synthetic kerosene [121]. How biomass can be converted into kerosene will be discussed in Chapter 2.3.

The type of kerosene mainly used for large airplanes is known as Jet A-1. Jet A-1 differs from Jet A fuel in a lower freezing point, which favors for long international flights. Jet B has a higher volatility and is used only in Arctic regions. Similar as other types of kerosene, Jet A-1 has strict regulations regarding the fuel specification. Most important specifications can be found in Table 1.1, based on DEF STAN 91-91, ASTM D1655 and ASTM D7655 for SAF. The aromatic content is restricted to avoid leaks in the engine and seals in the aircraft. Some production pathways for synthetic fuels do not meet the fuel specifications, such as aromatic content, but this may be resolved by blending with conventional fuels [72]. In case of synthetic fuels, a blending limit of 50% is allowed for nowadays aviation fuels. The remaining part should be conventional kerosene [30]. Otherwise approval is required before it can be applied as fuel for aviation.

Table 1.1: Jet fuel A-1 specifications with 50% synthetically produced kerosene [64]

Freezing point $[°C], max$	-47
Density at 15°$C[kg/m^3]$	775-840
Flash point $[°C], min$	38
Viscosity at -20°$C[cm^2/s], max$	0.08
Net heat of combustion [MJ/kg], min	42.8
Aromatic content [vol%]	8-25

1.1. Research objective

The growing aviation sector and the urgency to reach a more sustainable world shows that big improvements have to be made in the nearby future to meet the climate agreements. Replacing the fossil fuel based kerosene by a more sustainable variant will be a big step towards a more sustainable aviation sector. The research goal is to develop a model that continuously produces synthetic kerosene for Rotterdam-The Hague Airport. Several pilot plants are built to do experimental research on this topic in addition to the theoretical and computational research. A small pilot plant will also be built in Rotterdam, but not in the scale of the airport kerosene demand.

This study will investigate the production of synthetic kerosene that should deliver enough for Rotterdam-The Hague Airport in a completely sustainable way. The Netherlands consumed 3867 million kg kerosene in 2019 subdivided into all airports, but mainly Schiphol. Based on the amount of passengers, Rotterdam-The Hague Airport contributes to approximately 2.5% of this consumption which is around 100.000 ton kerosene per year. Since only 50% synthetically produced kerosene is allowed in a kerosene blend, the target will be to produce 50.000 ton kerosene annually. Required electricity will be supplied by solar and wind energy. Intermittent electricity supply and consequently syngas production will be compensated by biomass gasification. The biomass that is widely available and will be used in this model are wood pellets. Wood pellet market is a developing market in the world energy sector whereby the Port of Rotterdam acts as an important transit location.

Two methods to obtain syngas, (1) water electrolysis with DAC and (2) biomass gasification, are investigated in this study. Multiple studies are done on synthetic kerosene production by these methods separately from each other. But a combined process has not been investigated so far, especially not on this scale. This research will develop an integrated system of the two methods, which will make it complex and different from other studies.

This research will focus on the described problem statement, leading to the following research question where this study attempts to find an answer for.

- Is it feasible for Rotterdam-The Hague Airport to produce synthetic kerosene by water electrolysis with DAC and biomass gasification given the intermittent supply of electricity?

To answer the research question, several sub-questions need to be answered during the study. These are listed below:

- What are the bottlenecks in the system, based on an economical and technical feasibility study?
- What are the total costs of the production plant?
- How much electricity and consequently land-area is required for electricity production? And how will this be subdivided between solar and wind?
- How much CO_2-capture is required?
- How many useful side-products are produced in the system?
- Is there enough oxygen, derived from the water electrolyzer, available for biomass gasification?
  - What capacity for the oxygen storage is required?

1.1.1. Scenario description

Intermittent renewable electricity supply affects the hydrogen production from the PEM electrolyzer. Two scenarios will be investigated and represent maximum and minimum electricity supply to the system. Each scenario requires quantitatively different feedstreams. It is assumed that renewable electricity is solely produced by solar and wind energy, evenly distributed. Due to lack of information about preferences by the airport or possible locations for solar or wind farms in the Rotterdam area, it is impossible to determine a more specific distribution. Varying capacity factors throughout the year will result in the two following scenarios:

- **Scenario 1: high renewable electricity production**
  This is the most preferred situation. Abundant renewable electricity is generated and the PEM electrolyzer works at 100%. The capacity factors for both solar and wind are optimal (Table 1.2). Most syngas required for the production of kerosene will come from the DAC and PEM electrolyzer. The biomass gasifier will operate at only 40% of the nominal feed.
- **Scenario 2: low renewable electricity production**
  A minimum amount of renewable electricity will be available. From Table 2.3 it can be observed that the minimum solar production is during winter with a capacity factor of about 3%. While wind production in winter is normally at maximum but can decrease to only 20%, if we assume the 25-75% interval. The 10-90% interval is not considered since this will more be relevant for dynamic analyses because these low capacity factors will rarely occur over time periods of a month or longer. Only a small fraction (≈30%) of the syngas will be produced by the DAC and PEM electrolyzer. The residual syngas is produced via biomass gasification.

Table 1.2: Capacity factors of PV and wind power for the scenarios

capacity factor	Scenario 1	Scenario 2
Wind	50%	25%
Solar	20%	3%

1.2. Thesis outline

The report is divided into clear consecutive chapters. Chapter 2 comprises of relevant literature for this research study. Different types of gasifiers, electrolysers, DAC plants and production pathways are reviewed.

Chapter 3 outlines the Aspen Plus model developed to simulate the kerosene production process. Every component within the model is briefly discussed according to the literature review. The gasifier and gas cleaning steps are validated to justify the validity of the model.

In Chapter 4 the model results from Aspen Plus are examined, elaborated and finally concluded for both scenarios. These results are used for the cost analysis in Chapter 5. CAPEX and OPEX are determined to finally calculate the average fuel price. A sensitivity analysis is performed to examine the effect of the most important cost items on the average fuel price.

Finally, Chapter 6 concludes the study by answering the research question and corresponding sub-questions. In addition, a few recommendations for further research are given.

2

Literature review

This chapter will review literature based on previous research. In Section 2.1 the different building blocks to produce synthesis gas are discussed. There are different pathways to finally produce fuels, which is explained in Section 2.2. Biomass gasification forms an important part in this study and is discussed in Section 2.3, followed by the distillation part to obtain the different fractions (Section 2.4).

2.1. Building blocks for synthesis gas

Synthesis gas (syngas) is a mixture of hydrogen (H_2) and carbon monoxide (CO), at which CO is predominantly produced using carbon dioxide (CO_2). The pathways of getting to the aforementioned building blocks is discussed in this section. Electricity supply is an important part of the H_2 and CO production and therefore included. At last, biomass gasification also produces syngas, the availability of biomass and the principle of gasification will be explained.

2.1.1. Hydrogen

Hydrogen can be produced by the synthesis of water in an electrolyzer. H_2O will be supplied and converted into H_2. The total endothermic reaction that takes place inside an electrolyzer is shown in Reaction 2.1, where the enthalpy is a summation of heat (49 kJ/mol) and electricity (237 kJ/mol).

$$2H_2O \rightarrow 2H_2 + O_2 \ \Delta H^0_{298} = 286kJ/mol \tag{2.1}$$

The supply of clean water is important. Rotterdam is a location for abundant water supply with rivers and a sea nearby, although seawater can not be supplied directly to the electrolyzer. The salt needs to be separated from the water, which can be done by seawater reverse osmosis (SWRO) desalination [44]. Another alternative can be to utilise the river water. This water has a lower salt content, but might be contaminated. It will need additional steps to get rid of the contaminants or salt before it can be supplied to the electrolyzer. Besides external water supply, water produced as side-product at any point in the kerosene production chain might be recycled and used as input for the electrolyzer.

How the hydrogen is produced in the electrolyzer strongly depends on the electrolyte used. Important parameters to determine a suitable electrolyte for this process are current density, (future) capital costs, gas purity and ability to work with dynamic electricity supply.

Alkaline electrolysis (AEC) is the most common technique and dominates the market for more than 100 years [135]. It operates at a low temperature, $60°C - 80°C$, with NaOH and/or KOH liquid solution as electrolyte. The produced hydrogen has a purity of approximately 99% and requires 4.5-6.6 kWh_{el}/m^3 with a nominal stack efficiency of 65% LHV. Nickel alloys are used as catalysts in an AEC electrolyzer [29]. A disadvantage of the AEC is the low current density, slow start up time and slow loading response. Long start up time makes it difficult to function with the variable nature of renewable energy sources. AEC normally works with a steady power input. Future cost reductions will most likely be achieved by economies of scale [109].

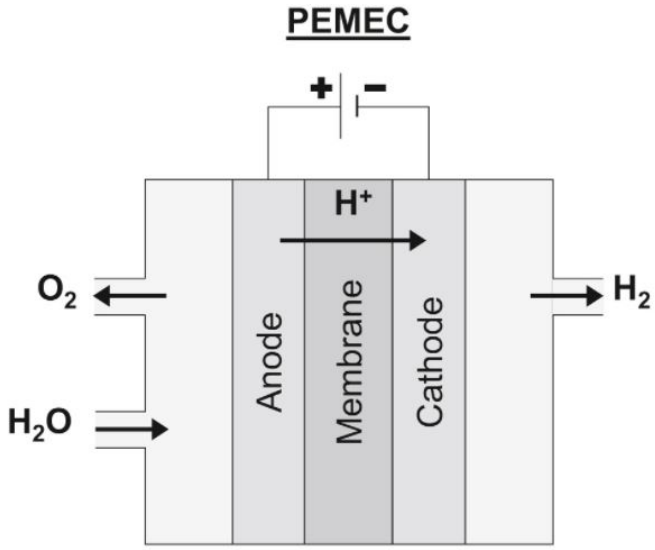

Figure 2.1: PEM electrolyzer [109].

Table 2.1: Specifications for four different electrolyzers [27] [29] [40] [46] [109]

	AEC	PEM	SOEC	AEM [88]
Operating temperature [$^{\circ}C$]	60-80	50-80	500-700	50-70
Operating pressure [bar]	10-30	20-50	1-15	-
Cell voltage [V]	1.8-2.4	1.8-2.2	0.7-1.5	-
Current density [A cm^{-2}]	0.2-0.4	0.6-2.0	0.3-2.0	1.15-1.5
System energy [$kWh_{el}m^{-3}$]	4.5-6.6	4.2-6.6	> 3.7	-
Nominal stack efficiency [% LHV]	63-71	60-68	up to 100	42-53
Production rate [m^3/h]	0.25-760	0.01-240	<40	-
Lower dynamic range [%]	0-40	0-10	>30	-
Respond rate (minimal load to full)	10 min	10 sec	-	-
Stack lifetime [h]	>100.000	>40.000	<10.000	-
Capital cost [€/kW]	370-900	480-1270	>2000	-

The production of a proton exchange membrane (PEM) (Figure 2.1) electrolyzer is quite similar to a PEM fuel cell. It was first introduced in 1960 to overcome the drawbacks of AEC [135]. PEM electrolyzers have a higher efficiency, fast response time and high output pressure making it suitable for hydrogen production and flexible operation, which is advantageous with intermittent power supply. The low dynamic range makes it even more attractive for renewable electricity usage. H_2 production can be decreased to 0-10% when electricity supply is minimal, which is the lowest of all discussed electrolyzers. The operating current density of 1 A/cm^2 is much higher than the AEC, while the operating temperature is comparable $(50^{\circ}C - 80^{\circ}C)$. But the precious metals used in the electrolyzer makes it more expensive than AEC. The costs can be decreased to only 1/4 of the current price if the hydrogen production increases till 1000 kg/d. RuO_2 and IrO_2 are now classified as best catalyst for PEM water oxidation and platinum (Pt) as best electrocatalyst for the cathode [27] [29] [109] .

The reaction that takes place at the anode side (Reaction 2.2) and on the cathode side (Reaction 2.3) will result in the total Reaction 2.1.

$$2H_2O(l) \rightarrow O_2(g) + 4H^+(aq) + 4e^- \tag{2.2}$$

$$4H^+(aq) + 4e^- \rightarrow 2H_2(g) \tag{2.3}$$

High water temperature solid oxide electrolysis (HT SOEC) is a new technology that can reach an efficiency of more than 90% if heat utilization is taken into account. This option is especially interesting if waste heat is available from geothermal, solar and/or nuclear sources. Operating tempera-

ture nowadays is still $650°C - 1000°C$, but research is developing a new configuration to lower this to $500°C - 700°C$. Current disadvantages are mostly due to material limitations, long start-up time, and poor dynamic response and therefore commercialization will probably not start in the coming years. Due to the long start-up time SOEC results in a poor dynamic response.

A potential advantage of the HT SOEC can be the direct production of syngas. The conversion of water and carbon dioxide can take place simultaneously [29] [109].

Another type of electrolyzer with a big potential is the anion exchange membrane water electrolyzer (AEMWE) [29]. Just like the PEM water electrolyzer, the AEMWE also uses a solid electrolyte and therefore produces high purity hydrogen. But the AEMWE shows low performance and durability compared to other methods. If the replacement of PEM with AEM is successful [88], advantages of both methods can be realized, but the AEMWE can be applied more widely. However, there are too many aspects such as materials, membranes and electrocatalysts that need more research before the full potential can be determined.

2.1.2. Carbon dioxide

Compared to water supply, the supply of carbon dioxide (CO_2) is more difficult. Pure CO_2 can be obtained by point source capture and direct air capture (DAC).

At first, the easiest method is transporting pure CO_2 that is produced in industry directly to the synthetic kerosene process, also known as point source carbon capture [45]. Although this option sounds very promising for the airport nearby Port of Rotterdam, it might cause problems the coming decades. The Port of Rotterdam wants to reduce their emissions drastically and ultimately to zero by 2050 [2]. But not only the Port of Rotterdam needs to reduce their emissions, every country faces challenges to reach the goals from the 2015 Paris Agreement [103]. A large CO_2 supply is needed to meet the desired amount for synthetic kerosene production. But if the industry meets the goals to reduce their carbon footprint, the availability to extract CO_2 from the industry can become insufficient for syngas production.

Secondly, CO_2 can be obtained by using direct air capture (DAC). DAC is a relatively new method and in the early commercial stage. It makes use of the CO_2 concentration in the air, which reached 400 ppm in 2018 and increases every year [15]. Although CO_2 is only a small fraction in the air, there is enough CO_2 available for multiple industrial applications. Various research studies around the world are studying different DAC methods, from which the following two methods are best known:

- One method is a system based on adsorption (Figure 2.2) where temperature swing adsorption (TSA) is the dominant DAC method. This method works at a temperature of approximately $80 - 100°C$. Adsorbents use amines to capture the CO_2 from ambient air, followed by a desorption process where the CO_2 is again detached from the amine [45]. Moisture swing adsorption (MSA) is another method in this category in which the CO_2 rich sorbent gets moisturized [66]. Specifications for an amine-based DAC can be found in Table 2.2.

Table 2.2: Specifications for an amine-based LT solid sorbent DAC [45]

Adsorption	Desorption		Energy demand			Cooling		$CO_2 purity$
T $[°C]$	T $[°C]$	P [bar]	kWh_{el}/t	kWh_{th}/t	by	T $[°C]$	by	%
Ambient	100	0.2	200-300	1500-2000	Waste heat	15	Air/water	99.9

Climeworks, a Swiss company based in Zurich, already built several DAC plants in Iceland, Germany and Switzerland based on this low temperature sorbent technique. The plant in Germany captured 80% of the CO_2 molecules in air and produced synthetic diesel in cooperation with Audi. They expect the large-scale costs for a plant to reach about $75€/t_{CO_2}$. Antecy, a Dutch company, cooperates with Shell to implement a pilot plant that works at moderate temperatures $(80-100°C)$. Another initiative from the Netherlands comes from Skytree, where CO_2 is captured on a porous plastic bed by electrostatic properties and regeneration takes place by humid swing [45] [60].

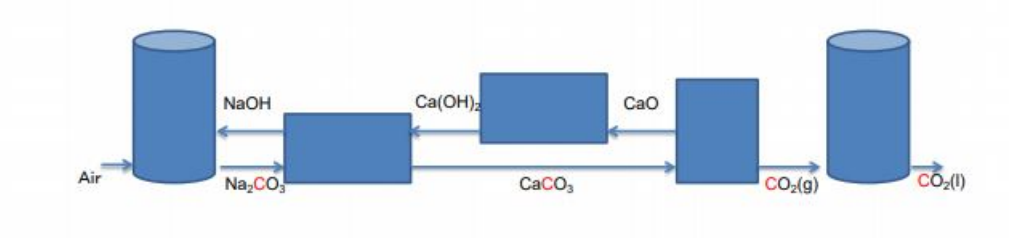

Figure 2.2: Schematic flow of DAC using liquid adsorbent. Captured carbon is indicated in red [60]

- A second DAC method is based on high temperature aqueous solutions. This method works with temperatures up to $900°C$ to release the CO_2, and therefore need substantially more heat than previous mentioned methods. The overall heat demand becomes 1420-2250 kWh per ton CO_2. Electricity is besides heat necessary to blow air through the contactor for which 366-764 kWh/ton electricity is needed.

The water demand for DAC gets significant when expanding to large scale plants. So water supply is again, after water supply for electrolysis, something to be taken care of. Regarding the costs, the DAC units contribute to approximately half of the annualised costs for a CO_2 capture plant. Solar PV panels and wind power plants, batteries, heat pumps and thermal energy storage (TES) provide the other half of the costs. Since the electricity supply depends on solar and wind, the costs for these plants are strongly determined by the location. Estimated costs for DAC will decline to 105 €/t_{CO_2} in 2030, 70 €/t_{CO_2} in 2040 to even 55 €/t_{CO_2} in 2050 [24]. Compared with the $CO_2 - tax$ of 30 €/t_{CO_2} in 2021 and 150 €/t_{CO_2} in 2030 makes DAC attractive for the future [65].

2.1.3. Carbon monoxide

Carbon monoxide (CO) with H_2 forms synthesis gas. There are several methods to obtain CO, from which all except one require CO_2 as feed stream.

The first method is equal to the first method mentioned for CO_2, namely point source capture. Carbon monoxide can be a side-product in numerous industrial processes. But it is, as well as direct CO_2 supply, highly unlikely that the CO supply will be sufficient to guarantee a permanent flow to meet the large kerosene demand.

Second, CO_2 reduction interest has grown the last few years for electrochemical, thermochemical and photochemical pathways. From these alternatives, electrochemical achieved the most interest since it has advantages over the other approaches. Such as the easily controllable reaction rate, ambient operating conditions, compactness and the option to fully recycle the supporting electrolytes. The other alternatives work at high pressures and temperatures [134]. If the required electricity is obtained from renewable sources it can potentially convert CO_2 into valuable fuels [129]. Certain challenges need to be overcome before electrochemical reduction of CO_2 can be commercialized. The biggest challenge is the insufficient stability and low catalytic activity which results in a low performance of the electrocatalysts. Two other challenges are the low energy efficiency of the process and the slow kinetics of CO_2 electroreduction [96].

Thirdly, carbon monoxide can be produced by hydrogenating carbon dioxide from a reverse water gas shift (RWGS) reaction, known as a catalytic reduction of CO_2 to CO. The captured CO_2 and H_2 will be converted following the endothermic Reaction 2.4. An exothermic methanation Reaction (2.5) can occur if the reaction temperature is not high enough.

$$CO_2 + H_2 \rightarrow CO + H_2O \ \Delta H^0_{298} = 41kJ/mol \tag{2.4}$$

$$CO_2 + 4H_2 \rightarrow CH_4 + 2H_2O \ \Delta H^0_{298} = -165kJ/mol \tag{2.5}$$

The minimum reaction temperature is $400°C$, but a common operating temperature for a high temperature RWGS reactor without catalyst lies between $800 - 900°C$. A catalyst can be added to increase the reaction rate and decrease operating temperature or a surplus of CO_2 or H_2 to shift the chemical

equilibrium. Lower temperatures decrease energy consumption but increase costs due to high dependence on the catalytic reaction. Most research is focused on copper-based catalyst systems, because high stability is achieved for CO_2 rich streams. Variations on the catalyst can enhance the performance of the RWGS. Ni-based catalysts, on the other hand, by addition of Fe or CeO_2 also results in high CO_2 conversion rates [133]. Elsernagawy et al. [41] used the copper-catalyst $Cu - ZnO/Al_2O_3$ because of lower price, lower methane formation and better performance at lower temperatures compared to alternative catalysts. Conversion rates of >90% can be achieved for this catalyst and depend on temperature, pressure and H_2/CO_2 ratio.

$Ru_3(CO)_{12}$ catalyst enables the reactions to take place at a much lower temperature of $80°C$, but ruthenium is expensive and scarce in nature [112]. Another low temperature RWGS method is non thermal plasma (NTP) which is a promising substitute for the conventional high temperature RWGS reaction. NTP has a compact design, fast ignition and high reactivity. Although the main disadvantages are a rich production of by-products and a low selectivity for the desired products. If these drawbacks can be overcome, it might have great potential [73].

Fourth and last, plasma splitting is a not yet commercially available but promising method. Plasma splitting uses a thermal plasma combined with the highly endothermic Reaction 2.6 to convert CO_2 into CO. Interest is growing the last years for gas conversion methods. Gas plasma can even react close to room temperature and only electricity need to be supplied. Because of the low temperature it does not need preheating and can be turned on and off quickly [22].

$$CO_2 \rightarrow CO + \frac{1}{2}O_2 \; \Delta H^0_{298} = 553kJ/mol \tag{2.6}$$

The conventional way is to pass the CO_2 through a carbon bed heated by a microwave. Microwave plasmas are very energy efficient for CO_2 conversion and therefore a promising method. They do not require electrodes, leading to low maintenance cost, and have a high electric energy utilization efficiency. In addition, no furnace is required to raise the reactor temperature since the temperature of the microwave plasma reactor is lower (outer wall temperature $(50 - 90°C)$) [47].

Bermúdez et al. [20] improved the process by replacing the carbon bed by a charcoal bed, which led to a CO_2 conversion of 95% and energy efficiency of 45%. Li et al. [71] heated the CO_2 gas in advance to 3000K to let the mixture react with coke or semi-coke in the carbon bed directly. This method maintained the 95% conversion, but reached a 75% energy efficiency. Converting CO_2 by plasma has promising advantages such as low investment and operating costs, no use of rare earth materials, quickly on and off and applicable for various renewable sources. But before plasma splitting can be commercialised it needs to overcome several drawbacks such as process capacity, catalysts tailored for the plasma environment and CO_2 conversion.

2.1.4. Electricity

Electricity will become an important factor in the proposed ways of synthetic kerosene production. To maintain a fully renewable pathway to kerosene, the electricity should be produced as sustainable as possible. Renewable electricity can be produced by wind, solar, tidal, geothermal, biomass and hydro energy. From aforementioned methods, wind and solar are most suitable for electricity generation in The Netherlands.

Solar panels generate approximately five times more electricity in summer than in winter (upper picture of Figure 2.3). Daily insolation can be estimated as $5.2kWh/m^2/day$ in summer and $1kWh/m^2/day$ in winter for The Netherlands. This yield increases 28% if the pathway of the sun is followed by the panel during the day [115]. The solar capacity factor can be estimated to be 10-25% in The Netherlands [107]. Panels may be placed on roofs, farms and potentially in windows. Solar farms require bare land-area compared to the other two alternatives.

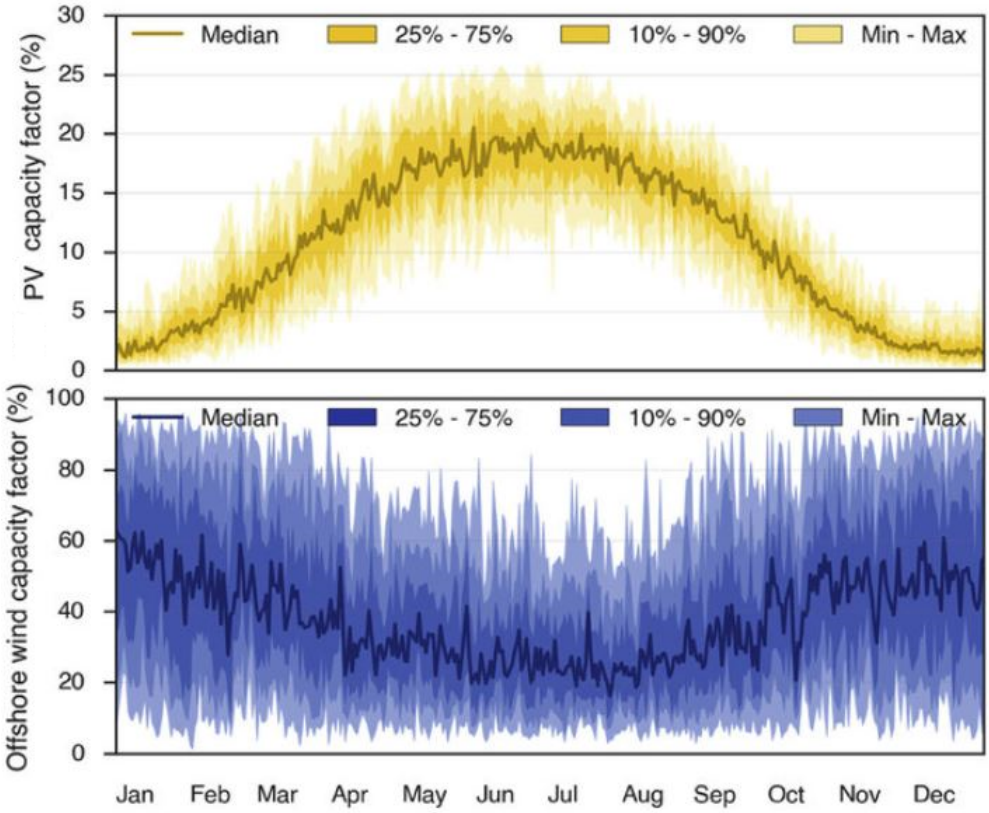

Figure 2.3: Expected mean capacity factor for offshore wind and solar energy for Great Britain in 2030 [118]

Wind power is generated by wind turbines placed offshore or onshore. Major improvements are made in recent years and globally installed capacity has grown significantly. Focus on offshore wind farms is growing, especially in The Netherlands with a long coastline. Onshore wind production faces social resistance (NIMBY) in highly populated areas. Wind power generation varies at different locations and temporally, fluctuating production per day and annually. Figure 2.3 shows the wind pattern for offshore wind in Britain, onshore wind exhibits a similar pattern. The mean capacity factor is clearly visible, but the graph also illustrates the enormous uncertainty. Capacity factor can reach values of only 10% up to 90%. Significantly higher than solar, where uncertainty is approximately ±5%. The wind capacity factor in the Netherlands is, according to a study of IEA [6], annually 24% for onshore wind turbines and 44% for offshore. Much higher capacity factors are reached offshore, which would encourage more offshore turbines. But this also depends on the available land/sea area and economics.

An advantage of wind power next to solar is the annual distribution combined. Solar power is dominant in summer, while wind power is generated more equally throughout the year. Although the production in summer is lower, which might be compensated by solar energy [118].

Another alternative might be biomass, but the sustainability hereof is questionable as discussed before. The remaining alternatives are not viable in The Netherlands due to geographical circumstances. Therefore wind and solar electricity generation will be most suitable for Rotterdam-The Hague Airport [105]. The distribution between them mainly depends on available land and electricity demand throughout the year. A higher electricity demand in summer requires more solar, while a higher demand in winter needs more wind power.

2.1.5. Biomass

Biofuels based on biomass takes on increasing interest. Increasing interest in new technologies usually depends on funding from governments or companies. Multiple countries incorporated biofuels in their newest policies. The United States launched the Renewable Fuel Standard (RFS) Program to reduce greenhouse gas emissions and reliance on imported oils by finding alternatives for fuels, such as jet fuel, which are price competitive. Incentives in agriculture and new plants are supported to reach their goals. The EU announced incentives to promote sustainable aviation fuel for the coming decade in the Renewable Energy Directive. The Dutch government cooperates with SkyNRG to promote biofuels for Schiphol Airport. China as well as Indonesia proposed increase of biofuel use in their policies [130].

Biomass can function as back-up production method for syngas production. Due to the intermittent electricity production by renewables, the supply of H_2 and CO will not be constant. But the FT reactor shows the best performance at constant operating conditions and hence continuous supply of syngas. The flexibility of biomass offers a perfect alternative for the fluctuating electricity supply. It is therefore a promising way to fill up the shortcomings of syngas production by electrolysis.

Biomass is widely available all around the world due to its variety. Algea, wood, agricultural waste, cooking oil and animal fats are some examples that can be transformed into useful sources for synthetic kerosene [124]. Wood and agricultural wastes have the highest mass conversion rates, 15% and 12% respectively, while manure only reaches 6% [114]. But not every option is as promising as it looks, some negatively affect the environment. A source that is relatively friendly for the environment, such as waste, and that is widely available is preferred.

Biomass may come from The Netherlands, or may be imported. In 2018, a total of 784 kton dried wood, chips and shreds, was available in The Netherlands [23]. Approximately 80% of this potential has been used from which 50% is exported. Improvement of biomass applications in the coming decades will quadruple the demand for biomass in 2050. An increasing demand and consequently biomass price will result in an increasing supply. 955 kton might be available in 2030 and this will further increase to 1324 kton in 2050. Expected increase in demand of woody biomass for transport fuels has not been taken into account, because of a lack of plans and initiatives.

Wood pellet market is one of the most developing solid biofuel market in the world energy sector. The USA, Canada and the EU are the main players in this field with a total production of 14Mt in 2015. From the European exports, the Baltic countries accounted for 35% of the total export because of their abundant forests and perfect accessibility for shipping. The market has developed last decade due to increased demand in the industrial sector and heating. In recent years, Asian countries also started scaling up their wood pellet market [94]. This growing interest in wood pellets worldwide makes the market become broader and offers opportunities for new trading partners. The Port of Rotterdam is an important transit port for the hinterland. Multiple storage facilities are present in the harbour before it is transferred to smaller ships, trains or trucks. This wide infrastructure is promising for a supply of wood pellets for the production of synthetic kerosene.

2.2. Production pathways for synthetic kerosene

There are several ways to produce synthetic fuels. But not all methods are suitable for kerosene production. The three most promising methods, using the discussed building blocks, are methanol, dimethyl ether (DME) and Fischer-Tropsch (FT) synthesis.

2.2.1. Methanol

The German company BASF built the first industrial scale methanol plant in 1923 at high pressure (250-350 bar) and temperature. This has been replaced by a low pressure (50-100 bar) plant since 1960. Methanol is produced according to the exothermic Reaction 2.7 or 2.8, and thus favours low temperatures.

$$CO_2 + H_2 \leftrightarrow CH_3OH + H_2O \ \Delta H^0_{298} = -49.4kJ/mol \tag{2.7}$$

$$CO + 2H_2 \leftrightarrow CH_3OH \ \Delta H^0_{298} = -90.6kJ/mol \tag{2.8}$$

Current research on methanol production focuses on increasing plant size because of economic advantages by scaling up. Quasi-thermal fixed bed reactors are currently used for production and replaced the former quench reactors. More research can be done to increase the methanol yield by CO_2 hydrogenation and reduce water production which causes problems [40]. But using alcohol as alternative fuel will result in a significant efficiency drop because of the higher weight and requires more space. In addition, the mass and volumetric heats of combustion are very poor [33]. Another drawback is that methanol is highly flammable and becomes toxic and corrosive. Moreover, methanol is predominantly used for the production of gasoline and not for kerosene [108].

2.2.2. Dimethyl ether

Dimethyl ether (DME) is a useful derivative from methanol, which is gaseous during ambient conditions and becomes liquid at moderate pressures. DME is present in cosmetic, agricultural chemicals and paint applications [114].

The plants were built after the methanol production plants replaced the high pressure process by a low pressure process and demand increased. First, methanol is produced from syngas (2.7-2.8) followed by hydrogenation of methanol according to reaction 2.9, the so-called two-step method.

$$2CH_3OH \leftrightarrow CH_3OCH_3 + H_2O \ \Delta H^0_{298} = -23.4kJ/mol \tag{2.9}$$

Due to the absence of carbon bindings and sulphur no soot or sulphur is emitted in the atmosphere. The energy density of DME is lower compared to FT-fuel, methanol and conventional fuels but contains a higher cetane number. Therefore it might be a promising solution to replace the conventional diesel for heavy-weight transport or replace cooking gas, but not for replacing the conventional kerosene. Combustion engine modifications have to be made to commercialise DME as fuel. Nevertheless, the greenhouse gas emissions can be reduced by 80% and emission of pollutants is minimized [40].

2.2.3. Fischer-Tropsch

Fischer-Tropsch (FT) process owes the name to the German scientists Franz Fischer and Hans Tropsch. Kerosene produced from FT is the first approved biofuel for commercial flights by ASTM in 2009 [130]. The FT reaction converts syngas into an intermediate product for liquid fuels called syncrude. Components as sulfur, nitrogen, aromatics and heavy metals are not produced in contrast to conventional fuel production [70], which is advantageous over the conventional production of liquid fuels. The following highly exothermic Reactions 2.10 and 2.11 take place inside the FT reaction for producing paraffins respectively olefins [114].

$$nCO + (2n+1)H_2 \rightarrow C_nH_{2n+2} + nH_2O \tag{2.10}$$

$$nCO + 2nH_2 \rightarrow C_nH_{2n} + nH_2O \tag{2.11}$$

Probability of chain growth, hydrogenation activity and readsorption chemistry of products determines the selectivity of the syncrude product and consequently the refining process. Side reactions take place inside the FT reactor that produce compounds other than paraffins and olefins. Oxygenates are a large by-product of FT synthesis and contain oxygen in their chemical structure (Reaction 2.12).

$$nCO + (2n)H_2 \rightarrow C_nH_{2n+1}OH + (n-1)H_2O \tag{2.12}$$

FT synthesis can be divided into two main categories, low-temperature FT $(200-240°C)$ and high-temperature FT $(300-350°C)$. The temperature of the process strongly determines the syncrude composition, as shown in Table 2.3.

Table 2.3: Syncrude composition for LTFT and HTFT (mass %) [110]

Fraction	HTFT	LTFT
Paraffins	>10%	Major product
Olefins	Major product	>10%
Oxygenates	5-15%	5-15%
Aromatics	5-10%	<1%
Naphthenes	<1%	>1%
Water	Major byproduct	Major byproduct

Length of the hydrocarbons depends on the probability of chain growth (α) and can be calculated according to the Anderson-Schulz-Flory (ASF) (Equation 2.13) distribution (Figure 2.4). The α-value depends on the type of catalyst, syngas composition, temperature and pressure. Typical α values for synthetic fuel production lie between 0.70-0.90, Dieterich et al. (2018) [40] reported an α of 0.85 for kerosene production. Higher temperatures will result in a lower α and lower average carbon number, a temperature of $300-350°C$ decreases the α till 0.65-0.70. An increasing H_2/CO ratio also results in a lower α, which is undesirable for kerosene production (Table 2.4) [11]. The FT synthesis usually operates near a H_2/CO ratio of 2.1:1, depending on the selectivity [124].

$$W_n = n(1-\alpha)^2\alpha^{(n-1)} \tag{2.13}$$

Table 2.4: Influence of FT operating conditions on product selectivity [11]

Selectivity parameter	Operating parameter being increased		
	Temperature	Pressure	$H_2:CO ratio$
Carbon number distribution	Lower α -value	Higher α -value	Lower α -value
Methane selectivity	Increases	Decreases	Increases
Alkene selectivity	-	-	Decreases
Oxygenate selectivity	-	Increases	Decreases
Aromatic selectivity	Increases	-	Decreases
Syngas conversion	Increases	Increases	-

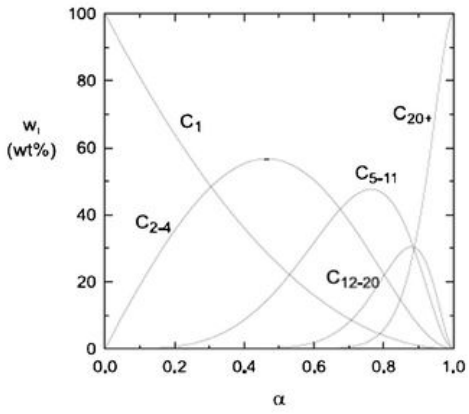

Figure 2.4: Anderson-Schulz-Flory product selectivity for FT [62]

C_{5+} paraffins, C_{20+} linear hydrocarbons and medium weight olefins are desirable products. These can be further processed into usable liquid transportation fuels [114], but there are certain deviations from this distribution [62]. At first, the methane selectivity is normally higher than estimated by ASF. Secondly, the C_2 selectivity is usually much lower compared to ASF. At last, there is more than one chain growth mechanism on the surface of a FT catalyst. More α values are required to estimate the distribution, but this will introduce undue complexity. A double α model is a reasonable compromise and behaves as a weighted sum of two ideal ASF product distributions. The model focuses on deviations of the ASF model at high carbon numbers.

A syngas conversion of approximately 80% in the FT reactor will result in the highest yield. Higher conversion decreases the yield due to lower partial pressure of carbon monoxide [93].

Catalysts

The performance and synthesis of a catalyst affects the syncrude composition. Ru, Fe, Co, Ni and ThO_2 are the best known catalysts or catalyst carriers, but only Fe and Co are industrially applied.

Ru-based catalysts for FT synthesis are more expensive and Ruthenium is scarce in nature. But Ru is reported the most active of these metals. The activity is higher for hydrogenation of CO below $150°C$ and less sensitive to H_2O [28]. Despite its price and scarcity, Ru can be able to function as promoter besides a Co-based catalyst. Nickel's hydrogenation efficiency is comparable with Ru, but more relevant for methanation.

Fe and Co are very effective in converting syngas into chemicals or fuels. High activity, low cost, easy access and flexible operating conditions in high and low temperature make that Fe-based catalysts are widely available and applied in industry. As regards $H_2/CO - ratio$, iron catalysts are useful for lower ratios (0.5-2.5) and are not suitable for H_2 rich syngas [119]. Consequently, iron catalysts are more convenient for alkene production.

Co-based catalyst on the other hand operates better in H_2 rich syngas ($H_2/CO = 2$) and is more relevant for middle distillate and heavy waxes production. This brings a high stability and low activity for the water gas shift (WGS) reaction. It produces mainly paraffins with few alcohols and olefins, which is advantageous because kerosene consists of paraffins. But cobalt is best suited in less severe conditions in terms of pressure and temperature.

The choice of catalyst depends on the FT method, feedstock and final objective of the process. From the above mentioned catalysts, Fe and Co are the only commercially available catalysts. They normally show the best compromise between price and performance [13] [74].

But this research will combine DAC and water electrolysis with biomass to anticipate on intermittent electricity supply. For this reason the syngas produced by biomass also needs to be considered by finding the appropriate catalyst. First, the hydrogen content of biomass syngas is relatively low. Fe-catalysts can work with low hydrogen content wherefore Fe is advantageous over Co-based catalysts. But the stream can be upgraded before the FT reactor and make cobalt suitable as well. Cobalt is preferred in a clean syngas stream and therefore requires purer syngas than a Fe-based catalyst.

Cleaning syngas in general is important to avoid catalyst deactivation by contaminants such as sulfur, chlorides, oxygen and nitrogen-containing compounds.

Secondly, water vapour is produced in biomass gasification. This affects the performance of the catalysts. Research found that Co and Fe catalysts are both similarly negatively influenced and thus no distinction can be made based on water vapour content.

Third, the operating conditions of the FT synthesis strongly affects the catalyst performance. Van Berge [19] developed an envelope, Figure 2.5, where the choice of Fe $(240°C)$ or Co $(220°C)$ catalysts depends on the reactor pressure and relative space velocity, the relation between volumetric flow rate and reactor volume [43]. Severe conditions, high temperature, high pressure and presence of impurities, are more suitable for using iron catalyst. Co-based catalyst on the other hand are comparatively more active under less severe conditions [74].

Based on these aspects, Co-based catalysts seems a better option for the FT process presumed that the FT reactor can operate with a Co-based catalyst. The higher selectivity for paraffins and applicability in H_2 rich streams are important parameters for the kerosene production with the proposed methods.

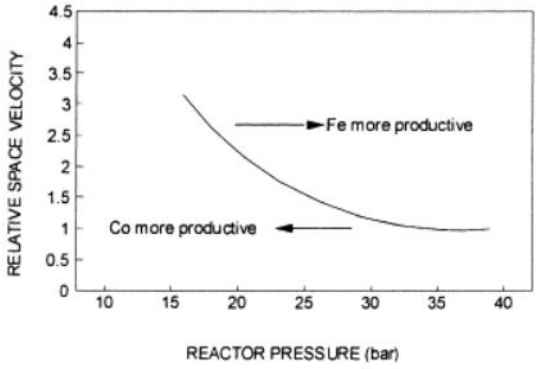

Figure 2.5: Productivity comparison between Fe- and Co-based catalyst [19]

Reactor type

Four different kinds of reactor types are available for the FT reaction: fixed bed, slurry bed, circulating fluidized bed (CFB) and fluidized bed reactor. An overview can be found in Table 2.5 and a visual impression in Figure 2.6. The operation mode of the aforementioned reactors can be divided into high $(300-350°C)$ and low $(200-240°C)$ temperature. Fe-catalysts work at high temperatures and chiefly produce low molecular weight olefins and gasoline. While low temperature FT produces high molecular mass linear waxes. Paraffins instead of olefins are preferred for the production of synthetic kerosene and therefore low temperature FT is more suitable [114]. By selecting an appropriate reactor it needs to be taken into account that the aviation sector will continue to expand and the availability of scaling up the reactor capacity is important.

Table 2.5: Reactor types for Fischer-Tropsch process [40]

	Multi-tubular fixed bed	Fixed slurry bed	Circulating fluidized bed	Fluidized bed
Operating temperature [$°C$]	220-240	220-240	320-350	320-350
Operating pressure [bar]	20-25	20-25	25	up to 40
Conversion	60% per pass	60% per pass	85%	>85%
Catalyst	Fe or Co	Fe or Co	Fe	Fe

A fixed bed reactor has tubes filled with catalysts and boiling water on the shell side. It produces mainly high carbon number products comparable to crude oil. The medium temperature needs to retain low to prevent the temperature rise up to the limit of $260°C$. Scaling up is easy, although the pressure drop becomes high in large reactors. Maximum production of this reactor is roughly 3000-4500 barrels per day [40].

(Fixed) slurry phase reactors are much easier to fabricate, simpler and operate at approximately $230°C$ and 20-25 bar [114]. The reactors use waxy products as heat carrier and suspension fluid for catalyst particles. The well mixed phase results in a perfect temperature control. The product selectivity will also function on higher average conversion. Another advantage is the cost efficiency, which is 25% higher compared to fixed bed. The pressure drop of a slurry phase is much lower than a fixed bed reactor, and therefore lowers the costs for re-compression. Catalyst removal can occur without turning off the reactor in contrast to the fixed bed reactor, which eliminates down-time. In addition, catalyst use in slurry phase per production unit is lower than fixed bed. At last, a slurry phase reactor is easy to be scaled up and can eventually reach 20.000 barrels per day [40].

On the other hand, several challenges and drawbacks come with the slurry phase. The viscosity in the reactor limits the catalyst loading and the thermal efficiency is only 60%. A challenge to make it economically feasible is the separation of catalyst and wax, especially for iron catalyst that is precipitated friable.

In general, the slurry phase reactor offers significant process and economic advantages over the fixed bed reactor. The isothermal behavior, lower costs and possibility to easily scale up the process makes the slurry phase FT reactor more attractive [43].

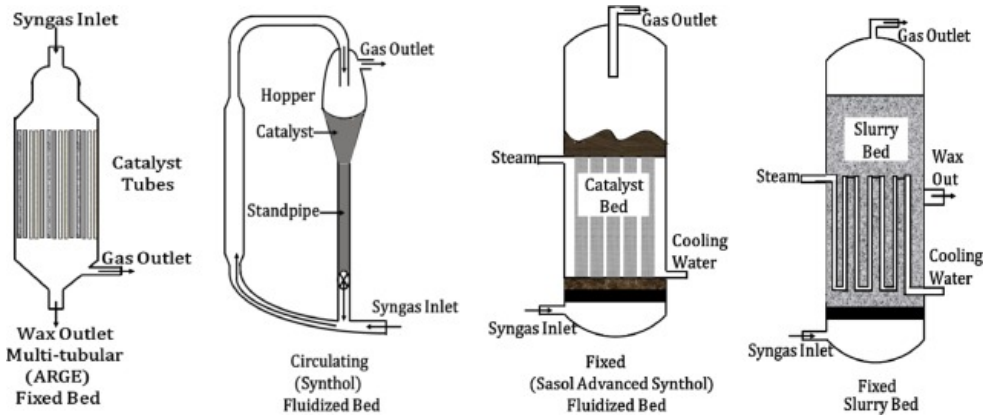

Figure 2.6: Fischer-Tropsch reactors, multi-tubular fixed bed, circulating fluidized bed, fluidized bed, fixed slurry bed [114]

Circulating fluidized bed reactors work with iron-based catalysts and operate at a higher temperature than previous mentioned reactors, namely above $300°C$ to avoid agglomeration of the catalyst by heavy waxes. But a CFB produces mainly (80%) low carbons ($< C_{10}$) and less kerosene range carbons or waxes. [40].

In a fluidized bed reactor, the cooling of the reactor occurs by tubes inside the reactor which operates in the bubbling regime. Easy heat removal and temperature mixing are provided by the good heat transfer of the beds [35]. The production of low carbon numbers ($< C_{10}$) contributes to approximately 80% of the outflow, such as the circulating fluidized bed reactor [40]. Wherefore CFB and fluidized bed are not suitable for kerosene production due to shorter hydrocarbon chains.

The FT-reactor produces tail gas besides hydrocarbons and water. Tail gas comprises of CO_2, $CH4$, N_2, water vapor, vapor hydrocarbons and unreacted syngas. There are three alternatives to use this tail gas useful within the system. At first, it can be recycled to the FT reactor to increase the liquid product yield. Secondly, the gas can be fed to the gasifier as additional feed besides the biomass. Finally, the gas can generate electricity by a power plant [111]. The best option depends on the system configuration.

2.3. Biomass gasification

There are several thermochemical processes to convert biomass. The main processes are pyrolysis, combustion and gasification.

Pyrolysis thermally decomposes organics with absence of oxygen and is the first step in combustion and gasification before total or partial oxidation of primary products. Reuse of side-products and less emissions are advantages of pyrolysis. Products are mainly used in chemical and power generation industries. But syngas and subsequently bio-fuels are also possible products, although low energy density and the corrosive nature makes it not very suitable for fuels [114] [127].

Biomass combustion can take place in a boiler and is used to produce heat, power or electricity. The boiler and operating conditions are determined based on the type of biomass [57]. But using the combustion process in the production of synthetic kerosene can only be useful if there is a lack of electricity or heat in the current system. Otherwise gasification to produce syngas is more promising to compensate the fluctuating supply of syngas by electrolysis due to intermittent electricity production by renewables.

2.3.1. Gasification technology

The gasification process converts biomass into syngas by using heat, pressure and a fluidizing agent. The produced syngas can be applied for electricity generation or synthetic fuel production via Fischer-Tropsch, ammonia or synthetic natural gas.

A gasifier can be described to consist of three successive steps: drying, pyrolysis and gasification. Drying is part of the pre-treatment of the biomass, along with screening, size reduction, magnetic separation and wet/dry storage. The drying phase heats up the biomass and causes the moisture to evaporate. Biomass mostly contains a certain amount of moisture that affects the performance negatively downstream. Algae for example can contain up to 40% moisture, while wood pellets or shreds are usually below 20% [114]. An upstream dryer is a pre-processing step of biomass that lowers the moisture content usually to <10%. This step is only required when the moisture content of biomass is above this 10% and mostly >20%. Every kilogram of moisture needs 2260 kJ to evaporate from the biomass [114]. Steam drying is preferred since the FT process produces low-quality steam that can be applied in the dryer [124].

The pyrolysis part of the gasification converts the biomass, according to the devolatilization reaction (R1) from Table 2.6, into gases, char and liquids. This will reach the gasification part where the main gasification reactions R2-R9 from Table 2.6 take place in the presence of a fluidizing medium. Partial oxidation reactions (PO1-PO3) occur when oxygen is present in the gasifier and tars will be converted according to Rtar-Rtar4. But the product gas composition strongly depend on the biomass composition (Table 2.7), operating conditions, reactor type, fluidizing medium and bed materials [76]. The temperature inside the gasifier depends on the feedstock and type of reactor. For woody biomass the operating temperature is usually $850 - 950°C$, while coal gasification operates at around $1000°C$. Defining the most appropriate temperature is important to achieve a high syngas yield and low tar production. The pressure of the gasifier will be similar to the Fischer-Tropsch reactor, 20-30 bar, but can work up to 40 bar.

The most well known reactors for gasification of biomass are fixed bed reactor, fluidized bed reactor and entrained flow gasifier. Plasma and unique gasifiers are also types of gasifiers but require more research before commercialization. Fixed bed are the simplest and most robust gasifiers predominantly used for small scale installations. The two types of fixed bed gasifiers are updraft and downdraft reactors. Their names are based on the flow direction, counter- or co-current, of the fuel and oxidant. Updraft gasifiers achieve a high thermal efficiency and perform better at high moisture biomass, such as residual waste. A disadvantage is the higher tar content which requires more gas cleaning afterwards. Downdraft gasifiers on the other hand produce less tar and the gas and fuel flow in similar direction. Scaling-up the downdraft gasifier is limited by the size of the throat, causing it unsuitable for large-scale plants.

Entrained flow gasifiers reach high temperatures which results in shorter life of components but can reach high carbon conversion and is suitable for large scale capacities such as fluidized bed. The high temperature makes it possible to get close to the equilibrium composition and consequently to a high

Table 2.6: List of gasification reactions [10] [48] [76] [91] [95]

Number	Name	Reaction	ΔH [kJ/mol]
R1	Devolatilization	Biomass → $Volatiles + C + Ash$	> 0
R2	Partial combustion	C + 0.5O_2 → CO	-111
R3	Complete combustion	C + O_2 → CO_2	-394
R4	Boudouard	C+CO_2 → $2CO$	172
R5	H_2O gasification	C + H_2O → $CO + H_2$	131
R6	CO oxidation	CO + 0.5 O_2 → CO_2	-283
R7	H_2 oxidation	$H_2 + 0.5O_2$ → H_2O	-242
R8	Water gas shift	CO + H_2O ↔ $CO_2 + H_2$	-41
R9	Steam methane reforming	$CH_4 + H_2O$ ↔ $CO + 3H_2$	206
	Partial oxidation reactions		
PO1	Methane	$CH_4 + 0.5O_2$ → $CO + 2H_2$	
PO2	Benzene	$C_6H_6 + 4.5O_2$ → $6CO + 3H_2O$	
PO3	Phenol	$C_6H_6O + 4O_2$ → $6CO + 3H_2O$	
	Tar conversion reactions		
Rtar1	Benzene	$C_6H_6 + H_2O$ → $3C + 2CH_4 + CO$	
Rtar2	Phenol	C_6H_6O → $CO + 0.4C_{10}H_8 + 0.15C_6H_6 + 0.1CH_4 + 0.75H_2$	
Rtar3	Toluene	$C_7H_8 + H_2$ → $C_6H_6 + CH_4$	
Rtar4	Naphthalene	$C_{10}H_8$ → $9C + 1/6C_6H_6 + 3.5H_2$	

Table 2.7: Proximate and ultimate analysis of two different types of biomass

	Wood pellets [3]	Wood chips [54]
Proximate analysis (wt % dry basis)		
Volatile matter	81.49	80
Fixed carbon	18.01	18.84
Ash	0.50	1.16
Moisture content (wt %)	8.70	20
Ultimate analysis		
Carbon, C	45.79	51.19
Hydrogen, H	5.54	6.08
Oxygen, O	39.43	41.3
Nitrogen, N	0.08	0.2
Sulfur, S	0.01	0.02
Chlorine, Cl	0	0.05
Net caloric value (dry basis) (LHV) [MJ/kg]	18.61	19.09

syngas quality. But entrained flow gasifiers are more known in the coal industry. Coal can be easily crushed into smaller particles, which is harder to achieve with biomass. Reaching the preferred particle size for biomass is a high energy intensive process.

Fluidized bed gasifiers can work with flexible fuel and load and reaches high heat transfer. An advantage of this reactor is that it can operate under pressurized conditions. This makes it very suitable for processes that work above atmospheric pressure, such as FT. A fuel conversion of $85 - 95\%$ can be reached, which is comparable with a fixed bed downdraft gasifier. The reactors are divided into circulating fluidized bed (CFB) and bubbling fluidized bed (BFB), where a CFB works with high gas velocities and BFB with low. Both have an operating temperature which is limited to $800 - 900°C$ to prevent melting of the bed material, although the feedstock conversion rate is usually high. But a catalyst is required to reach the equilibrium of the gasification reactions. The lower temperature and also short residence times result in the existence of methane and tar. The geometry and mixing properties makes this reactor type very suitable for scaling up. Siedlecki [113] made a brief overview of the differences between a CFB and BFB for an industrial plant (Figure 2.7).

Considering the heat supply for the reactor, the fluidized beds can be divided into direct and indirect

Property	BFB	CFB
fluidization regime	bubbling bed	fast bed
mixing	very good	excellent
solids feed flexibility (size)	fines not desirable	fine & coarse material
tar yield (g m_n^{-3})	avg.: 12 (moderate)	avg.: 8 (lower than BFB)
carbon conversion (%)	lower than CFB	typically 88–96
carbon loss by entrainment	significant	low
particle concentration in the gas (g m_n^{-3})	average: 4	average: 20
bed height / fuel burning zone (m)	1–2	10–30
therm. throughput (MW m^{-2})	1.2–1.6	5–7
process control	less complex	more complex
scale-up potential	good	very good

Figure 2.7: Overview of differences between industrial scale BFB and CFB [113]

heating. Indirect heating separates the gasification and combustion stage in two different parts. The heat delivered to the gasifier is produced in the combustion chamber, where steam is usually used as fluidizing agent. This method of heating produces a higher hydrogen content and lower CO_2 fraction, but more methane. It seems that this process is most likely for substitute (synthetic) natural gas. Some well-known indirect heated CFB concepts are the Pyrox process, MILENA gasifier from ECN, Battelle's Silvagas process and a by TU Vienna developed Fast Internally Circulating Fluidized Bed (FICFB) (Figure 2.9) [83].

The Pyrox process was the first developed method in 1970's originally from Japan, targeted for solid waste material gasification. A commercial scale plant operated 8 years, built in 1983, with a capacity of 450 t/d using municipal solid waste (MSW). In Woodland, California a pilot plant with a capacity of 5 t/d for wood pellets is commissioned.

MILENA operates in CFB mode surrounded by a BFB combustor with it's first lab-scale plant in 2004. Plans and research studies have been done for large scale (12 MW_{th}) plants in recent years.

The Battelle's Silvagas process had an operating plant from 1997-2001 using wood pellets with a fuel use up to 350 t/d [83].

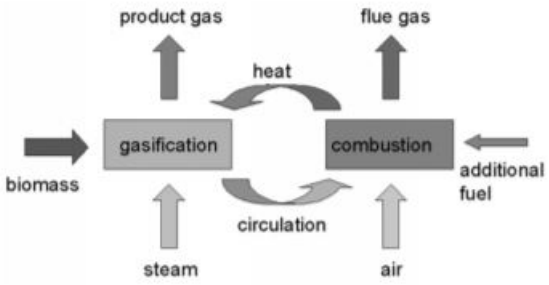

Figure 2.8: Principle of FICFB gasification process [55]

FICFB has been invented in late 1990's and resulted in several plants, from which a 32 MW_{th} unit in Gothenburg, Sweden, is the biggest [83]. It has a quite similar technology as the MILENA gasifier, except that the gasification reactor is a BFB instead of CFB. Steam is used as fluidizing agent and the operating temperature is maintained between $850 - 900°C$, while the combustor operates at a slightly higher temperature $(950 - 1000°C)$. An overview of the FICFB principle is shown in Figure 2.9.

Direct heating (Figure 2.9a) on the other hand heats up the feed stream inside the gasifier. Oxygen is supplied to the gasifier to balance the heat of combustion of the oxidation reactions. Here it becomes inevitable that some fraction of the product gas will also be combusted. This is one of the reasons why indirect heating has been invented, to avoid combustion of product gas. The fluidizing agent consists of a mixture of steam and air/oxygen [113].

Siedlecki [113] did extensive research on CFB gasification with wood pellets. Multiple bed materials, such as sand, olivine and magnesite, have been tested from which magnesite showed the highest H_2/CO ratio (1.7-2.7). Bed material is mainly used for heat storage and heat transfer between the

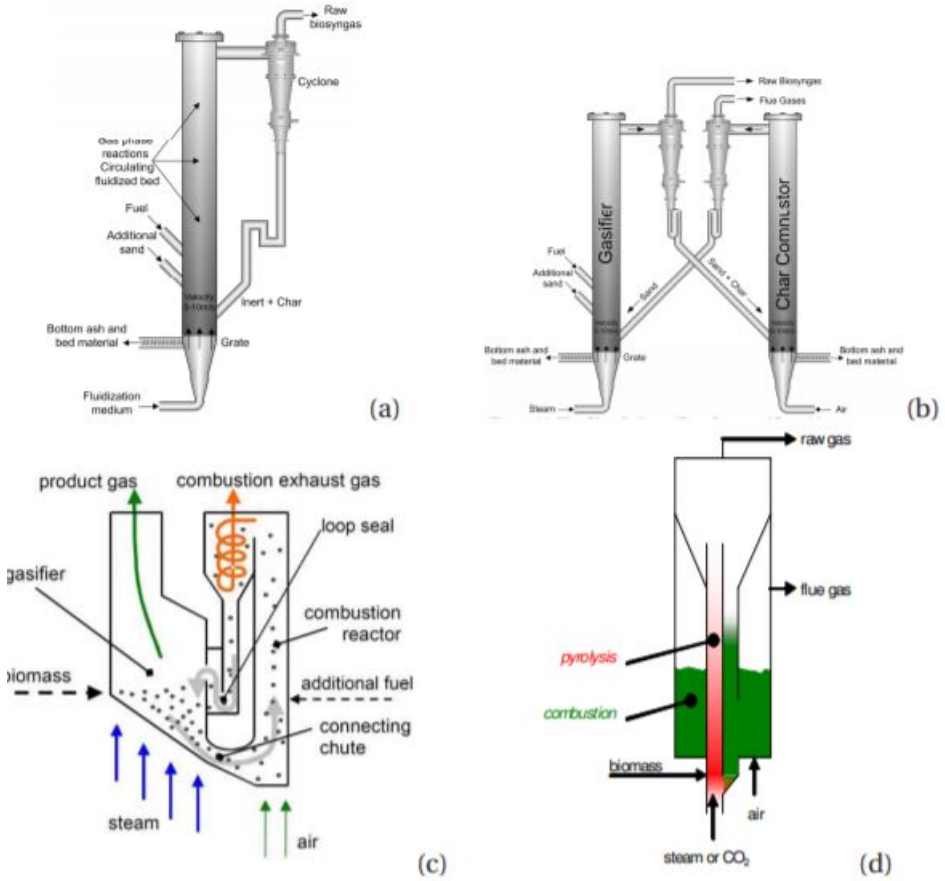

Figure 2.9: Four CFB gasifiers a) directly heated; b) indirectly heated duel CFB, Battelle; c) indirectly heated FICFB, TU Vienna; d) indirectly heated MILENA, ECN [113]

particles undergoing endothermic and exothermic processes. Heat is stored in the bed material and transferred to processes that require heat by intense mixing of the bed inventory. Usually bed material remains inert as quartz sand is normally applied. But some types of bed material may have a significant impact on the process. Causing catalytic activity on some involved reactions or interaction with fuel constituents and changing the physical properties. Higher activity for ongoing reactions mostly result in higher tar conversion rates and improved gas quality. The change in physical properties, on the other hand, can cause bed agglomeration which is highly undesirable. But materials can also absorb components, for example CO_2, affecting the H_2/CO ratio and CO_2 emission from the gasifier. Main problems with bed materials are the high costs, low attrition resistance and continuous deterioration of their mechanical strength over the reaction time.

Another direct heated gasifier is built by the Institute of Gas Technology (IGT) and operates under pressurized conditions. It produces medium calorific gas, broad range of H_2/CO ratio and is oxygen fired, causing no nitrogen pollution [52]. A pressurized IGT demonstration plant built in 1991 designed for 70 ton/day of sugarcane is located in Hawaii [67].

Air, CO_2, steam or a steam-oxygen mixture can function as medium in the fluidized bed reactors. Air is the most common fluidization medium but comes with nitrogen which dilutes the syngas. But the MILENA and FICFB gasifiers use air while producing a product stream with essentially zero nitrogen. Gasification by steam is endothermic and is very energy intensive, but the heat produced in a FT reactor or other exothermic processes can be used to saturate H_2O. Steam is often preferred since it produces syngas with higher hydrogen content, maximizes the heating value and has efficient tar and char reduction [87]. The optimum conditions for steam to biomass ratio (SBR) and equivalence ratio (ER) depends on the type of gasifier used. The equivalence ratio (ER) and steam-to-biomass ratio (SBR) can be defined according to Equation 2.14 and Equation 2.15.

$$ER = \frac{external\ O_2\ supply/fuel\ supply\ (d.a.f.)}{stoichiometric\ O_2\ requirement/unit\ of\ fuel\ input\ (d.a.f.)} \tag{2.14}$$

$$SBR = \frac{steam\ mass\ flow}{biomass\ feed\ flow} \tag{2.15}$$

The oxygen can be supplied by the system itself, although an oxygen quality of at least 90 mol% is required [111]. The electrolysis of water by the PEM electrolyzer produces very pure oxygen that can easily meet the conditions. One drawback is the required oxygen storage. Oxygen production is high when biomass gasification will be low, and vice-versa. Which means that oxygen required for the gasifier is needed when PEM electrolysis produces small amounts of oxygen.

There are several methods to store oxygen. If oxygen is cooled below boiling point $(-183°C)$, it will become liquid. Liquid oxygen, abbreviated to LOX, is less difficult to transport and store than gaseous oxygen. Another method is storing oxygen under high pressure in tanks, but this is more bulky and costly [36].

2.3.2. Gas conditioning

The produced raw syngas by the gasification reactor requires gas conditioning to reach clean enough syngas for the FT reactor. Gas conditioning extrudes components from the raw syngas before it can be fed to the FT reactor, such as particulate matters, tar, water, H_2S, NH_3 and halides [124]. Maximum allowable quantities of these contaminants can be found in table 2.8.

Table 2.8: Maximum allowable contaminants in FT synthesis [114]

Contaminant	Maximum allowable [μ L/L]
Particulate matter	0
Condensable tars	< 0.01
Tars (heteroatoms)	< 1
Alkali	< 0.01
NH_3	< 0.02
H_2S	< 0.01
Halides (HCl)	< 0.01

Particulate matters consist of ash and unconverted carbonaceous materials and are inevitable produced by gasification. The amount of particles is strongly determined by the gasifier design. Removal is essential because it affects processes downstream and exceed the emission limit of environmental regulation if it remains in the flue gas. Gas turbines and combustion engines accept small particle concentrations, but for Fischer-Tropsch synthesis complete separation is required. Commonly a cyclone separator with a bag filter or scrubber is applied to remove >99.9% of particulates [12] [124].

Tar is a dark brown or black viscous liquid of hydrocarbons and free carbon. It is an undesirable mixture and consists of condensable hydrocarbons and aromatic compounds up to five rings. It can be removed within the gasifier or in the post-treatment, which is less economically attractive. The tar content depends on the the type of gasifier, but higher temperature (above $800°C$) usually results in lower tar contents [38]. Same result is observed with increased pressure. On the other hand, tar content increased when steam is used as agent instead of air due to lower gasification temperature.

Tars can clog equipment, lower syngas quality and deactivate catalysts downstream. Therefore tar removal is important right after the gasification to prevent damage downstream. Tars can be cracked by non-thermal plasma, elevated temperature or catalysts. Thermal decomposition operates at temperatures of 1100 till $1300°C$ and is simple and effective, but expensive due to high energy demands. Alternatively, a water scrubber can be used as post-treatment to decrease the tar and contaminant content in the raw syngas [99], although water scrubbing only reaches a tar removal efficiency of only 30%. But an oil scrubber can reach an efficiency of around 80-98% [25] [122]. Vegetable and canola oil are regularly used for oil scrubbing, otherwise fossil oil is an option. ECN patented an oil-based gas washer, OLGA, that focused on the tar behavior instead of tar content. The liquid tar is collected by cooling $(320 - 340°C)$ the product gas inside the scrubber. But the inlet and outlet temperature of the cooler should be high $(> 400°C)$ to minimise tar condensation and fouling. To prevent water formation, temperature of the oil scrubber may not decrease below dew point [21].

Catalyst deformation in scrubbing takes place at relatively low temperatures. Ni-catalysts are mainly employed commercially, but suffers from sintering and coking. Plasmas are very effective, but due to high energy requirements and operating intricacies not used in large-scale facilities.

Wet scrubbing is a cold gas cleaning technique where also a fraction of tar is absorbed in water. This method is attractive in the context of efficiency and costs, but the waste-water cleaning can be challenging. Cold gas cleaning removes besides tar also alkali, chlorine and PM. Alkali can also be extracted by condensation, but adsorption has a higher capacity and operates at almost all temperatures.

Catalysts for tar are also useful to crack ammonia and operate at $500°C$, but elevated temperatures of $700 - 800°C$ are recommended to prevent coking. Thereafter, ammonia removal happens by absorption in water.

Sulfur can be removed by high and low temperature technologies. High temperature makes use of physical or chemical adsorption, whereby metal oxides are the most promising sorbents. Low temper-

ature is based on chemical absorption, physical absorption, or a combination of both processes. Commercially applied physical absorption methods are Selexol, Rectisol and Purisol. Selexol and Purisol both show high solubility for H_2S and may be applied for combined H_2S and CO_2 removal. Rectisol on the other hand uses chilled methanol as physical solvent which shows high removal efficiency for H_2S and CO_2, making it suitable for Fischer-Tropsch process. Relative solubility's of chilled methanol can be found in Appendix A. But the operating temperature is a downside of the process, requiring expensive and complicated cryogenic process stages [123]. Amines can be used as solvent with an absorber/stripper column to extract H_2S as well as CO_2 from the raw syngas stream [90]. The appropriate method is determined according to the partial pressures in the feed and product stream [120] (Figure 2.10).

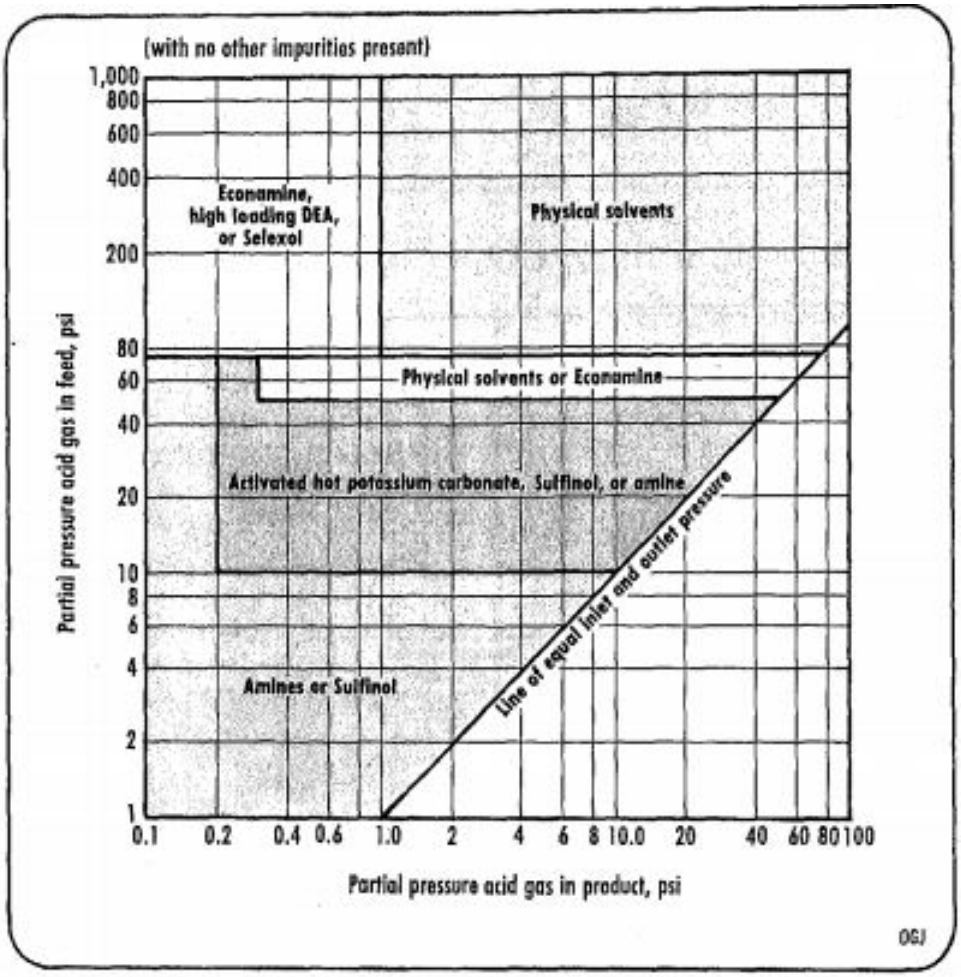

Figure 2.10: Appropriate method for simultaneous removal of H_2S and CO_2 [120]

At last, a sorption enhanced water gas shift reactor (SEWGS) can be used to obtain the desired H_2/CO ratio for FT. The SEWGS is basically the water gas shift reaction (R8 from Table 2.6) and operates at around $200 - 300°C$. The SEWGS Reaction 2.16 is an equilibrium reaction where H_2O or CO_2 can be added to adjust the H_2/CO ratio [64].

$$CO + H_2O \leftrightarrow H_2 + CO_2 \; \Delta H^0_{298} = -41kJ/mol \tag{2.16}$$

The syngas is converted into hydrocarbons with different lengths, water and unconverted syngas by the FT reactor. Several components will be removed from the stream before fed to the distillation column. This can be done in a decanter. Small hydrocarbons $(C_1 - C_5)$ are separated by a flash separator and can be recycled to a steam reformer.

Currently hydrogen production is for 95% based on fossil fuels, mostly by steam reforming (SMR) of natural gas. SMR converts methane (CH_4) and other small hydrocarbons (Reaction 2.17) in the

presence of steam/water into hydrogen, CO and CO_2 over a nickel catalyst according to the endothermic reaction R9 from Table 2.6. This operates at a pressure of 20-30 bar and temperature around $850°C$ with a steam to methane ratio around 2.5-5 [64]. Average conversion rates of 74-85% are achieved, whereby higher conversion rates are reached in large-scale SMR plants [100].

$$C_nH_{2n+2} + nH_2O \rightarrow nCO + (2n+1)H_2 \tag{2.17}$$

Autothermal reforming (ATR) is another method to convert methane into syngas in presence of steam by Reaction 2.18. It operates at a relatively high temperature of $950 - 1050°C$ and pressure 30-50 bar.

$$2CH_4 + O_2 + CO_2 \rightarrow 3H_2 + 3CO + H_2O \tag{2.18}$$

ATR has a higher methane conversion than SMR and corresponds better with the H_2/CO ratio of Co-based and Fe-based catalysts. Therefore ATR is used for methanol synthesis and production of higher molecular-weight hydrocarbons via FT process. Secondly, the H_2/CO ratio can be varied which makes it suitable for second generation fuels. On contrary, pure oxygen is required in a 0.55-0.6 oxygen/hydrocarbon ratio. Figure 2.11 illustrates the conversion rate with varying aforementioned parameters [31].

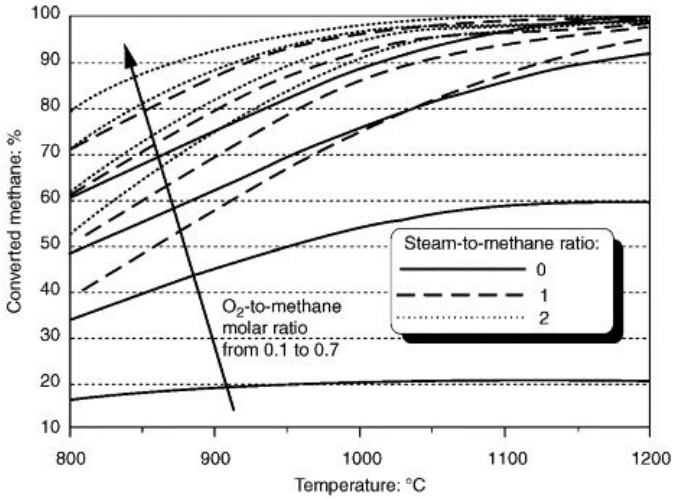

Figure 2.11: Theoretically calculated fraction of methane that is converted in an autothermal reformer as a function of temperature, $O_2 - to - methane$ ratio and steam-methane ratio at 40 bar [31]

2.4. Distillation

The residual stream with long hydrocarbon chains (C_{5+}) is fed to the distillation column. The column is used to retrieve the different fractions, such as gasoline $(C_4 - C_{10})$, diesel $(C_{11} - C_{22})$, waxes (C_{22+}) and the preferred kerosene $(C_9 - C_{15})$. The number of stages and reflux ratio can be estimated according to the Winn-Underwood-Gillilind, which is based on volatilities. While the feed tray can be determined with Kirkbride's method [18]. The pressure inside the column can be assumed constant if it's not a vacuum column where pressure at the top and bottom are significantly different.

Kerosene roughly consists of hydrocarbons and is referred to as middle distillate. Other fractions like gasoline and diesel might be useful for other applications on the airport. Waxes, light hydrocarbons and other fractions can be converted into kerosene by different processes. Waxes can be cracked by thermal or catalytic cracking. Catalytic cracking takes place at high temperature and relatively low pressure in the presence of a catalyst. Thermal hydrocracking on the other hand takes place at high temperature and pressure with hydrogen. But this method is energy intensive and requires specialized machinery [92]. A purge stream is required to prevent accumulation of unreacted components.

Leckel [68] has done extensive research on the performance of the Sasol iron-catalyzed hydrocracker to predominantly produce diesel. Although diesel is slightly different from kerosene, much hydrocarbons can be equally in both fuels. Table 2.9 provides the yield and selectivity for a hydrocracker operating at 35 bar and 360 $^\circ C$ with a wax conversion rate of 84%. A higher pressure results in a higher diesel/naphtha ratio but decreases the wax conversion.

Table 2.9: Selectivity and yield rates of an iron catalyst hydrocracker (35 bar, 360 $^\circ C$, 84 wt.% wax conversion, hydrogen/wax ratio of 1500/1 L_n/L)[68]

	Selectivity (wt.%)	Yield (wt.%)
C1-C4	10	11
C5-C9	15	13
C10-C22	75	63
C23+	-	13

Lower chains $(C_6 - C_8)$ can be upgraded till kerosene by alkylation or oligomerization or used as gasoline. Upgrading is not necessarily required since gasoline is also widely used on airports for other forms of transports, the same holds for diesel. Therefore only waxes and $C_1 - C_5$ will be recycled to optimise kerosene production.

3

Model development

In this chapter the model is described and validated. Aspen Plus is the simulation program used for this study, as explained in Section 3.1. Previous relevant literature making use of Aspen Plus is discussed and model assumptions are given. Section 3.2 describes the components present in the model. At first, for each part a theoretical foundation is given for the decisions made based on the literature study. Secondly, the schematic of the part developed in Aspen Plus is explained. Validation of gasification, tar removal and H_2S/CO_2 removal takes place in Section 3.3 to justify the validity of the model.

3.1. Methodology and model assumptions

For this study, Aspen Plus version 8 is used to model the synthetic kerosene production process. Aspen Plus simulates chemical processes in steady state where reactors, compressors, pumps etc. are modelled as unit operation blocks. Materials, process conditions and energy streams are used to perform simulations and calculate optimum conditions and specifications for the unit blocks. Most calculations were made according to the Peng-Robinson Equation of State (EoS) (Equations 3.1-3.3), which is recommended when working with hydrocarbons and high pressure. For several components in the process it is recommended to apply other EoS. But this will be discussed during model setup in Section 3.2.

$$P = \frac{RT}{v-b} - \frac{\alpha a}{v^2 + 2bv - b^2} \tag{3.1}$$

$$a = 0.45723553\frac{R^2T_c^2}{P_c} \; b = 0.07779607\frac{RT_c}{P_c} \tag{3.2}$$

$$\alpha = [1 + \kappa(1 - \sqrt{\frac{T}{T_c}})]^2 \tag{3.3}$$

Several research studies have made use of Aspen Plus that are partially related to this research study. Han et al. (2017) [53] modelled a downdraft biomass gasifier to produce syngas with hardwood chips by Aspen Plus. Another Aspen Plus model that produces syngas by biomass gasification is done by Yahya and Gambardella (2017) [132]. Tijmensen et al. (2002) [124], Navas-Anguita et al.(2019) [85] and Campanario and Gutiérrez Ortiz (2017) [26] modelled the production of syngas via biomass as well, but in a more comprehensive way including the eventual synthetic fuels. Er-rbib et al. (2012) [42] has produced synthetic fuels by dry reforming of methane using Aspen Plus.

Electrochemical cells, such as PEM or AEC, are not readily available as operation block in Aspen Plus. Only a custom cell stack is available. Sánchez et al. (2020) [106] developed an Aspen Plus model that simulates an AEC plant.

The intermittent electricity supply turns the problem into a dynamic problem, but this research study will be focusing on the extreme situations in steady state. The dynamic behavior is more important in

shorter time periods than discussed in this study. Time frames of a day or shorter will require dynamic analyses while this study focuses on the longer frames where steady state analyses gives a satisfactory result. Performing dynamic analyses will be a recommendation for further research.
Some assumption will be made due to modelling limitations and to finish the study within prescribed time, these are listed below:

- The process is assumed to run on steady state operation.
- Particle size distributions of biomass and other components is not considered.
- Biomass is assumed to be free of ash
- Char resulting from pyrolysis is simulated as pure carbon (graphite).
- Tars are simulated as four compounds, benzene, phenol, toluene and naphtalene.
- The pressure drops are assumed to be zero for the components unless mentioned otherwise.
- Enthalpy and specific heats of biomass are calculated by Aspen Plus, where biomass is modeled as a non-conventional solid.
- CO_2 capture (DAC) in-depth research will not be done in this report. Available reports will be used to determine the operating parameters and cost analysis. But a further study does not fit in the scope of this project.
- Water fed to the system is assumed to reach the required specifications when it arrives, except from temperature and pressure. Doing research on pollution in rivers, canals and seawater nearby Rotterdam and consequently the required cleaning methods lies beyond the scope of the project. Excluding the recycled water from within the system, here required upgrading steps will be integrated to meet the electrolyzer specifications.
- Electricity will be completely supplied by the connected solar panels and wind turbines. Low electricity production does not result in electricity supply by the grid but a lower production of hydrogen by the electrolyzer and an increasing syngas production by biomass gasification.
- The electricity grid of the airport will always assumed to be stable.

The model (Figure 3.1) will be a combination of two separate ways to produce synthetic kerosene. The part from the Fischer-Tropsch reactor and further downstream including distillation is equal for both parts. So the model can be subdivided into three different parts. The two different pathways, (1) DAC with water electrolysis and (2) biomass gasification, till the Fischer-Tropsch reactor and (3) from the FT reactor further downstream. At first, the two pathways will be built separately where one pathway includes part 3. When both models show adequate results, they will be merged. Recycle streams and a heat integration network is possible if the three parts are connected, because of interconnecting streams.

The incoming streams, (1) H_2O, (2) air/CO_2 and (3) biomass (wood pellets), depend on the 2 described scenarios. An overview of the complete process developed in Aspen Plus can be found in Appendix B. Section 3.2 will briefly discuss and elaborate each operation block.

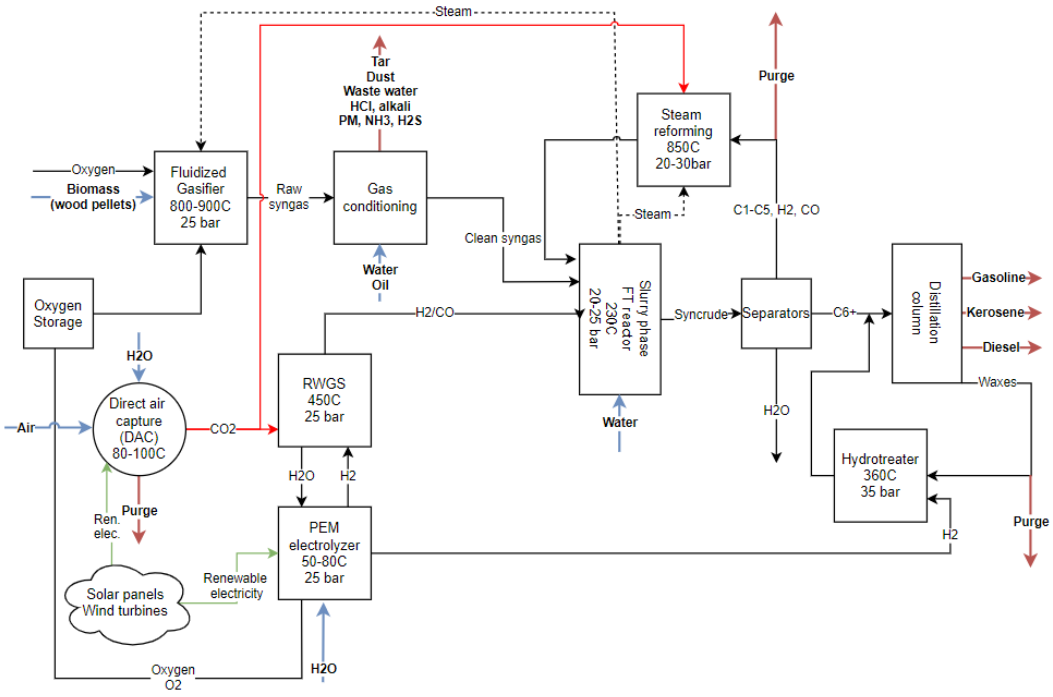

Figure 3.1: Block diagram of the combined system of synthetic kerosene production. Blue lines are inlet streams, red lines are outlet streams.

3.2. Model setup

3.2.1. PEM electrolyzer

Hydrogen is a key component in the system and can be produced by water electrolysis. The endothermic Reaction 2.1 requires heat and electricity to convert H_2O into H_2 and O_2. Different electrolyzers are available, where current density, (future) capital costs, gas purity, respond rate and dynamic range are parameters to take into account. Table 2.1 shows the specification for the most used type of electrolyzers, AEC, PEM, SOEC and AEM. From which AEM is not a commercial option yet, since more research is required [88].

Because renewable energy will meet the electricity supply, an electrolyzer has to operate under varying conditions. AEC and PEM can lower their production to approximately 10%, while SOEC requires at least 30%. Together with a high capital cost, high operating temperature and smaller stack lifetime makes SOEC less attractive than AEC and PEM.

Both, AEC and PEM, have similar operating conditions, although AEC has a higher production rate, longer stack lifetime and slightly lower capital cost. On the other hand, PEM can operate below 10% of nominal production and reaches a faster respond rate.

To conclude, PEM electrolyzer has an advantage over the AEC electrolyzer because a lower dynamic range in combination with fast respond rate is advantageous with intermittent electricity supply. Therefore the PEM electrolyzer will be applied in this study.

Schematic electrolyzer

Modelling an electrolyzer in Aspen Plus is a combination of multiple operation blocks (Figure 3.2). At first, a H_2O feedstream at atmospheric pressure and $22°C$ will increase to operating pressure (25 bar) through a pump PUMP-H2O, where all pumps have an efficiency of 75%. A pressure of 25 bar is chosen because the FT-reactor downstream operates between 20-25 bar. It is therefore convenient to maintain the same pressure throughout the system to optimise the energy balance. A Fortran calculator block H2O-IN determines the desired H_2O feedstream H2OIN, based on the H_2O recycle streams. Fortran is a programming language especially suited to numeric computation and scientific computing.

Recycled H_2O is mixed with the feedstream in MIX-H2O and send to the first heat exchanger HX1-

PEM and thereafter to a second heat exchanger HX2-PEM. These heat exchangers increase the inlet temperature and decrease the outlet temperature of the electrolyzer to optimise the energy balance. A RGibbs PEMREA simulates the membrane, where Reaction 2.1 takes place. The chemical equilibrium is restricted to a predefined molar outflow, depending on the scenario.

The outflow contains a mixture of predominantly H_2O, O_2 and H_2, while in reality O_2 and H_2 will never collide in an electrolyzer. A separator H2O2-SEP will perfectly separate the O_2 from H_2, where unreacted H_2O is evenly distributed between both outlets. The outlet containing O_2 will flow through HX1-PEM to a flash separator O2H2O-FL. Similarly, H_2 outlet stream passes through HX2-PEM and be fed to a flash separator H2H2O-FL. Both flash separators separate H_2O from O_2 or H_2, after which the H_2O stream is recycled. No purge stream is necessary since inerts can not accumulate in the electrolyzer. A pressure drop will take place inside the heat exchangers, even as other heat exchangers in the model. Pressure drops in HXs depend on the stream pressure, $\Delta P = 0.5$ bar for p>30 bar, $\Delta P = 0.3$ bar for 10>p<30, $\Delta P = 0.2$ bar for p<10 bar [124].

Produced oxygen will function as gasifying medium in the biomass gasifier. In reality, an oxygen storage tank will capture the O_2 and feed it to the gasifier when necessary. But since Aspen Plus is a steady state program, storage is not included in the model.

Required electricity for the stack is calculated in an external file and will not be integrated in the Aspen Plus model.

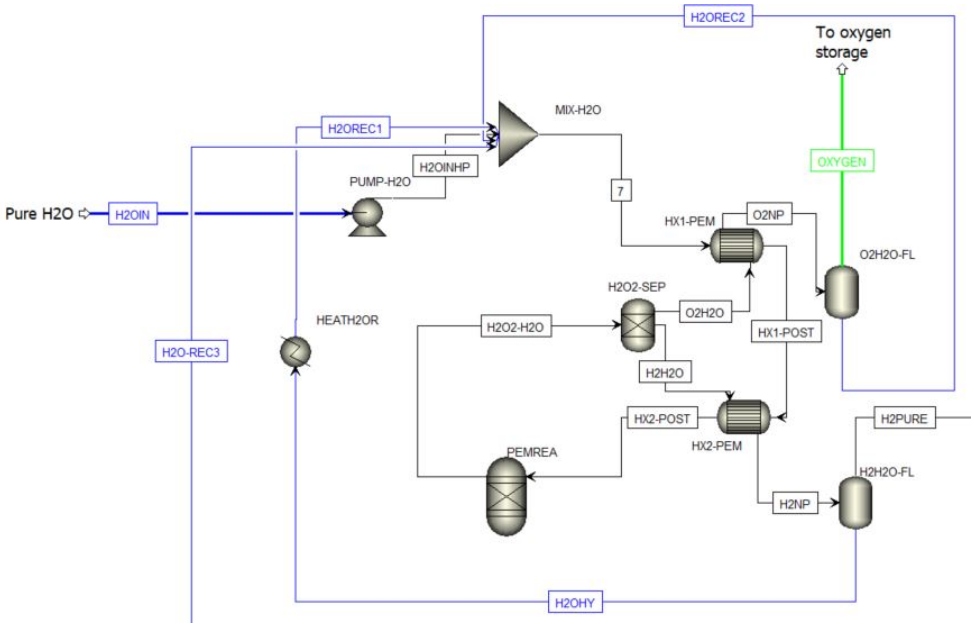

Figure 3.2: Schematic of the PEM electrolyzer developed in Aspen Plus

3.2.2. RWGS reactor

CO is besides H_2 the other building block for synthesis gas. CO will be produced according to Reaction 2.4, where the required CO_2 is obtained from the DAC plant. The modelling of the DAC unit is beyond the scope of this study and hence not included in the Aspen Plus model. Economical and technical parameters required for mass and energy balances as well as cost analysis will be retrieved from literature data. The CO_2 feedstream will arrive in the system with operating conditions similar as the DAC outlet mentioned in Table 2.2.

High temperatures, $800-900°C$, are usually required to obtain a high CO_2 conversion. Same conversion rates can occur at lower temperatures, around $450°C$, by making use of a catalyst. Copper-based catalyst show high stability under high CO_2 concentrations and the performance can be improved by variations of copper-catalysts. Elsernagawy et al. [41] conducted an extensive research on the reverse water-gas shift process and choose the copper-based catalyst $(Cu-ZnO/Al_2O_3)$ for the reactor. Optimal CO selectivity and CO_2 conversion of 94.7% was reported for a setup with H_2/CO_2 ratio of 3:1 and

operating at 10 bar and $450°C$. Increased pressure resulted in slightly lower conversion rates (91-94%), same holds for lower temperatures.

Schematic RWGS

The RWGS is modelled as RGIBBS reactor operating at 25 bar, equal to the pressures from up- and downstream equipment. Temperature is maintained at $450°C$, increasing the temperature to $500°C$ leads to insignificant increase of conversion. CO_2 is obtained from the DAC unit and enters the model at a temperature of $100°C$ and 0.2 bar, as shown in Table 2.2. A multistage compressor DAC-MCOM will increase the pressure to 25 bar, equivalent to the pressures of RWGS and SMR respectively. It contains 5 stages with a cooler placed on the first stage and a specified outlet temperature of $100°C$ [78]. The resulting pressurized CO_2 stream is split in DAC-SPL before it continues to the two reactors.

H_2 enters the RWGS directly after it is produced in the electrolyzer. A Fortran subroutine RWGSCALC regulates the inlet flows to reach the desired H_2/CO_2 ratio of 3:1. In addition, a CO_2 conversion of 91.7% (obtained from [41]) is assumed for the RWGS Reaction 2.4.

The product stream contains besides syngas also a large H_2O fraction. H_2O can result in unacceptable catalyst deactivation in the Fischer-Tropsch reactor and should therefore be separated from the stream. A Flash separator RWGS-FLS operating at 25 bar and $75°C$ separates 95% of H_2O from the stream. The resulting stream will be mixed in FT-MIX with the syngas streams from biomass gasification and the SMR before fed to the FT reactor.

3.2.3. FT reactor

The FT process is an essential part of this study. Syngas is converted into an intermediate product for liquid fuels, known as syncrude. Paraffins are preferred for kerosene production, hence LTFT is chosen due to higher paraffin production than HTFT [110]. The syncrude composition after the FT reactor can be found in Table 2.3. Carbon number distribution for paraffins and olefins is determined according to Reaction 2.13 from ASF. Typical α-values for synthetic fuel production are 0.70-0.90. For optimal kerosene production Tijmensen et al. [124] reported an α of 0.85.

Adding the right catalyst is important to reach a high performance. Ru, Ni, ThO_2, Fe and Co are the best known catalyst (carriers), from which Fe and Co are the only industrially applied. Fe-based catalysts offers high activity, low cost, easy access and flexible operating conditions for high and low temperature.

Co-based catalysts are more relevant for middle distillate and heavy waxes production. Mainly paraffins are produced with small fractions of alcohols and olefins. This makes Co-based catalysts more attractive for kerosene production. To take into account, Co-based catalyst show best performance in H_2 rich syngas $(H_2/CO) = 2$ and are best suited for less severe conditions. Therefore gas cleaning, especially from biomass gasification, becomes more necessary. At last, cobalt-catalysts are applied in the most relevant FT plants of today by Sasol and Shell [110].

Four types of reactors are described in Section 2.2.3, from which multi-tubular fixed bed and fixed slurry bed are the only possible options for LTFT. A multi-tubular fixed bed reactor offers a maximum production of roughly 3000-4500 barrels per day, but faces a high pressure drop in large reactors. Fixed slurry phase reactors on the other hand are much easier to fabricate and causes a lower pressure drop. But above all, slurry bed offers a 25% higher cost efficiency and can reach a total production of 20.000 barrels per day [40]. To conclude, slurry phase reactor has significant process and economic advantages over fixed bed reactor and is therefore more attractive to implement in this model.

Schematic FT reactor

The reactor block to model the FT reactor in Aspen Plus is a stoichimetric reactor FT-REAC (Figure 3.3). Temperature inside the reactor is assumed to maintain at $230°C$ with a pressure of 25 bar. One reaction for every syncrude component is added to the FT-REAC, where an external Excel file calculates the fractional conversion of CO for each reaction. Highest yield is achieved for syngas conversion of 80% [93], so only 80% of the incoming CO will be converted. Table 3.1 compares the syncrude composition of the Aspen Plus model with literature data.

The property method Redlich-Kwong-Soave (RKS) is applied for the FT reactor. LTFT process produces hydrocarbon mixtures and light chemical species that involves vapour-liquid multi-component stream [110].

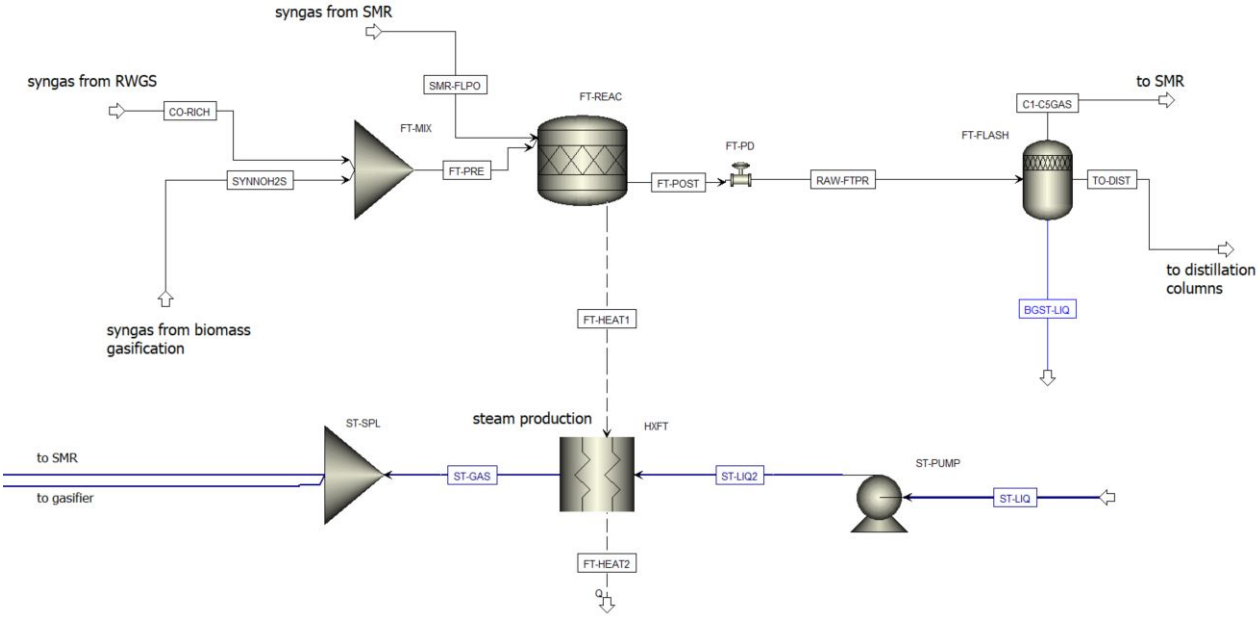

Figure 3.3: Schematic of the FT reactor with steam production developed in Aspen Plus

Table 3.1: Syncrude components for Aspen Plus model in mass %

Fraction	Components	Literature [110]	Aspen Plus model
Paraffins	$C_1 - C_{60}(C_nH_{2n+2})$	Major product	72.1%
Olefins	$C_1 - C_{60}(C_nH_{2n})$	>10%	11.3%
Oxygenates	CH_2O, CH_3OH	5-15%	14.6%
Aromatics	Benzene, Toluene, Xylene	<1%	0.6%
Naphthenes	Cyclopentane, Cyclohexane	>1%	1.4%

A valve right after the FT reactor simulates the pressure drop of 5 bar [124] taking place inside the FT reactor, since there is no option to model the pressure drop inside the RStoic. The exothermic reactions of the FT process produce significant amounts of heat. Water, separated from the syncrude in a FT-FLASH, will utilise the heat to vaporize. A heat exchanger HXFT increases the water temperature to $225°C$ to make it directly suitable for the gasifier and SMR.

Besides water, FT-FLASH separates tail gas and liquid hydrocarbons. Tail gas comprises of unreacted syngas and small hydrocarbons $(C_1 - C_5)$ destined for SMR and subsequently recycling.

3.2.4. Steam methane reforming

Steam methane reforming (SMR) is predominantly used for hydrogen production by fossil fuels. Small hydrocarbons react into CO, H_2 and CO_2 with presence of steam. SMR plants usually operate at 20-30 bar, for economic reasons, and a temperature of $820 - 880°C$. The pressure is a trade-off between conversion and volumetric productivity. A nickel-based catalyst, Ni/Al_2O_3, is employed to activate the reforming reactions. Main reactions taking place in the SMR can be found below.

$$C_nH_{2n+1} + nH_2O \rightarrow nCO + (2n+1)H_2 \tag{3.4}$$

$$CO + H_2O \leftrightarrow CO_2 + H_2 \tag{3.5}$$

$$CO + 3H_2 \leftrightarrow CH_4 + H_2O \tag{3.6}$$

A hydrogen rich outlet stream with $H_2 : CO$ ratio of 5:1 is typical. This can be reduced by lowering the steam to methane ratio or co-feeding CO_2 to obtain an acceptable $H_2 : CO$ ratio for FT synthesis [64].

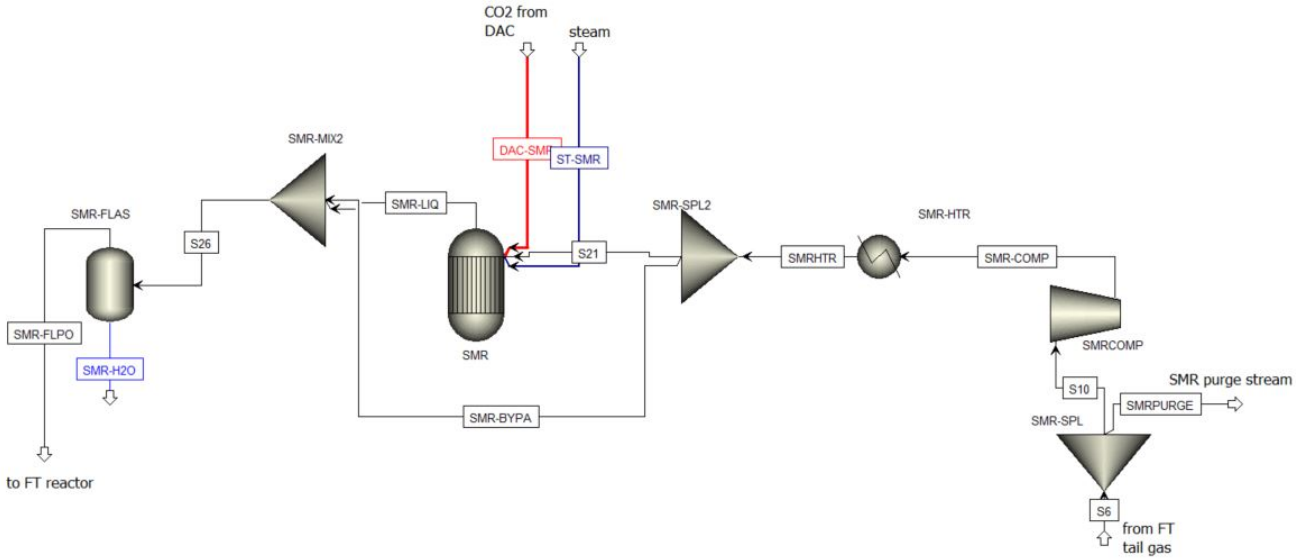

Figure 3.4: Schematic of the SMR process developed in Aspen Plus

Schematic Steam Methane Reformer

A first flash separator FT-FLASH removes the highest fraction of low hydrocarbons and unreacted syngas. Further downstream a second flash separator FT-FLAS2 is installed to decrease pressure to atmospheric for the distillation process. Here, most residual small hydrocarbons are separated from the stream heading to the distillation column.

The two streams C1-C5GAS and C1-C5 are pressurized to the SMR operating pressure of 25 bar, similar to FT reactor and most other blocks in the system, by a compressor SMRCOMP with an efficiency of 75%. A heater SMR-HTR will increase the inlet temperature of the reactor. Normal inlet temperatures range between $540 - 580°C$, while outlet temperatures are $820 - 880°C$. The heater increases the temperature to $560°C$, before entering the SMR reactor.

A REquil reactor SMR in Aspen plus simulates the SMR reactor. Here, all reactions reach equilibrium by solving stoichiometric chemical and phase equilibrium equations. This will result in total conversion of hydrocarbons, where average conversion rates for SMR plants lie between 74% and 85% [100]. To simulate a lower conversion rate, 20% of the inlet stream is split in SMR-SPL2 before the reactor and mixed (SMR-MIX2) thereafter and represents the fraction that usually does not convert. Saturated steam enters the reactor at 25 bar with saturation temperature $225°C$ and a steam-to-methane ratio of 2-3. The high operating temperature and outlet temperature is $850°C$. CO_2, produced by the DAC plant, can be co-fed to decrease H_2/CO ratio to match FT plant requirements.

3.2.5. Distillation

Distillation is the final process step to obtain synthetic kerosene. A distillation column is used to retrieve the different fractions. Main focus of this research is kerosene $(C_9 - C_{15})$, but useful side products like gasoline $(C_4 - C_{10})$ and diesel $(C_{11} - C_{22})$ are also obtained. Waxes (C_{22+}) consist of the heaviest hydrocarbons and can be used for common applications such as candles or lubrication. But another alternative is to hydrocrack waxes into smaller hydrocarbons.

Hydrocracking is subdivided in thermal and catalytic cracking. Thermal hydrocracking requires high temperature and pressure causing it to be highly energy intensive and need specialized machinery [92]. Catalytic cracking on the other hand takes place at relatively low pressure. The hydrotreater in this study is based on a study of Leckel [68], who investigated the Sasol catalyzed hydrocracker. Different configuratios regarding the pressure, hydrogen/wax ratio and temperature were investigated. Accordig to this study, it can be concluded that the optimal conditions for kerosene production are 35 bar and $360°C$ with a H_2/wax ratio of 1500/1 L_n/L. A lower H_2/wax ratio will only decrease the C_{23+} conversion.

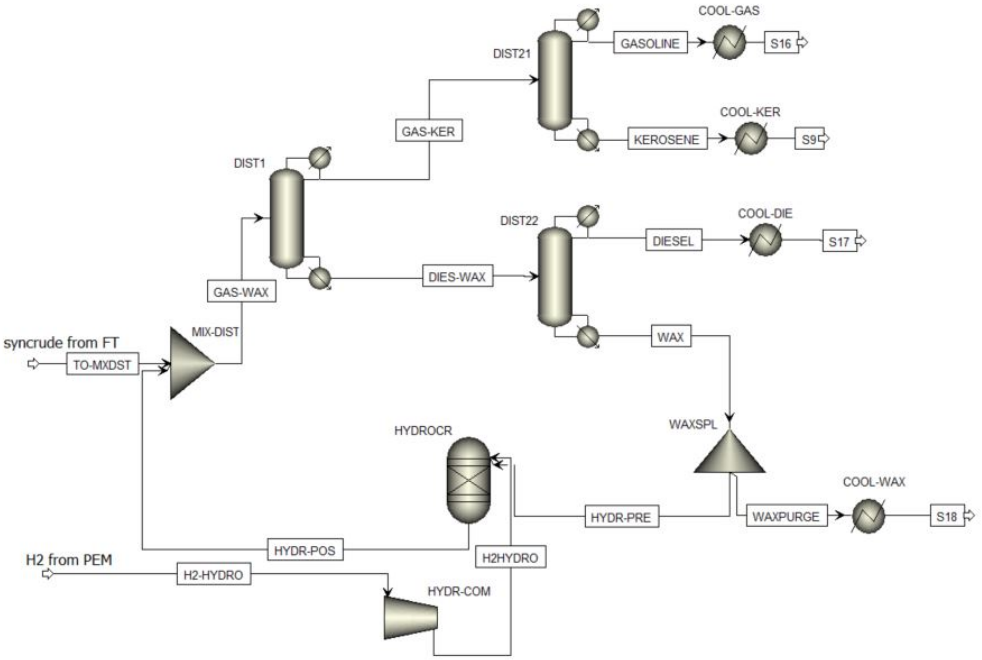

Figure 3.5: Schematic of the distillation process with hydrocracker developed in Aspen Plus

Schematic distillation

The distillation column is split into three separate DSTWU columns in the Aspen Plus model as shown in Figure 3.5. A DSTWU column performs shortcut design calculations with a partial or total condenser for two-product distillation or single-feed. A mixer MIX-DIST mixes the hydrocarbons from the FT reactor with the product stream from the hydrocracker.

DIST1 is the first column splitting the stream at C_{17}, resulting in a bottom stream of diesel and waxes while gasoline and kerosene leave on top. Kerosene is the bottom product of the second column DIST21, where gasoline is the top product. At last, the third column separates heavy waxes from diesel by splitting the stream at C_{22} (DIST22). Each outlet stream is redirected to a cooler (COOL-GAS, COOL-KER, COOL-DIE and COOL-WAX) to meet atmospheric temperature of $15°C$ for storage.

Specifications of the three mentioned columns can be found in Table 3.2. Recovery rates of the distillation columns are optimised to obtain densities that approaches the fuel specifications. Densities found in this model are slightly lower than required [64]. Chiefly because aromatic content is low for kerosene produced by this method. Aromatics are allowed up to 25 vol.% (Table 1.1) and have higher density than observed for kerosene in this model. Hence, a higher aromatic content will increase the kerosene density such that it meets the specifications. This problem will easily be resolved after blending with conventional kerosene.

Table 3.2: Specifications for distillation columns in Aspen Plus model

	DIST 1	DIST21	DIST22
Reflux ratio	2	3	3.8
Condenser Pressure (bar)	1.2	1.2	1.2
Reboiler Pressure (bar)	1.3	1.3	1.3
Top outlet temperature ($°C$)	117	77	335
Bottom outlet temperature ($°C$)	364	226	419

Waxes are redirected to an iron-catalyzed hydrocracker through a splitter WAXSPL. To avoid accumulation of unfavorable components, a fraction of the wax stream is separated, but can be used as useful by-product. Hydrogen required for the cracking process is derived from the electrolyzer, and pressurized in a compressor HYDR-COM to operating pressure of the hydrocracker. A RYield

HYDROCR simulates the hydrocracker, operating at equal temperature and pressure as Sasol hydrocracker (35 bar, $360^{\circ}C$). Mass yields within the model can be found in Table 2.9, assuming a wax conversion of 84 wt.%. The hydrotreater is modelled relatively easy and it is recommended to do further research to optimise the hydrotreater, but this is beyond the scope of this research study.

3.2.6. Biomass gasification

The second option for syngas production, besides electrolysis, starts with the biomass gasifier. A great variety from types of biomass can be used as feedstock for gasification. This research will use wood pellets as feedstock, predominantly for the modern and future availability of this source, as discussed in 2.1.5. In addition, wood pellets are dense, easy to transport and have a low moisture content. The proximate and ultimate analysis of the wood pellets is shown in Table 2.7. Moisture content is only 8.7% which means that the pre-processing step drying is not necessarily required.

Chapter 2.3 elaborately discussed the different types of gasifiers and the commercially available gasifiers. This research will make use of an autothermal fluidized bed gasifier which can operate with flexible load and pressurized conditions. A brief literature study was needed to find relevant data for such a plant that utilises oxygen and steam as fluidizing medium. A demonstration plant in Hawaii developed by the Institute of Gas Technology (IGT) has done a thorough study on their gasifier [126]. From their 12 ton-per-day process development unit (PDU) was validation data available and the technical specifications of the plant. This study will model the gasifier as the IGT such that results can be validated with the IGT gasifier located in Hawaii.

Sand is integrated in the model although it does not react with any component. But sand contributes to a large fraction normally in a fluidized bed gasifier and consequently has a significant effect on the product gas composition. Therefore, if sand would not be included the product flow is different and will not meet the original data from the IGT plant [126].

Peng-Robinson EoS is applied in the Aspen Plus model of the gasifier, while DCOALIGT and HCOALGEN (a property model for non-conventional components) are used to calculate the density and enthalpy of the non-conventional components. A gasifier is in reality one reactor, but in Aspen Plus usually modelled as multiple different operation blocks. This model will decouple the gasifier into four different reactors. The four reactors can be explained by the three zones shown in Figure 3.6: pyrolysis, oxidation and reduction. The fourth reactor is placed after the pyrolysis zone to let the inerts react.

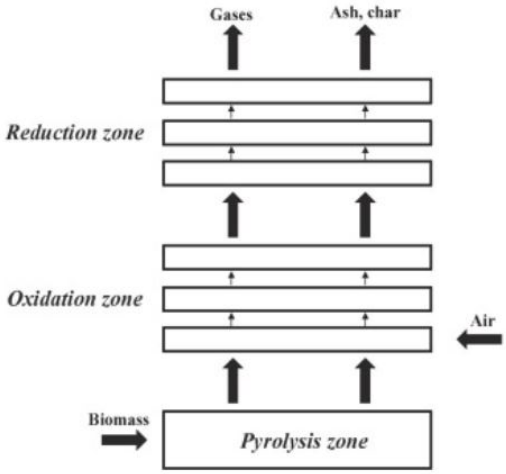

Figure 3.6: Overview of the gasifier model, where the fluidizing medium air is replaced by steam and oxygen [95]

Schematic biomass gasification

A schematic of the Aspen Plus model developed is shown in Figure 3.7. The wood pellets are fed to the first reactor in stream Biomass. Wood pellets are modelled as non-conventional solid according to the composition mentioned in Table 2.7. Pyrolysis is the first zone, modelled in a RYield reactor block PYROL. A RYield is used when the molar or mass yield is known for the products of the reactants. The product is calculated according to correlations shown in Table 3.5 which calculates the mass yields,

results hereof can be found in Appendix C. L. Abdelouahed et al. quantified the results of a study into an empirical correlation where the bed material is the only variable [10]. This model assumes the temperature of the bed material constant and equal to the gasifier temperature which is $911°C$, but it is recommended to include temperature fluctuations in further studies. The temperature is well within the range in which the empirical experiment has been performed $(700 - 1000°C)$. An external Excel subroutine will calculate the mass yields after which the yields are entered in the RYield block in Aspen Plus. Char mass yields are then calculated to achieve mole balance and mass balance based on the pyrolysis product. For simplification, char is assumed to be pure carbon (graphite). The method for determining this pyrolysis product is equal to Sridharan [116] his Aspen Plus gasifier model.

The pyrolysis product then enters a RStoic INERTREA, a stoichiometric reactor in Aspen Plus. Here, nitrogen and sulfur reacts into NH_3 and H_2S. The reactor is assumed to be adiabatic, heat produced by the reactions is absorbed by the stream to simulate an actual gasifier. These components do not react further in the reactor and are therefore separated in a separator block INERTSEP from the main stream and will re-enter the product stream after the last gasifier reactor block.

Table 3.3: Main input parameters for the Aspen Plus gasifier block

Parameter	Value
Gasifier temperature	$911°C$
Gasifier pressure	25 bar
Biomass inlet pressure and temp.	1 bar and $25°C$
Moisture content biomass	8.7%
ER	-[a]
Oxygen inlet pressure and temp.	25 bar and $300°C$
SBR	-[a]
Steam inlet pressure and temp.	25 bar and 220-230$°C$
Bed material flow rate [kg/h]	1.1x Biomass input

[a] Depends on scenario

Schematic oxidation zone

A first RPlug reactor block PLUG1 simulates the oxidation zone of the gasifier. The steam and oxygen is entering the gasifier in this reactor with a SBR and ER ratio as shown in Table 3.3. Oxygen comes from the electrolyzer where pure oxygen is produced during H_2 production, but it is first stored in an oxygen storage. The high quality steam is produced with heat from the FT reactor. Steam at a pressure of 25 bar has to reach a temperature between 220 and $230°C$ to saturate.

An inert bed material sand (siliciumoxide) is added to the stream. In direct gasification the temperature of the bed material is a key parameter. Most reactions taking place in the gasifier are endothermic and the bed temperature will be used to optimize the producer gas quality [95]. Reactor dimensions are retrieved from the 11 ton-per-day IGT plant in Hawaii and can be found in Table 3.4. For every oxidation reaction taking place in the oxidation zone the reaction kinetics can be found in Table 3.6. The reaction temperature is maintained at $911°C$ which is equal to the IGT gasifier.

Table 3.4: IGT gasifier design specifications [126]

Parameter	Value
Height [m]	7.32
Diameter [m]	0.29
Volume [m^3]	0.49
Volume RPlug [m^3]	0.25

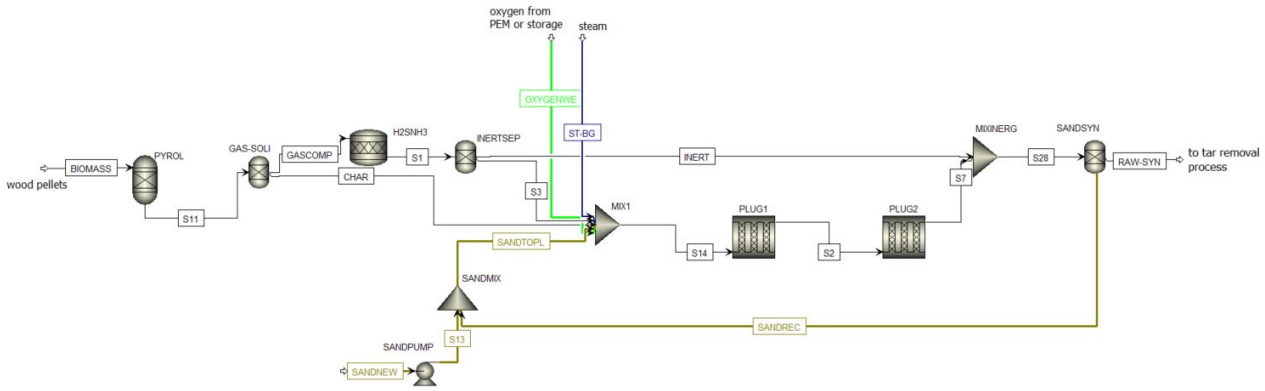

Figure 3.7: Schematic of the fluidized bed gasifier developed in Aspen Plus

Schematic reduction zone

Finally, a second RPlug reactor block PLUG2 simulates the reduction zone above the oxidation zone. The reactions taking place in this reactor can also be found in Table 3.6. Now, all reactions taking place inside a gasifier have been modelled, the inert stream with NH_3 and H_2S joins the resulting stream of PLUG2 in MIXINERG. The sand as bed material will be separated from the stream and recycled to the inlet of the oxidation zone.

Table 3.5: Correlations for the pyrolysis process in the gasifier. Mass yields are calculated by $Y_i = aT^2 + bT + c$ with T in Kelvin [10].

Product	a (10^{-5})	b (10^{-2})	c
CH_4	-4.341	10.12	-51.08
H_2	1.362	-2.517	12.19
CO	-3.524	9.770	-24.93
CO_2	3.958	-9.126	64.02
C_2H_4	-6.873	14.94	-76.89
C_2H_6	0.8265	-2.105	13.38
C_6H_6	-3.134	7.544	-42.72
C_7H_8	-0.4539	0.687	1.462
C_6H_6O	1.508	-3.662	22.19
$C_{10}H_8$	-0.8548	1.882	-9.851
H_2O	5.157	11.86	84.91

Table 3.6: Reaction kinetics considered in the gasification model

Reactor	Reaction	Kinetics [kmol/m$^3 * s$]	Source
PLUG1	R2/R3	r = 1.426*10$^5 exp(-\frac{59.9(kJ/mol)}{RT})[O_2]f$ f=3	[91]
	R6	r = 5.62*10$^9 exp(-\frac{133(kJ/mol)}{RT})[CO][O_2]^{0.5}$	[131]
	R7	r = 5.159*10$^{15} T^{-1.5} exp(-\frac{28.519(kJ/mol)}{RT})[H_2]^{1.5}[O_2]$	[101]
	POmeth	r=1.58*10$^{12} exp(-\frac{202(kJ/mol)}{RT})[CH_4]^{0.7}[O_2]^{0.8}$	[48] [95]
	PObenz	r=2.40*10$^8 T^{-0.1} exp(-\frac{126(kJ/mol)}{RT})[O_2]^{1.85}$	[48] [95]
	POphen	r=0.655T exp(-$\frac{80.2(kJ/mol)}{RT}$)[C$_6H_6O$]$^{0.5}$[O$_2$]	[48] [95]
PLUG2	R4	r=1.05*10$^{10} exp(-\frac{135(kJ/mol)}{RT})[C]$	[48] [95]
	R5	r=200exp(-$\frac{49.9(kJ/mol)}{RT}$)[C][H$_2O$]	[48] [95]
	R8	r=0.278exp(-12.6 (kJ/mol)/(RT))*[CO][H$_2O$] $- \frac{[CO_2][H_2]}{k_{eq}}$ $k_{eq} = 0.022exp(\frac{34.730}{RT})$	[95]
	R9	r=3*10$^8 exp(-\frac{125(kJ/mol)}{RT})[CH_4][H_2O]$	[48] [95]
	Benzene	r=21.11exp(-$\frac{61(kJ/mol)}{RT}$)$\frac{m_{char}}{V_R}$[C$_6H_6$]	[10]
	Toluene	r=21.11exp(-$\frac{61(kJ/mol)}{RT}$)$\frac{m_{char}}{V_R}$[C$_7H_8$]	[10]
	Phenol	r=95798exp(-$\frac{79(kJ/mol)}{RT}$)[C$_6H_6O$]	[10]
	Naphthalene	r=21.11exp(-$\frac{61(kJ/mol)}{RT}$)$\frac{m_{char}}{V_R}$[C$_{10}H_8$]	[10]

3.2.7. OLGA tar removal

The produced raw syngas is solely for the production of synthetic fuels via the Fischer-Tropsch process. A FT reactor requires an input with a low amount of contaminants. In Section 2.3.2 and Table 2.8 all relevant and present contaminants have been discussed. Two processing steps are introduced to clean the syngas and meet the stoichiometric feed ratio. Other mandatory gas conditioning steps are not modelled in Aspen Plus, but will be added in the cost analysis. This section will focus on the tar removal process, next section will focus on H_2S/CO_2 removal.

As discussed in Section 2.3.2, tars can cause damage to catalysts downstream and lower the syngas quality. Tar removal is therefore an essential part of the syngas cleaning. Several methods have been introduced, for instance thermal decomposition and water or oil scrubbing. Thermal decomposition operates at high temperatures ($> 1100°C$) and hence require high energy demands. Water scrubbing is a cold gas cleaning technology where tar compounds are directly absorbed in water. However, a challenging waste water cleaning is necessary for streams containing toxic tar compounds [114]. An oil scrubber on the other hand can reach high tar removal efficiencies. Vegetable oil, canola oil or even fossil oil are suitable as oil compound in the oil scrubber.

ECN patented an oil-based washer, named OLGA, to remove tar. Besides tar also a fraction of H_2S is removed. The oil removal method used in this study is based on this OLGA concept. But the OLGA concept is designed to operate at atmospheric pressure while this study uses a pressurized column for absorption [21]. Using a pressurized absorber over an atmospheric absorber has a similar reason as the gasifier, because the FT reactor is also pressurized. The inlet temperature of the syngas is just above the tar dew-point, which is the point where the tar in the syngas condenses. Condensed tars

can cause corrosion and deposition downstream.

The oil scrubber in this study will make use of methyl-oleate, the biggest fraction of biodiesel and used in similar studies [116] [117]. A suitable phase equilibrium model is important for optimal performance of the scrubber. Srinivas et al. [117] compared several equilibrium models to obtain an appropriate liquid-liquid equilibrium (LLE) model. Non-random two-liquid (NRTL) and universal quasichemical (UNIQUAC) functional-group activity coefficients (UNIFAC) both show satisfactory results. The components used in this model are similar as the study of Srinivas et al. [117] hence NRTL will be the property method used in this oil scrubber. Missing binary interaction parameters were estimated using the UNIFAC method.

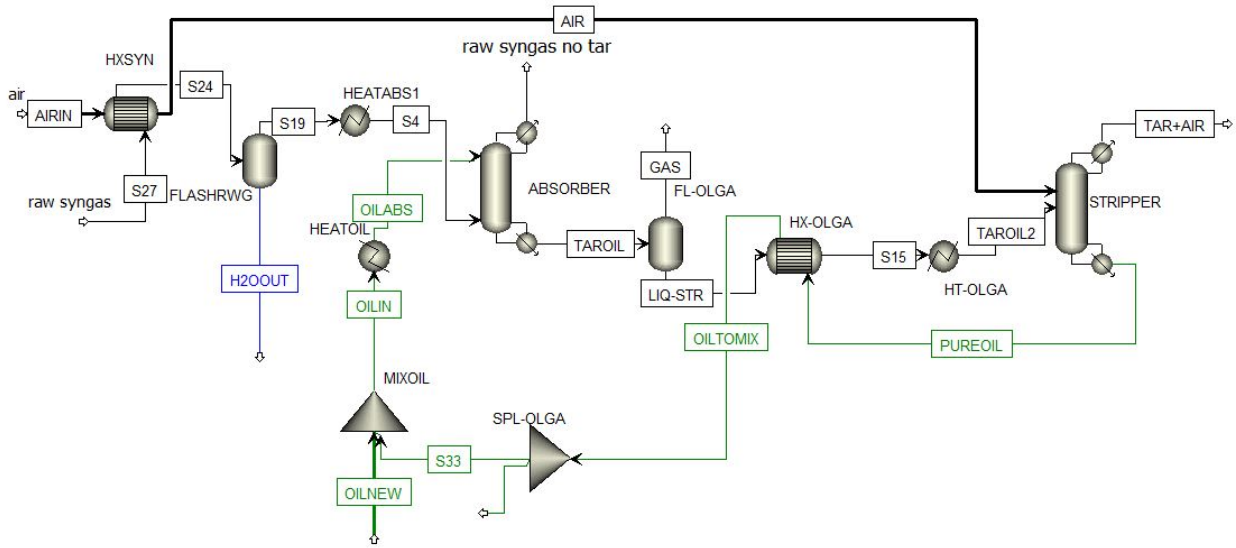

Figure 3.8: Schematic of tar removal process developed in Aspen Plus

Schematic OLGA tar removal

The oil scrubber consists of an absorber to absorb the tar followed by a stripper that separates the oil from the tar, after which the oil will be recycled (Figure 3.8). RADFRAC columns from Aspen Plus will simulate the absorption and stripping column of the oil scrubber. A RADFRAC column is a rigorous model for simulating all types of multistage separations.

The ABSORBER and STRIPPER simulate the absorption and stripper column respectively. Oil is fed to the top stage of the column and the syngas at the bottom, operating conditions for the flows can be found in Table 3.7. No condenser or reboiler is present in any of the two columns. The absorber operates at a pressure of 25 bar (Table 3.8), similar to the gasifier and FT reactor. Over 99% of tar is removed from the syngas stream including a small amount of H_2S and NH_3. The bottom stream is fed to a flash FL-OLGA to decrease pressure to the stripper operating pressure, atmospheric. A heat exchanger HX-OLGA followed by a heater HT-OLGA increases the temperature of the stripper feed stream to $190°C$ and decreases the recycled oil temperature. The stripper temperature will be lower than the boil temperature of oil to avoid significant oil losses. Preheated air works as stripping agent in the stripper. Air is heated by HXSYN placed after the gasifier, where the product stream reaches a high temperature.

Table 3.7: Flow conditions and tar content for tar removal process

	Raw syngas	Sweet syngas	Oil	Air
Temperature [$°C$]	120	85	82	78
Pressure [bar]	25	25	1	1
Tar content [mg/N^3]	7.6*10^5	0.32		

Most oil ends in the stripper bottom stream, but a small fraction leaves on top as scrubbing liquid loss. Common losses lie between 4% and 9% [116], this model loses 4-6% of scrubbing oil with an air/raw syngas ratio of 1. A Fortran code will calculate the required new oil to maintain a constant oil feed to the absorber. The splitter SPL-OLGA splits off a small fraction of the recycled oil to avoid accumulation of unwanted compounds. Optional an additional column can be integrated to separate the heavy tars from the light tars.

Table 3.8: Column specifications for tar removal process

	Absorber	Stripper
Number of stages	13	10
Pressure [bar]	25	1
Condenser	No	No
Reboiler	No	No

3.2.8. Hydrogen sulfide (H_2S) and CO_2 removal

Biomass is relatively free from sulphur, but small fractions of sulphur can already cause catalyst poisoning and corrode metal surfaces. Fischer-Tropsch process requires a syngas stream containing less than $< 0.01 mg/m^3$ of sulphur compounds, H_2S in this model [114]. On the other hand, CO_2 contributes to a large fraction of the raw syngas. Although CO_2 is not mentioned in Table 2.8, a high CO_2 content does influence the FT-process. Less CO_2 will increase the selectivity for C_{5+} and hence is advantageous for kerosene production.

It might be beneficial to remove H_2S and CO_2 separately from the raw syngas stream. But $CO_2 - H_2S$ separation is difficult due to low relative volatility of CO_2 and H_2S at high CO_2 concentrations. Reaching the desired separation will require huge columns and comes with high energy demands [50]. A study of Tijmensen et al. [124], where FT-liquids have been produced by biomass gasification, found out that CO_2 removal adds more than 10% to the total capital costs.

As discussed in Section 2.3.2, finding the appropriate method depends on the partial pressure of the acid gas in the feed and product stream. Both streams have a high partial pressure resulting in a physical solvent method. An amine based scrubber has also been investigated and can be found in Appendix E. But a physical solvent method is more appropriate for this system.

High H_2S and CO_2 removal efficiency can be achieved using Rectisol, making use of chilled methanol. The Rectisol process can produce high quality syngas, operate flexible and makes use of inexpensive and easily available solvent which makes Rectisol an attractive method [102]. As can be seen in Appendix A, chilled methanol reaches high relative solubilities for these components.

Schematic H_2S/CO_2 removal

Model setup for the removal process of H_2S and CO_2 is comparable to the tar removal process. A first column, ABS-H2S, represents the absorber where syngas is fed at the bottom and chilled methanol on top (Figure 3.9). The syngas stream coming from the tar removal process is cooled to $-20°C$, at a pressure of 36 bar. Chilled methanol enters at atmospheric pressure and $-3°C$, in a methanol/syngas ratio of 2.9. A high operating pressure of 40 bar is maintained to reach high removal efficiency, which is discussed in Section 3.3.3 during validation.

Before the stripper column, three consecutive flash separators separate a large fraction of CO_2 and H_2S from the methanol. When only the stripper was placed for separation, high methanol losses were observed. In a flash separator, gasses leave on top and the liquid stream at the bottom. FL-1, FL-2 and FL-3 represent the flashes, where temperature and pressure decreases ($FL{-}1 = 75°C\ and\ 20\ bar, FL{-}2 = 50°C\ and\ 10\ bar, FL-3 = 35°C\ and\ 5\ bar$) in each flash separator. Approximately 80% CO_2 and 35% H_2S is separated within these flashes, the residual fraction is removed by a stripper STR-H2S. Column specifications for the stripper, as well as absorber, can be found in Table 3.9.

Table 3.9: Column specifications for H_2S/CO_2 removal process

	Absorber	Stripper
Number of stages	16	28
Pressure [bar]	40	1
Condenser	No	No
Reboiler	No	Yes (Kettle)
Distillate to feed ratio (mass)		0.1

A splitter MEOHPURG separates a small fraction of the liquid bottom stream from the stripper to avoid accumulation of unfavorable components. The largest fraction is send to a cooler MEOH-CLR to meet the inlet temperature of $-3°C$ for the absorber. A mixer MEOHMIX combines the recycled methanol stream with new methanol to meet the methanol/syngas ratio. Required new methanol is calculated according to a Fortran block. Product stream composition, even as syngas feedstream, of the absorber is shown in Table 3.10.

Table 3.10: Mole fractions of the present components before and after the absorber

	Raw syngas	Pure syngas
H_2O	0.02	0
CO_2	0.38	0.09
H_2	0.41	0.63
CO	0.19	0.29
H_2S	3800 mg/Nm^3	<0.1 mg/Nm^3
NH_3	13070 mg/Nm^3	<0.1 mg/Nm^3
Temperature [$°C$]	-20	-1
Pressure [bar]	36	40

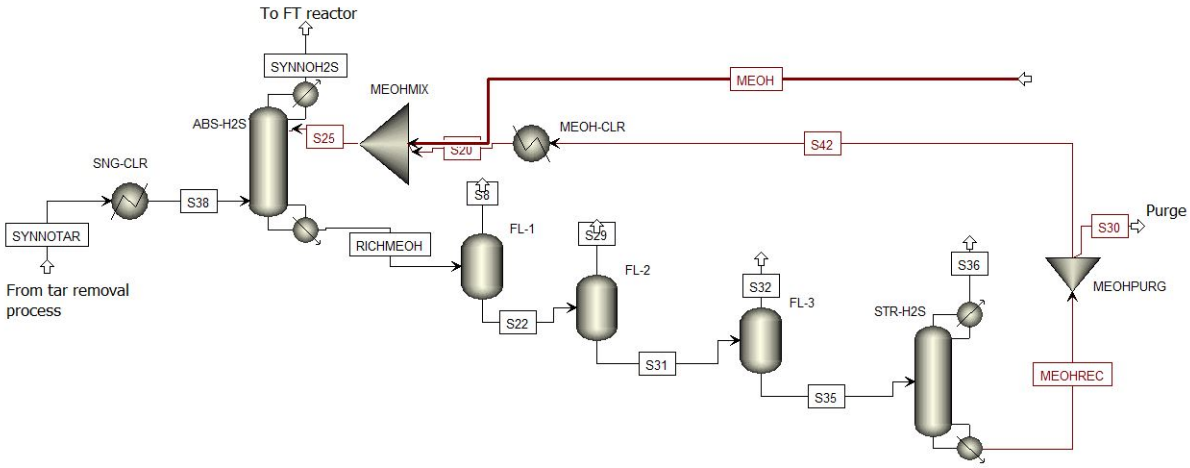

Figure 3.9: Schematic of CO_2/H_2S removal process developed in Aspen Plus.

3.3. Model validation

3.3.1. Fluidized bed gasifier

Experimental data from the IGT gasifier is not widely available for a pressurized gasifier with steam/oxygen as gasifying agent. But Tijmensen et al. [124] and Han et al. [53] has reported results for a biomass driven direct heated IGT gasifier. The parameters of the different experiments had been entered into the Aspen Plus model to obtain similar results. Table 3.11 shows the comparison between the Aspen Plus model and the experiments from literature. The sum squared deviation method was used to estimate the accuracy of simulation results.

$$RSS = \sum_{i=1}^{N} (\frac{x_{i,e} - x_{i,sim}}{x_{i,e}})^2 \tag{3.7}$$

$$MRSS = \frac{RSS}{N} \tag{3.8}$$

$$Mean\ error = \sqrt{MRSS} \tag{3.9}$$

An average error of 0.21 is calculated for the three different setups from IGT gasifier. The largest proportional deviation is the CH_4 concentration. This Aspen Plus model does not contain CH_4 in the product stream of the gasifier, while the experiments show small fractions of CH_4. Zero CH_4 is usually predicted above $800°C$ in equilibrium modeling. The underestimation can be explained by the difference between an ideal reactor at chemical equilibrium and a real gasifier [53]. The lower LHV can also be explained by the absence of methane. Same holds for H_2 concentration, a study reported an overestimation of H_2 concentration for chemical equilibrium simulation when compared to experimental results [95]. IGT.2 shows this behavior where H_2, as well as CO, is overestimated due to absence of CH_4. Which is in agreement with the reaction containing $CH4$, R9.

Table 3.11: Gasifier validation for IGT gasifier, with present component fractions

Component	IGT.1 [52] T=920°C, P=25 bar, ER=0.38, SBR=0.8	Model 1	IGT.2 [124] T=968°C, P=20.3 bar, ER=0.3, SBR=0.6	Model 2	IGT.3 [124] T=982°C, P=34 bar, ER=0.3, SBR=0.34	Model 3
H_2	0.240	0.200	0.157	0.220	0.208	0.267
CO	0.115	0.113	0.078	0.123	0.150	0.142
CH_4	0.005	0.000	0.057	0.000	0.082	0.000
CO_2	0.160	0.170	0.177	0.169	0.239	0.203
H_2O	0.480	0.518	0.506	0.487	0.318	0.385
$LHV_{dry\ gas}[MJ/Nm^3]$	8.11	7.42	10.06	7.67	10.72	7.62
$Mean\ error_{without\ CH_4}$		0.10		0.35		0.19
$Mean\ error_{with\ CH_4}$		0.46		0.55		0.48

According to Table 3.11, it can be concluded that the simulating results are in good agreement with the experimental data. Since no data is available for sensitivity analyses of pressure, temperature, steam-to-biomass ratio and equivalence ratio, trendlines will be interpreted for the performance of wood pellet gasification. This alternative validation method has been used in previous simulation works where experimental results were hardly available [80] [87]. Temperature, steam-to-biomass ratio and equivalence ratio will be varied to validate the gasifier behavior.

Temperature

Temperature is varied between 750 and $1050°C$ for obtaining the gas composition shown in Figure 3.10.

The trend can be described according to Le Chatelier's principle in gas-phase systems. Chemical equilibrium will shift towards the reactants for exothermic reactions and opposite happens with endothermic reactions, equilibrium shifts to products. Boudouard (R4), H_2O gasification (R5) and steam methane reforming (R9) are the present endothermic reactions, favoring higher temperatures for their forward reaction. While exothermic reactions favor the backward reaction with increased temperature.

It can be observed that the H_2 fraction decreases slightly with higher temperature. A similar pattern is observed in several other studies [53] [69] [80] [83] [87] [91] [95]. Hydrogen content usually peaks when all methane reacted according to R9. At higher temperatures, the water gas shift reaction R8 reverses and creates more CO and H_2O. CO_2 content and H_2 decreases with similar slope, which validates the reverse WGS reaction.

Higher temperatures shift chemical equilibrium towards CO production for both endothermic (R5 and R9) and exothermic reactions (R6 and R8). CO_2 is consumed in the exothermic reactions R6 and R8 for higher temperatures, which is in agreement with other studies. Methane is completely consumed by the endothermic reaction R9.

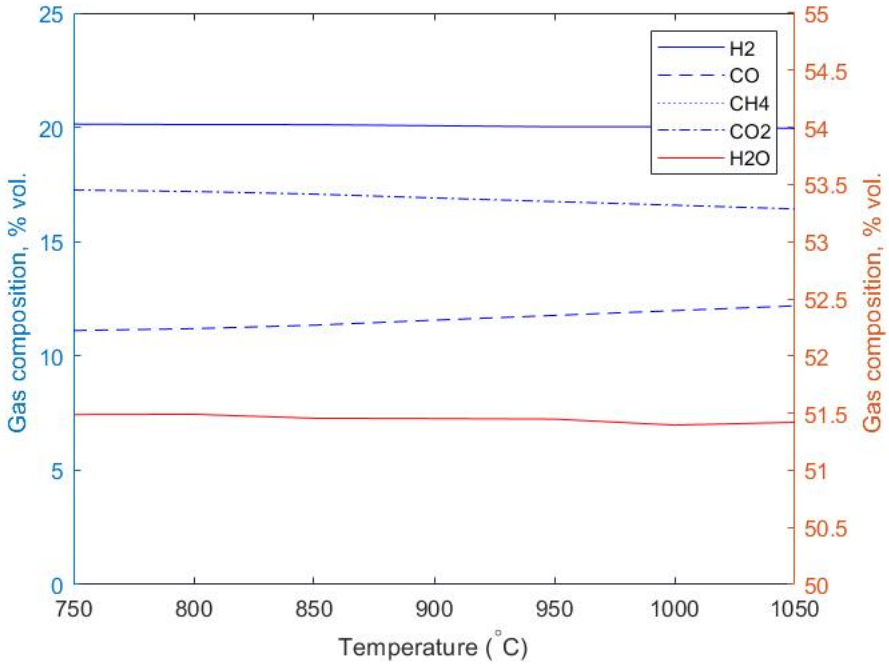

Figure 3.10: Product gas composition for the Aspen Plus model with varying temperature (P=25 bar, SBR=0.8, ER=0.38)

The effect of temperature on the LHV is shown in Figure 3.11. LHV is defined as the amount of heat released by full combustion of a fuel minus the heat of vaporization of water in the combustion product, and is calculated according to Equation 3.10. Y represents the volume fraction of each component on dry basis [80].

$$LHV_{gas} = 10.79Y_{H_2} + 12.62Y_{CO} + 35.81Y_{CH_4} \tag{3.10}$$

Since H_2 is consumed and CO is produced, it can be observed from Reaction 3.10 that LHV will increase because CO has a higher contribution to LHV than H_2.

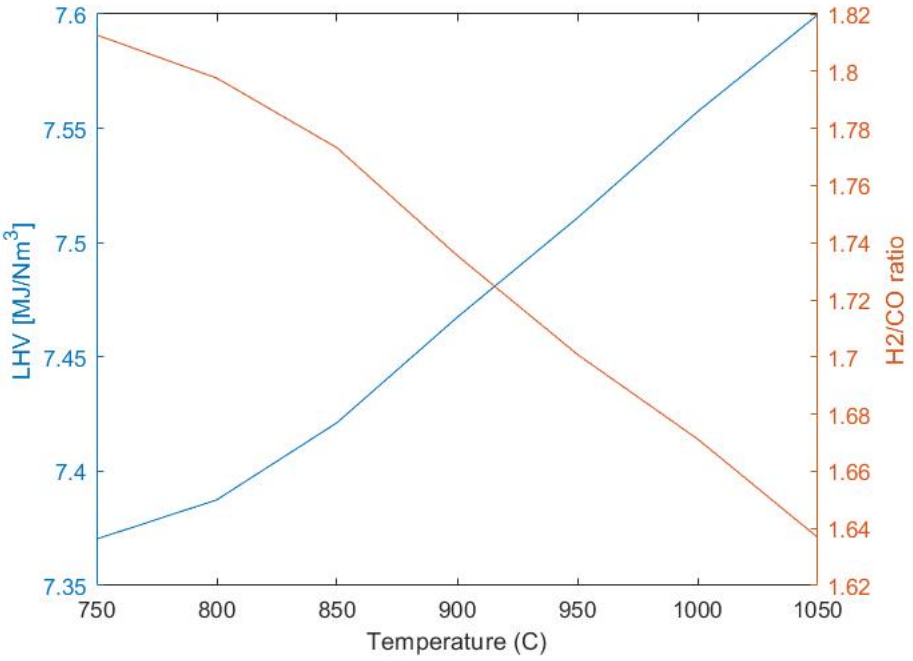

Figure 3.11: LHV and H_2/CO ratio for different temperatures (P=25 bar, SBR=0.8, ER=0.38)

Steam to Biomass ratio (SBR)

The effect of the SBR to the product gas composition is shown in Figure 3.12. More steam enhances H_2O gasification, water gas shift (R8) and steam methane reforming (R9) reactions. CO, CO_2 and H_2 is produced, while CO is negatively influenced by steam injection due to R8. Similar trends have been found by other studies [53] [54] [69] [80] [87]. The observed trend is more clear when the components are modelled in vol. % dry basis, as shown in Appendix D. It can be observed that the SBR has a small positive effect on the H_2/CO ratio, while LHV decreases slightly by increased SBR (Figure 3.13). Therefore it is beneficial to feed only a small amount of steam because steam production requires significant amounts of heat.

However, predicting the real trends is difficult because temperature fluctuations due to changing steam input is completely ignored in the Aspen Plus model [86].

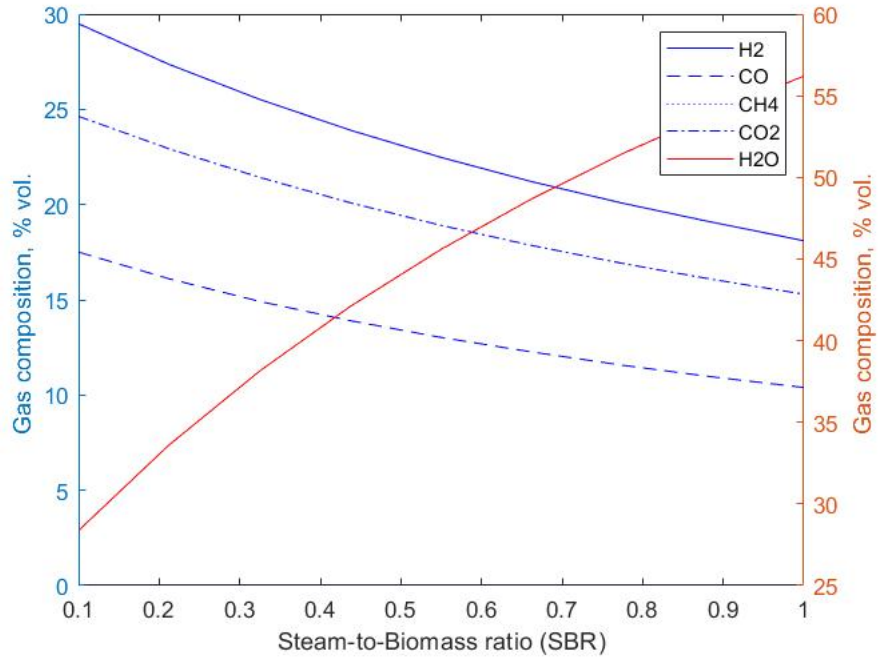

Figure 3.12: Product gas composition for the Aspen Plus model vs. SBR (T=900°$C, P = 25bar, ER = 0.38$)

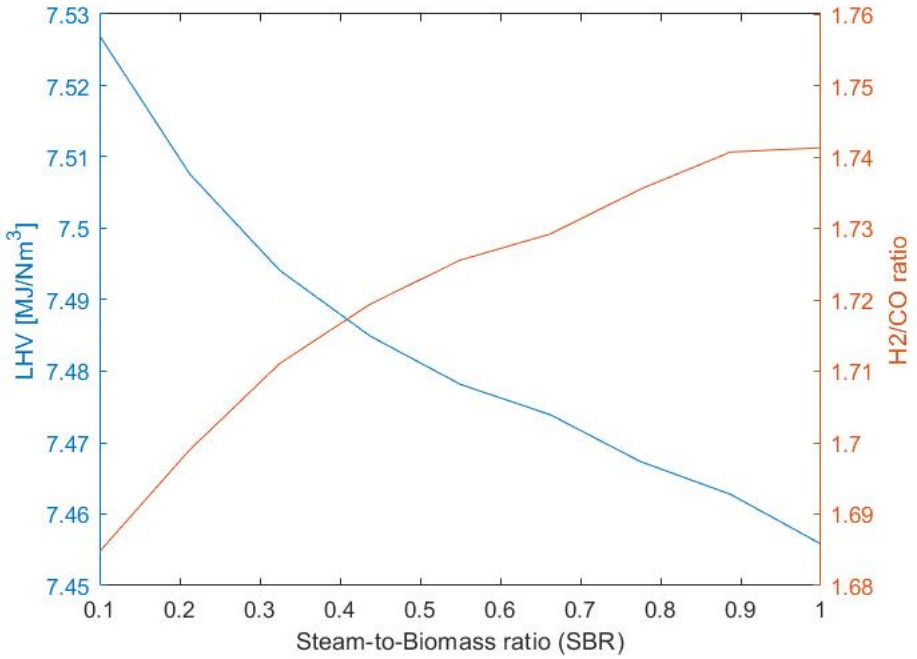

Figure 3.13: LHV and H_2/CO ratio for different temperatures vs. SBR (T=900°C, P=25 bar, ER=0.38)

Equivalence ratio (ER)

The ER has a strong influence on the gasification products. A higher ER means that more O_2 is available for the oxidation reactions R2/R3/R6/R7. This results in a decrease of H_2,CO and CH_4 and increase of CO_2, as shown in Figure 3.14. Comparable results are observed in other studies [25] [53] [69] [95]. Syngas LHV decreases by increased ER ratio (Figure 3.15). The decrease of CO takes place in higher pace than H_2 hence the H_2/CO ratio increases.

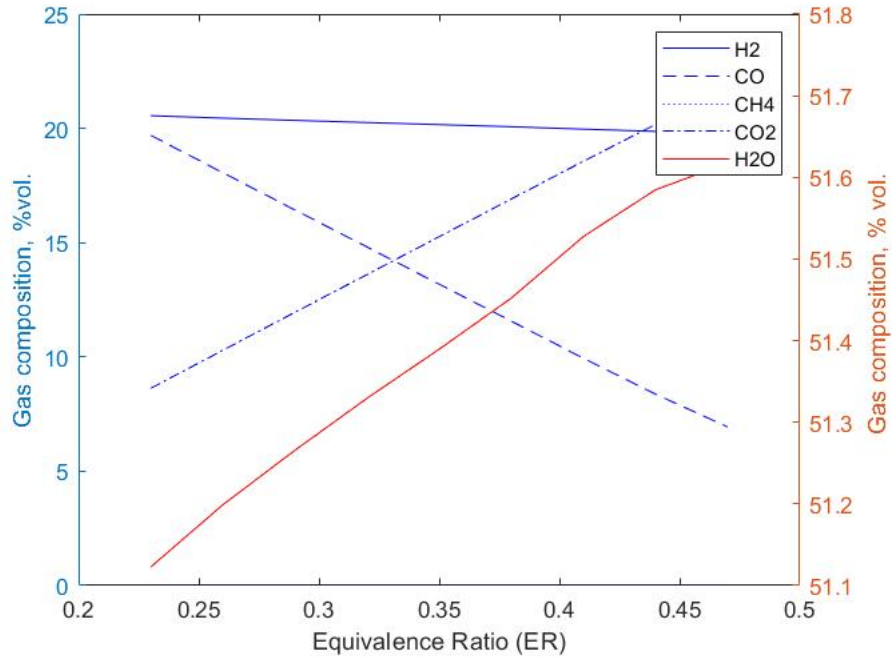

Figure 3.14: Product gas composition for the Aspen Plus model with varying SBR (T=900°C, P=25 bar, SBR=0.8)

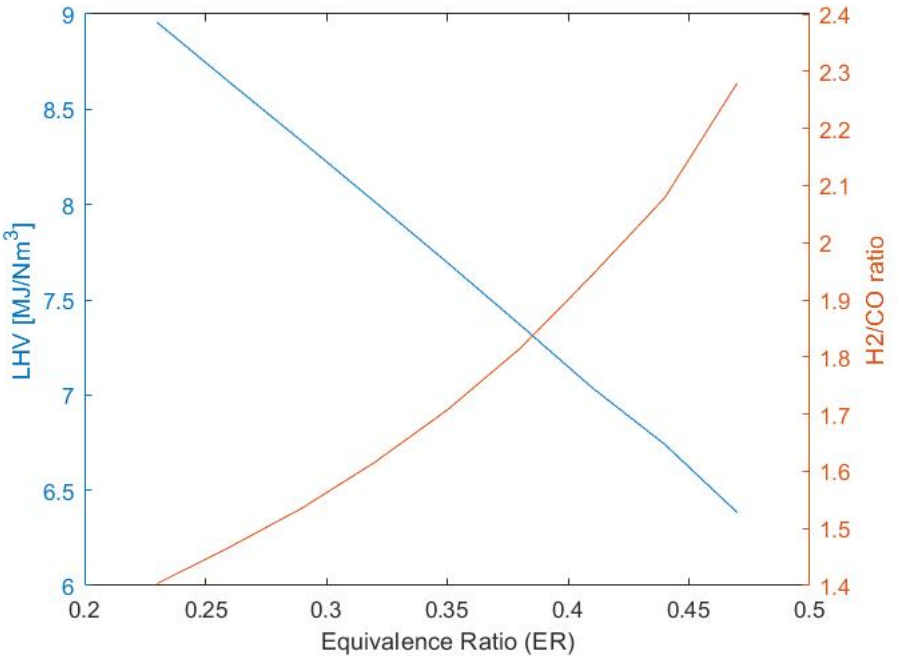

Figure 3.15: LHV and H_2/CO ratio for different temperatures (T=900°C, P=25 bar, SBR=0.8)

3.3.2. OLGA tar removal

Most literature research on OLGA tar removal takes place at atmospheric or low pressure, while high pressure research data is scarcely available. The only high pressure OLGA process similar to this research study is done by Sridharan [116] and Srinivas et al. [117]. They performed an Aspen Plus analysis at 20 bar, little less than the 25 bar of this study. Several parameters determine the tar concentration in the syngas outlet stream. Figure 3.16 shows the effect of the number of stages and pressure

inside the absorber, for a fixed volume and oil flow. It can be observed that increasing the stages or pressure has a positive influence on the syngas outlet tar concentration, but will also increase energy demand and costs. Although, the higher pressure is not necessarily a problem since unit operations up- and downstream operate at similar pressure. The required tar concentration of $10mg/Nm^3$ is achieved with less stages at higher pressure. In addition, the higher the pressure the closer the curves are to each other.

Figure 3.17 shows the results of the tar removal process from the model developed in this study, where the number of stages and pressure is fixed at 25 bar and 13 stages. It can be observed that the trend follows an exponential pattern. This pattern is also found in the aforementioned studies [116] [117]. A bio-diesel/raw syngas ratio of 2.2 is required to reach a purified syngas stream with less than $10mg/Nm^3$ of tar.

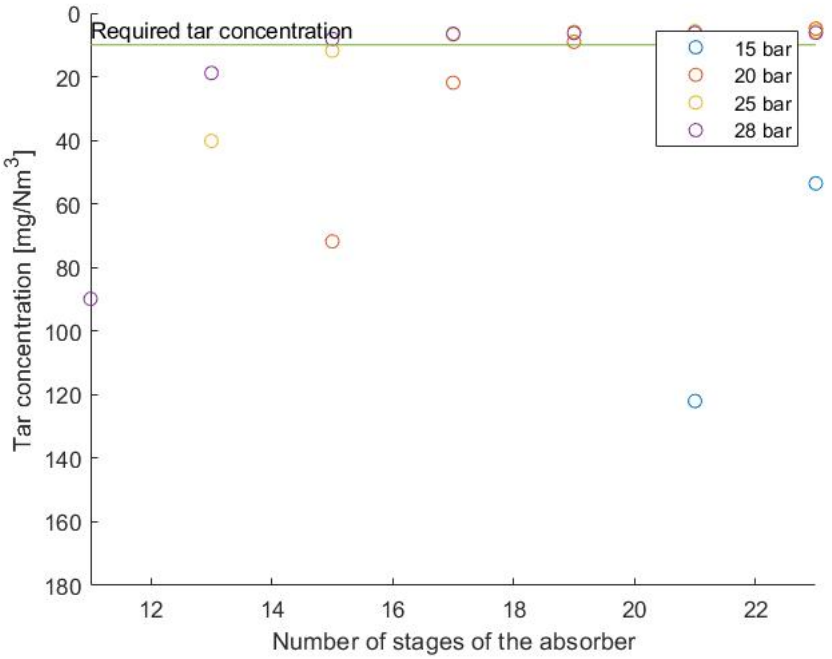

Figure 3.16: Sensitivity analysis for pressure and number of stages for the absorber on the tar concentration. The inlet oil flow is fixed at 1.9 $kg_{bio-diesl}/kg_{raw\ syngas}$.

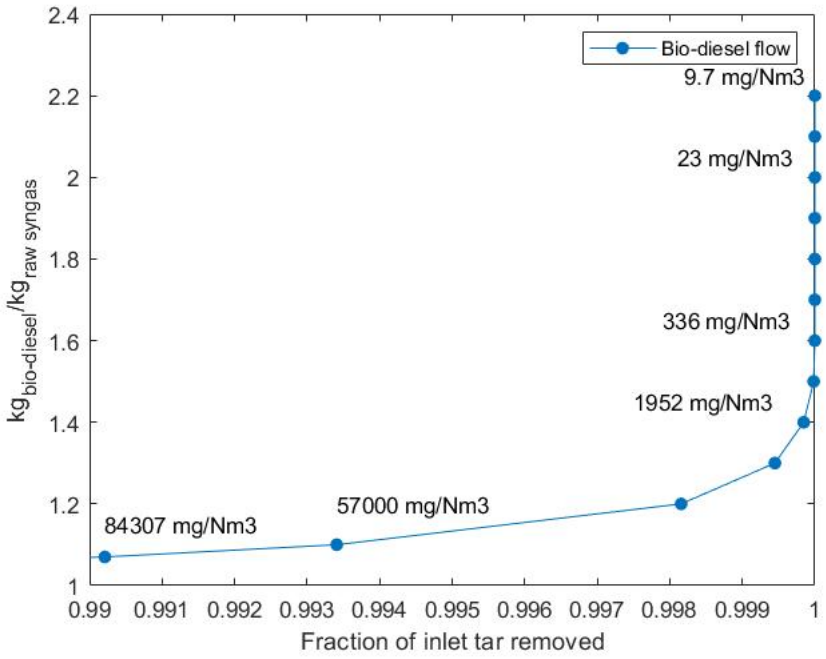

Figure 3.17: Solvent required to purify syngas. Absorber has 13 stages and operates at 25 bar. Syngas inlet stream:$120°C$, 25 bar. Oil inlet stream:$82°C$, 1 bar.

3.3.3. H_2S and CO_2 removal

Removal of H_2S and CO_2 takes place with an absorber/stripper combination, including three flash separators in front of the stripper. Main focus of this removal process is to decrease H_2S ratio below $0.1 mg/Nm^3$ (Table 2.8), where also a large fraction of CO_2 is removed. For this validation the number of stages, pressure and methanol/syngas ratio is examined. Note, results shown does not take the recycle stream into account. Final results of the model, with recycle stream, may deviate.

In Figure 3.18 the number of stages and pressure is varied to investigate H_2S concentration in the product stream. Similar as the tar removal process, increasing the pressure or number of stages will increase H_2S removal. Although, curves get closer when pressure is further increased. The preferred H_2S concentration is reached after 12 stages with 10 bar, but when the pressure is 40 bar it is already achieved after 6 stages. Even so, CO_2 removal is much higher at higher pressures or when the number of stages increases (Appendix F).

Increasing the methanol/raw syngas ratio also has a positive effect on the removal efficiency. Preferred H_2S concentration is reached easily, but for a CO_2 removal of >99% a methanol/raw syngas ratio of at least 2.4 is required.

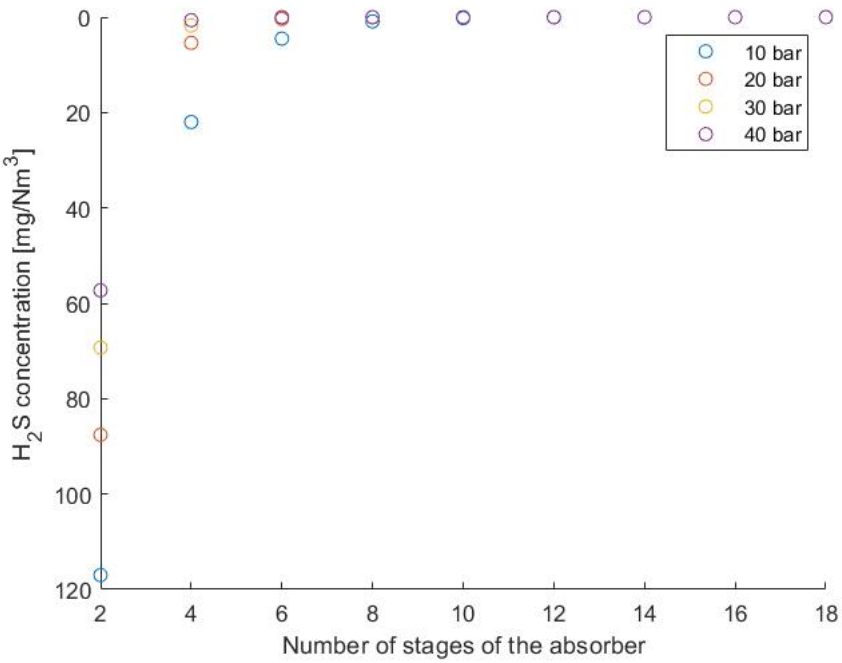

Figure 3.18: Sensitivity analysis for pressure and number of stages for the absorber on the H_2S concentration. The inlet methanol flow is fixed at 2.5 $kg_{methanol}/kg_{raw\ syngas}$.

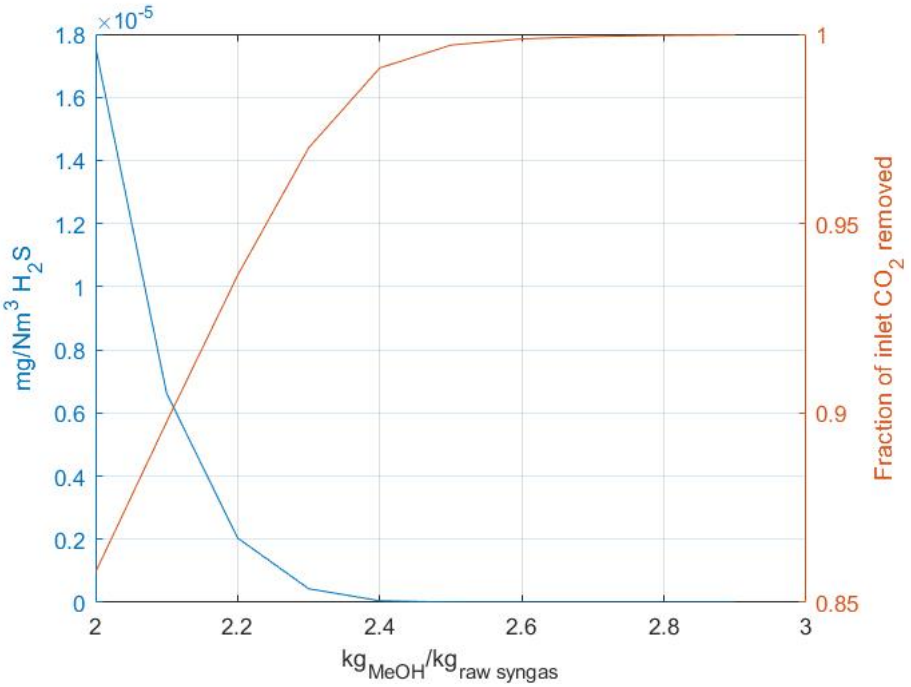

Figure 3.19: Methanol required to remove H_2S and CO_2 from raw syngas. Absorber has 12 stages operating at 36 bar. Raw syngas inlet conditions: $-20^{\circ}C$, 36 bar. Methanol inlet stream: $-3^{\circ}C$ and 1 bar.

4

Results

In Chapter 3 the Aspen Plus model is described. This chapter analyses the model adapted for two scenarios in Section 4.1 and 4.2, to finally conclude the results in Section 4.3.

The results will be obtained for two different scenarios described in Section 1.1.1. These are based on the extreme situations that might take place during a year, regarding the electricity supply. Renewable electricity has a fluctuating behavior which has an effect on the dynamic range of the electrolyzer. The scenarios depend on the availability of electricity, namely high or low. This represents day/night or summer/winter fluctuations throughout the year. Energy efficiency for kerosene production exclusively will be calculated according to Equation 4.1. Equation 4.2 takes other useful byproducts like gasoline and diesel also into account by calculating the energy efficiency of the process.

$$\eta_{energy,kerosene} = \frac{Kerosene}{Biomass + Electricity_{PEM} + Electricity_{pumps/compressors}} \tag{4.1}$$

$$\eta_{energy,fuel} = \frac{Kerosene + Gasoline + Diesel + Wax}{Biomass + Electricity_{PEM} + Electricity_{pumps/compressors} + Electricity_{DAC}} \tag{4.2}$$

The scenarios will be compared according to key performance indicators (KPIs). KPIs are required electricity production, biomass, produced/consumed oxygen, above mentioned energy efficiencies and CO_2 emission during the process.

4.1. Scenario 1

The first scenario represents a period of time where renewable electricity is maximized. Hence, most syngas will be produced by water electrolysis while only a small fraction originates from the gasifier. Dynamic load of the gasifier is reduced to approximately 40% of the nominal output.

Almost 70% of syngas is produced by PEM electrolysis and the RWGS. To meet the CO_2 demand for optimal RWGS conditions, a total of 38 ton/h has to be retrieved from the DAC plant. The still remaining syngas fraction (30%) is obtained by biomass gasification. 43 ton/h of wood pellets and 18 ton/h of oxygen is fed to the fluidized bed gasifier. Compared to oxygen production for this scenario, there is a positive net flow of oxygen. 342 MW of electricity is needed, whereof 320 MW originates from PEM electrolysis. Electricity demand for PEM is calculated according to a system energy of 5 kWh_{el}/m^3 (Table 2.1), assuming a H_2 gas density of $0.084 kg/m^3$.

A final kerosene production of 5.90 ton of kerosene is achieved, resulting in approximately 50.000 ton/y. A thermal efficiency of the process is 35% taking all fuels into account, comparable with results reported in Campanario and Gutiérrez Ortiz [26]. CO_2 emission end up to be 2.4 ton_{CO_2}/ton_{fuel}. A summary of the main parameters can be found in Table 4.1, or a more extended table in Appendix G.

4.2. Scenario 2

The second scenario represents low renewable electricity supply. This takes place when solar and wind energy are scarcely available. Approximately 80% of the syngas in this scenario is obtained from biomass gasification operating at maximum capacity, for which almost 100 ton/h of biomass is required.

Dynamic load of PEM electrolysis has decreased to 30%, producing much less oxygen as well. A negative net flow of oxygen is observed for this scenario, hence deficiencies must be made up by stored oxygen. Only 123 MW is required to meet the electricity demand for PEM, DAC and pumps/compressors.

A Thermal efficiency of 33% is achieved for fuel production. On the other hand, 3.2 ton_{CO_2}/ton_{fuel} is emitted. Results can be found in Table 4.1 or more comprehensive in Appendix G.

Table 4.1: Main parameters compared for scenario 1 and 2

	Scenario 1	Scenario 2
Inputs		
Biomass [ton/h]	43.04	98.51
H_2O [ton/h]	34.74	12.37
CO_2 [ton/h]	38.2	12.6
Electricity [MW]	340.8	122.7
Outputs		
Kerosene [ton/h]	5.90	6.32
Gasoline [ton/h]	4.41	4.53
Diesel [ton/h]	2.52	2.70
Wax [ton/h]	2.85	3.05
Oxygen net flow [ton/h]	24.14	-25.14
Efficiencies		
$\eta_{energy,fuels}$	34.79 %	32.84 %
ton_{CO_2}/ton_{fuel}	2.4	3.2

4.3. Scenario conclusion

During a year the system will fluctuate between the two described scenarios, depending on the available renewable electricity. Calculated thermal efficiencies and CO_2 emissions are more advantageous in scenario 1, because syngas is produced in a cleaner process. On the other hand, much more electricity is required. Final size and capacity of components in the process are based on the scenarios. Scenario 1 will determine the stack size of the PEM electrolyzer and maximum electricity production capacity from solar/wind power.

Scenario 2 on the other hand determines the size of the biomass gasifier and downstream gas cleaning units. From the FT reactor and further downstream, both scenarios have similar results.

The gasifier will have a length of 7.3 meter with a diameter of 4.1 meter, reaching a biomass capacity of approximately 100 ton/h. To reach the desired hydrogen production by PEM electrolysis, a stack of 93 electrolyzers is needed. Similarly, a DAC plant with a capacity of almost 40 ton/h is needed. In order to meet the maximum electricity demand of 342 MW, solar and wind have to supply 171 MW each. Required land-area for solar PV can be calculated according to Equation 4.3.

$$A = \frac{P_{Wp}}{PSI * \eta_{PV}} \tag{4.3}$$

Where the required area (A) depends on required power (P_{Wp}), Peak Sun Insolation (PSI) and solar panel efficiency (η_{PV}). PSI for The Netherlands can be equal to 1000, with a solar panel efficiency of 20% results in a total area required equal to $0.855 km^2$ [39].

In order to calculate the number of wind turbines required and consequently land-area, the single power output of a turbine has to be determined. Large wind turbines, especially offshore, are nowadays

10 MW. Leading to approximately 17 wind turbines to meet the electricity demand. Following the rules of thumb, a wind farm design as shown in Figure 4.1 is assumed [104]. Whereby the two additional turbines are placed in the first two rows. Rotor blades for 10MW turbines can have different diameters, depending on the design company. When the 10MW turbine from DTU [128] is assumed, the total rotor diameter is 178.3m. This would at least need an area equal to 1250m*2850m, equivalent to $3.6km^2$. Note, more designs will suffice, but required area will be similar.

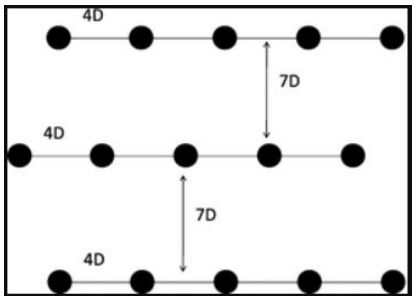

Figure 4.1: Wind farm layout for 15 turbines, following the rules of thumb [104]

The oxygen net flow represents the sum of oxygen production by PEM electrolysis and consumption by the gasifier.

If the solar and wind pattern of Figure 2.3 can be assumed, most renewable electricity will be produced in May. On the other hand, December obtains the lowest production of renewable electricity. These conclusions can be drawn when installed solar/wind ratio is 50/50. When assuming scenario 1 and 2 as best and worse case scenarios, on monthly average there will be no shortage of oxygen. This is beneficial since daily storage requires far less oxygen capacity than monthly storage.

A day where scenario 2 is dominant is required to determine the storage capacity, which turns out to be in December. On energieopwek.nl [7] the daily solar and wind production is written down. Up to 10GW of renewable electricity can be produced during peak times in May, compared to only 2GW on days in December. This results in oxygen shortage throughout the day equivalent to 400-500 tons of oxygen. Storage of oxygen usually takes place in liquid stage, because density increases and consequently volume decreases. For 400-500 tons of oxygen a storage capacity of $300 - 400m^3$ is required. Since these shortages can last longer than a day, it is recommended to install a larger storage capacity. However storage capacity this size is not commercially available, maximum capacity for commercial storage is up to $70m^3$. Placing multiple smaller tanks instead of one large storage tank can be an alternative. An elaborated analysis on monthly and daily basis can be found in Appendix G.

5 Cost analysis

This chapter calculates the capital costs (Section 5.1) and operational costs (Section 5.2) using results obtained in Chapter 4. These costs are required to calculate the average fuel price in Section 5.3. An estimation is made for 2030 and 2050 to examine future feasibility of the project in Section 5.4.

Economical feasibility is besides technical feasibility important to determine the attractiveness of a project. This chapter will make a rough estimation for the total costs of the process. Total cost data is based on component level, obtained from literature. Total costs of the components are multiplied with specific percentages to calculate final installed costs. Capacity affects the costs for a component, hence a scaling component R is used to scale capacities according to Equation 5.1 [124].

$$\frac{Costs_b}{Costs_a} = (\frac{Size_b}{Size_a})^R \tag{5.1}$$

Finally, most costs from literature data is historical data and based on previously built plants, therefore the costs are scaled to 2020 according to the Chemical Engineering Plant Cost Index (CEPCI).

Projected cost in year n depend on a year m with index value I_m and cost C_m (Equation 5.2) [77].

$$C_n = \frac{I_n}{I_m} * C_m \tag{5.2}$$

Shown model capacities are obtained from the energy and mass balances from the Aspen Plus model. The largest value from both scenarios for each component is applied to determine the maximal required capacity.

Removal processes for particulate matters, cyclone, baghouse filter and condensing scrubber, are taken into account for the cost analysis while not integrated in the Aspen Plus model. Storage facilities placed at the airport today are assumed as storage for this new plant and therefore ignored in the cost analysis. Final installation costs are still very uncertain and come with an uncertainty range of approximately ±30%.

5.1. Capital costs

Two different cases are distinguished by determining the total installation costs and operating costs. In case *'with electricity production'* the cost for wind turbines and solar panels is included. Total CAPEX becomes 1.075 billion euros (Table 5.1), where solar and wind power contribute to almost 50%. Another significant fraction is formed by engineering, fees and start-up costs. Considering the two production methods, biomass gasification covers approximately 10% of the costs while PEM and DAC reach 15%. Although, solar and wind power is part of the latter hence this method is dominating the CAPEX.

The second case *'without electricity production'* ignores wind turbines and solar panels, because it contributes to a large fraction and the system can work without this part. Presumed that required electricity is taken from the grid and is part of the OPEX. Total CAPEX reduced to 408 M€, more than halved because engineering etc. also decreased. Costs for other components remained the same as the other case.

Table 5.1: Total installation costs, inflation is taken into account when determining base and final costs [98] [124] [125] [136]

	Base scale[a] [MW_{th} LHV]	Base cost [a] [MUS$]	Scale factor	Model scale [a] [MW_{th} LHV]	Costs [M€]
Pre-treatment					
Storage	69.54	1.35	0.65	493	4.7
Iron removing	69.54	0.42	0.7	493	1.6
Conveyers	69.54	0.42	0.8	493	2.0
Grinding	69.54	0.55	0.6	493	1.8
Feeding system	69.54	3.45	1	493	3.4
IGT Gasifier	400 MW_{th} HHV	51.0	0.7	493	43.9
Gas conditioning					
Cyclone	69.54	3.78	0.7	493	0.01
Baghouse filter	69.54	2.38	0.65	493	7.3
Condensing scrubber	69.54	3.78	0.7	493	12.8
Tar removal process[b]					15
Rectisol process[b]					18
PEM electrolyzer	1 kW	875 €/kW	1	110 MW	95
DAC	1.000.000 ton_{CO_2}	200M€	1	300.000 ton_{CO_2}	60
RWGS	2400 kmol/h	0.66	0.6	3036 kmol/h	0.6
FT reactor	100 MW_{th}	24.54	1	70	14.8
SMR	400 MW_{th}	44.52	0.7	15	3.9
Distillation	150 m^3/h	0.27	1	2250 m^3/h	3.6
Hydrocracker	4.1 ton/h	9.3	0.55	2.5	6.0
Compressors	13.2 MW_e	17.63	0.85	10.8	12.8
Pumps	0.14 MW	0.12	1	0.08	0.1
Heaters	0.27 MW	0.10	1	21	6.4
Flash separators	1 MW	0.22	1	8	1.5
Heat exchangers[c]		105$/$m^2$	1	10.469m^2	0.9
Electricity production					
Wind turbine		2M€/MW	1	171 MW	342
Solar panels		1M€/MW	1	171 MW	171
Engineering[d]	15% of investment costs				121.5
Fees/overheads/profits	10% of total investment				82.9
Start-up costs	5% of total investment				41.5
	with electricity production			**Total costs**	**1075**
	without electricity production			**Total costs**[e]	**408**

[a] Units are similar in this column for all components unless mentioned upon.
[b] Price is an estimation based on [124] [136]. Cost for Rectisol is higher because cooling network is required.
[c] Heat transfer coefficient in W/m^2K for HX-OLGA=1420 [116], HXSYN=850 [116] HX1-PEM/HX2-PEM=370 [5], HXFT=11.3 [5]
[d] Engineering is already included in costs for FT reactor, SMR and RWGS.
[e] Also reduced by *engineering/fees.../start-up costs* for electricity production.

5.2. Operational costs

Operating costs are build up from depreciation and expenses, calculated on yearly basis. The two aforementioned cases are treated separately, even as the described scenarios. At first, case *'with electricity production'* where scenario 1 is found to be more attractive than scenario 2. Depreciation and maintenance costs contribute to 85M€, hence the majority of OPEX is determined by material expenses (Table 5.2). Methanol and biomass are dominant factors covering 50% or more of OPEX, especially for scenario 2 where biomass gasification is dominant.

Secondly, in case *'without electricity production'* total OPEX is higher than previously mentioned case. Depreciation and maintenance costs diminished drastically, but do not compensate for higher electricity costs. In scenario 2 electricity demand is minimal hence the effect of electricity costs decreases, resulting in lower OPEX than scenario 1 and a smaller difference between the two described cases. But in total, case *'with electricity production'* is more attractive than case *'without electricity production'*.

Table 5.2: Operational expenditures (OPEX) [32] [51] [124]

	Base cost	Model scale		Costs [M€/y]	
		Scenario 1	Scenario 2	Scenario 1	Scenario 2
With electricity production					
Yearly depreciation[a]	5% of investment			53.8	53.8
Maintenance	3% of investment			32.3	32.3
Personnel[b]	0.7 M€/100MW$_{th}$ LHV			2.8	2.8
Waste water treatment	0.21 M€/75MW$_{th}$ LHV	99 MW	171 MW	0.3	0.5
Biomass	135 €/t	377 kt/y	867 kt/y	50.9	117.0
Oil	437 €/t	84797 t/y	70080 t/y	37.1	30.6
Methanol	350 €/t	173448 t/y	251412 t/y	60.7	88.0
Process water	0.68 €/m^3	1007400 m^3/y	595680 m^3/y	0.7	0.4
			Total	**238.6**	**325.4**
Without electricity production					
Yearly depriciation[a]	5% of investment			20.4	20.4
Maintenance	3% of investment			12.2	12.2
Personnel[b]	0.7 M€/100MW$_{th}$ LHV			2.8	2.8
Waste water treatment	0.21 M€/75MW$_{th}$ LHV	99 MW	171 MW	0.3	0.5
Biomass	135 €/t	377 kt/y	867 kt/y	50.9	117.0
Oil	437 €/t	84797 kt/y	70080 kt/y	37.1	30.6
Methanol	350 €/t	173448 kt/y	251412 kt/y	60.7	88.0
Process water	0.68 €/m^3	1007400 m^3/y	595680 m^3/y	0.7	0.4
Electricity	0.07 €/kWh (2020) [1]	2987 GWh	1077 GWh	209.1	75.4
			Total	**394.2**	**347.3**

[a] Depreciation period = 20 years
[b] A scaling factor of 0.25 is used

5.3. Average fuel price

An important parameter to determine the economic feasibility of a project is cash flow, as defined in Equation 5.3.

$$CF_j = S_j - E_j \tag{5.3}$$

The cash flow for a year j (CF_j) is the total income (S_j) minus the expenses (E_j). To determine the final fuel costs and obtain a $CF \geq 0$, it is assumed that gasoline, diesel, waxes and kerosene all have an economical value, regardless of their quality or average carbon number. OPEX assumes a depreciation period of 20 years, causing the installation costs paid off completely after 20 years. To generate revenue, an average fuel price of at least $1.74€/kg$ or $2.24€/kg$ for scenario 1 respectively 2 should be applied, when electricity production is taken into account. If electricity is taken from the grid, average fuel prices of $2.87€/kg$ and $2.39€/kg$ are required for scenario 1 and 2. It can be observed that for both scenarios the case that integrated electricity production in the network seems to turn out best. Calculated average fuel price of this study exceeds the 1.54€/kg for conventional fuels (2018) [4].

Compared to other research studies, calculated fuel prices within this research are usually more expensive. Tijmensen et al. [124] reported fuel prices of 13-30€/GJ for FT-liquids, where this study varies between 39-64€/GJ for all cases (Table 5.4). Shivananda and Dasappa [11] made an overview of multiple research studies and found fuel prices between 0.50€/kg and 2.00€/kg for different types of biomass. Dieterich et al. [40] reported production costs of 1.60-3.50€/kg for fuels produced by biomass gasification or carbon capture. These prices coincide with results found in this research study. A reason for higher fuel prices can be the integration of two production methods, whereby only one is running on full load. Biomass gasification functions as back-up when renewable electricity production is low, resulting in a lower capacity factor for the gasifier. But costs, especially depreciation costs for the gasifier and gas cleaning equipment, are made leading to an increased fuel price.

5.4. Future cost estimation 2030 and 2050

In the last decades huge developments have been made in technologies used within this process. Table 5.3 shows future cost estimations for 2030 and 2050. These estimations are also relevant because large-scale projects depending on multiple players can take years before the actual start of construction. Components not mentioned in the table are assumed to remain fixed at the 2020 value.

The reduced costs affect the total installation cost of the production facility. Yearly depreciation costs in OPEX will subsequently decrease, resulting in lower fuel prices. Adapted CAPEX, OPEX and fuel prices for 2030 and 2050 are shown in Table 5.4.

Table 5.3: Future cost estimations in 2030 and 2050 [24] [46] [59]

	Base	2030	2050
DAC [€/kW]	200	105	55
PEM [€/kW]	1000	250-1270 (750)	130-307
Wind turbine			
Onshore [€/kW]	1350 (2018)	720-1215	585-900
Offshore [€/kW]	2250	1530-2880	1260-2520
Solar panel [€/kW]	1000	660	370

Reduced costs for 2030 and 2050 all affect the CAPEX and subsequently OPEX by reduced costs for depreciation and maintenance. Fuel price has decreased around 0.25€/kg between 2020 and 2050 for case *'with electricity production'* compared to only 0.09€/kg in case *'without electricity production'*. Integrating electricity production was already more attractive for the 2020 case, but the price difference between the cases increases with time.

Still, future average fuel prices are relatively high compared to prices from conventional fuel. But expected increase on carbon tax can potentially reduce the gap between conventional and synthetic kerosene [65].

Considering wind turbines, they are expected to increase to 15-20MW in two decades. Capacity factors will also increase, 30-55% in 2030 or 32-58% in 2050 compared to 34% in 2018 for onshore turbines. Offshore reached 43% in 2018 and might increase to 36-58% in 2030 or 43-60% in 2050 [59]. Predicted future cost for wind power in CAPEX is based on the average price of on- and offshore turbines. If, finally, only offshore turbines will be applied fuel price will increase slightly. Exclusively onshore turbines results in lower fuel prices.

Table 5.4: CAPEX, OPEX and fuel price estimations for 2030 and 2050

	Scenario 1			Scenario 2		
	2020	2030	2050	2020	2030	2050
With elec. production						
CAPEX [M€]	1075.1	855.3	649.5	1075.1	855.3	649.5
OPEX [M€/y]	238.6	220.9	204.5	325.2	307.7	291.3
Fuel price [€/kg]	1.74	1.61	1.49	2.24	2.12	2.00
Fuel price [€/GJ]	39	36	33	50	47	44
Without elec. production						
CAPEX [M€]	425	340.1	255.3	425	340.1	255.3
OPEX [M€/y]	394.2	388.8	382.0	347.3	341.9	335.1
Fuel price [€/kg]	2.87	2.83	2.78	2.39	2.35	2.30
Fuel price [€/GJ]	64	63	62	53	52	51

5.5. Sensitivity analysis

Fuel prices are, based on CAPEX and OPEX, highly determined by PEM, DAC, wind/solar power, biomass, methanol and electricity price. Effect of the three first mentioned factors is examined in Section 5.4. Biomass, in this research study wood pellets, is an essential feedstream and will undergo market changes the coming decades due to increased interest in biomass. Methanol market is also highly sensitive for the world economy and forms a significant fraction of the OPEX. DAC and PEM costs are highly dependent on the electricity price, that is influenced by the growing renewable electricity supply. A sensitivity analysis is performed for each factor to determine the effect on the average fuel price.

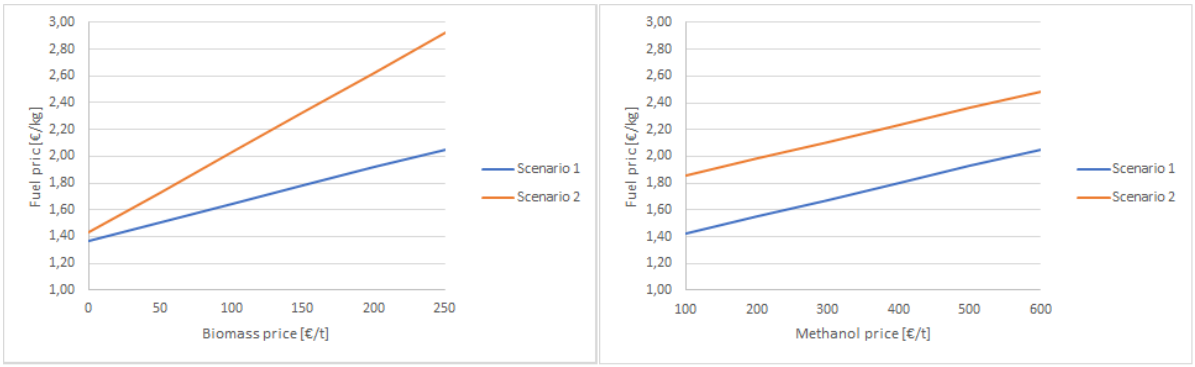

(a) (b)

Figure 5.1: Calculated average fuel price for different biomass (a) and methanol (b) price for the case *'with electricity production'*. Other parameters are fixed and established as reported earlier.

5.5.1. Biomass

Besides changing market conditions for wood pellets, changing to another biomass source will also influence the OPEX. Therefore it was decided to perform a sensitivity analysis on the biomass price to examine the effect on the fuel price (Figure 5.1a). Fuel price is doubled and reaches 2.92 €/kg for a biomass price of 250 €/ton in scenario 2. This increase is milder for scenario 1, where biomass contributes to a much smaller fraction in the OPEX.

5.5.2. Methanol

Methanol is mainly the second highest cost item in OPEX. The price for methanol strongly depends on the world economy. Previous events like Gulf War and financial crises dropped methanol prices drastically [58]. In Figure 5.1b methanol price is varied between 100 and 600 €/ton. It can be observed that within this range the fuel price differs 0.70 €/kg maximum. When methanol price is reduced to 100 €/kg, the average fuel price becomes 1.42 €/kg for scenario 1 or 1.85 €/kg for scenario 2. The price difference of approximately 0.40 €/kg is a result of the higher methanol consumption in scenario 2.

5.5.3. Electricity

Electricity prices can fluctuate the coming decades and contributes to a large fraction of the OPEX. Especially in the case *'without electricity production'* where electricity is taken from the grid. It is observed that the fuel price fluctuates between 1.30 and 3.70 €/kg for scenario 1 where DAC and PEM are operating on full load (Figure 5.2). For scenario 2 the price difference is less because electricity contributes to a smaller fraction in the OPEX. In addition, when electricity price exceeds 0.04 €/kWh the second scenario shows lower fuel prices. Electricity price will strongly determine the feasibility of this project.

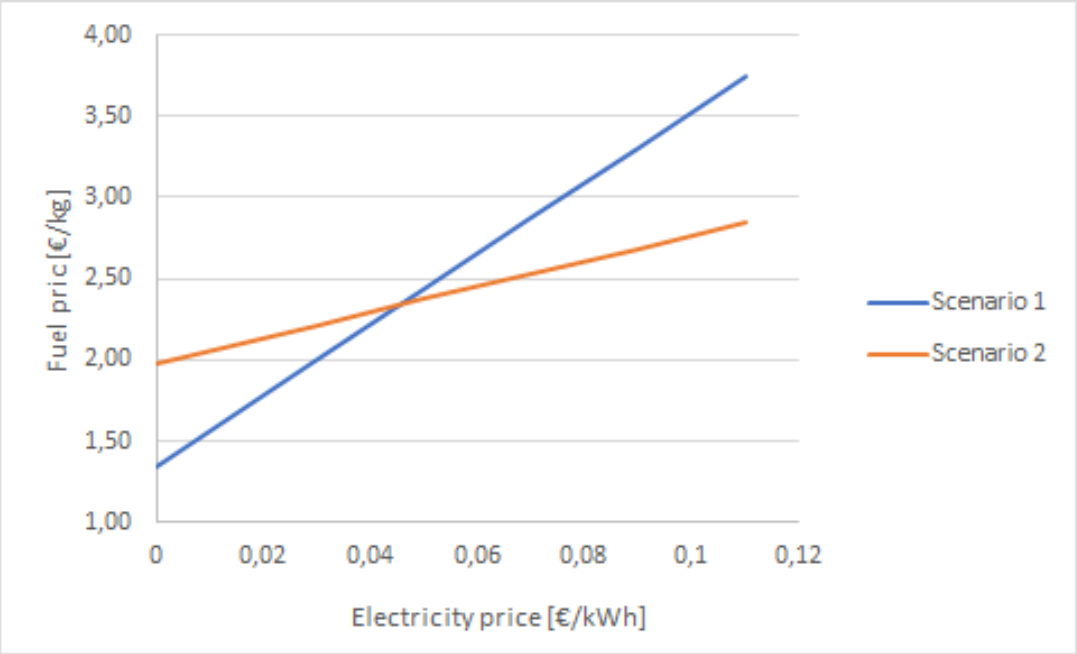

Figure 5.2: Calculated fuel price for different biomass price for the case *'without electricity production'*. Other parameters are fixed and established as reported earlier.

5.6. Discussion

- A RWGS reactor is not required after the gasifier to obtain the H_2/CO ratio. But changing conditions of the gasifier affects this ratio, after which a RWGS might be necessary to meet the ratio. No RWGS decreases flexibility of the system but has a positive effect on the CAPEX.

  Same holds for the biomass gasifier, the calculated capacity is relatively high. Two smaller gasifiers with lower capacity instead of one with a high capacity is an alternative. It will increase reliability of the model, in case of failures, but increases the CAPEX.

- Separating CO_2 from H_2S is a cost and energy intensive process, but might be promising [124]. Initially, adding this separation step will increase the CAPEX. But pure CO_2 can be fed to the RWGS reactor instead of feeding CO_2 from the DAC plant. This will decrease the required capacity of DAC plants and consequently CAPEX. But the purity of CO_2 from the CO_2/H_2S separator is probably less than CO_2 obtained from the DAC plant. Therefore further research is recommended to explore this alternative.

- Kerosene is easy to store and transport. This research study assumes a constant production of kerosene resulting in a total of 50.000 ton/y. The most renewable production method is by water electrolysis and DAC. But biomass gasification is added to remain a constant production. Another approach can be to increase kerosene production during peak electricity production and store the kerosene. Syngas by biomass gasification can be minimized and so will CO_2 emission. Dynamic range of components present in the model have to be investigated to determine the feasibility of this alternative approach.

- CO_2 taxes are not taken into account for the cost analysis. This would increase the OPEX, especially for the biomass gasification where CO_2 is emitted. CO_2 taxes are estimated to increase coming decade, making the electrolysis process more attractive [65].

- CAPEX for wind turbines is strongly dependent on multiple factors and may even increase. Placing wind parks further offshore and in deeper water increases costs for foundations and grid connection. Raw material prices also increase, steel and copper prices for example significantly increased the last decades. At last, competition between turbine suppliers is limited which causes higher prices than estimated [63].

- This research study makes use of purely wood pellets with low moisture content, hence a dryer is not required. But when other types of biomass or feed streams become promising, it is plausible that moisture content is too high. Flexibility of the gasifier will be increased when adding a dryer, but would cost approximately $47M€$ [124].

- Obtained gasoline fraction does not meet the gasoline specifications yet. Aromatic content is low and oxygenates must be removed before use. Some problems can be resolved after blending. But additional steps downstream are recommended to meet the gasoline specifications.

6

Conclusion

The main objective of this research study was to investigate the technical and economical feasibility of large scale synthetic kerosene production, for Rotterdam-The Hague Airport. Due to intermittent renewable electricity supply, biomass gasification is integrated besides water electrolysis to fill up shortcoming of syngas production. A constant kerosene production is realized by a combination of the two aforementioned methods.

From the literature study it was concluded that Fischer-Tropsch process is most suitable to produce kerosene. Two different scenarios were sketched to represent periods of low and high renewable electricity production respectively. An Aspen Plus model was created and validated with corresponding literature data to establish the validity of the model.

The two scenarios were implemented to predict and analyze the model results. For each scenario results were generated according to the KPIs: required electricity production, biomass, produced/consumed oxygen, CO_2 emission and energy efficiency. Finally, a (future) cost analysis was performed to calculate CAPEX, OPEX and the average fuel price. The results are used to get a better understanding of the system and to explore the opportunities and bottlenecks.

At the beginning of the research one key question was consolidated, together with six sub-questions. This research study is concluded by answering the sub-questions and finally the main research question.

- **What are the bottlenecks in the system, based on an economical and technical feasibility study?**
  At first the economical bottlenecks. In Chapter 5 a thorough cost analysis has been made to give a clear vision of the CAPEX, OPEX and average fuel price. Biggest contributor (48%) to the installation cost were wind and solar power, followed by PEM electrolysis and DAC plants. But costs for aforementioned components undergoes rapid developments leading to lower costs in the future. Hence the contribution of these components will decrease in time, but remain dominant.

  Regarding the average fuel price, CAPEX and OPEX have to decrease to make this process profitable. Fuel prices of 1.74-2.87€/kg are observed for 2020, decreasing to 1.61-2.83€/kg in 2030 and 1.49-2.78€/kg in 2050. Highest prices belong to the case *'without electricity production'*, where wind/solar power is not integrated in the system and electricity comes from the grid. Currently the calculated average fuel price lies above market price, making the project less attractive. But if taxes increase for conventional fuel and renewable projects are subsidized, synthetic fuels becomes more attractive and the process more feasible.

  At last, PEM electrolysis is not yet economically attractive. Most RD projects focus on increasing operating current density (to reduce CAPEX) and improve efficiency (to reduce OPEX). Carbon tax can increase electrolysis interest even more in the future [49].

Technical bottlenecks for PEM electrolysis comprises of membranes, catalysts, mass transport effects, current density distribution with low catalyst loadings and more. These challenges need to be overcome when increasing production to MW scale [34].

DAC faces similar challenges for scaling up. Currently few pilot plants are built. But the relatively high cost make large scale plants still challenging. In technical perspective, DAC plants have a high water and energy consumption. Mostly heat provided is derived from fossil fuels, although this can be resolved by waste heat from the process.

Another technical bottleneck is oxygen storage. However, this will be explained in another sub-question down below.

- **What are the total costs of the production plant?**
  The total costs of the production plant are strongly dependent on electricity supply. This system including the costs for solar panels and wind turbines comes with a total cost of $1075M€$. When they are not integrated and added to operational costs taking electricity from the grid, total installation costs decrease with more than $500M€$ to $408M€$.

- **How much electricity and consequently land-area is required for electricity production? And how will this be subdivided between solar and wind?**
  From Chapter 4 it can be found that at peak moments electricity demand becomes 342 MW. In order to determine land-area and wind/solar ratio, further research and communication with the airport and municipal is recommended. Wind turbines can not be placed nearby runways, hence for placing wind turbines the airport is highly dependent on other players. Solar panels may be placed on airport buildings or elsewhere. Since realising large-scale renewable projects is complex and no communication has taken place with other players within this research, no clear ratio can be determined and therefore it is assumed that wind/solar ratio is 50/50. An estimation is made for the required land-area, which resulted in an area equal to $0.9km^2$ for solar panels and $3.6km^2$ for a wind farm. To note, area for the wind farm is calculated for 10MW turbines.

- **How much CO_2 capture is required?**
  Based on the two scenario analyses, scenario 1 showed the highest demand of CO_2. A maximum capacity of approximately 40 ton/h or 350.000 ton/y is required. Optionally, the CO_2 emitted by the gasification process may be used. But, as mentioned in Chapter 3, separating CO_2 from H_2S is very cost and energy intensive. On the other hand, recycling CO_2 reduces the number of DAC units required.

- **How many useful side-products are produced in the system?**
  The main objective of this system is kerosene production (53.000 ton/y), but other fractions are also retrieved from the process. Gasoline (39.000 ton/y) and diesel (23.000 ton/y) are side-products applicable in other types of transportation found at the airport. Waxes (26.000 ton/y) are applied in other markets and industries. The project becomes more feasible when side-products can make a financial contribution.

- **Is there enough oxygen, derived from the water electrolyzer, available for biomass gasification? And which storage capacity is required?**
  Based on the analyses about oxygen production and consumption in Appendix G, several conclusions can be drawn. At first, over a year more oxygen is produced than consumed. Resulting in enough oxygen to meet the demand of the gasifier. Secondly, on a monthly basis on average more oxygen is produced than consumed except January and December. Although, during these winter months shortage only occurs for days and not throughout the month. This means that seasonal storage is not required, hence only shortages resulting from days with low renewable electricity production have to be covered.

  Assuming one day of low electricity supply will result in a shortage of 450 ton, equivalent to approximately $350m^3$ when stored as LOX. Since consecutive days with shortage is highly plausible, more storage capacity is advised. Storage tanks in this order of magnitude are found in literature theoretically [56], but are practically difficult to realise. More realistic capacities are at maximum $70m^3$. An alternative can be to install multiple smaller storage tanks.

- **Is it feasible for Rotterdam-The Hague Airport to produce synthetic kerosene by water electrolysis with DAC and biomass gasification given the intermittent supply of electricity?**

  This research intended to make a clear techno-economic analysis to investigate the feasibility of this project. The sub questions already discussed important subjects required to formulate a comprehensive answer to the research question.

  The combination of two different production methods to obtain syngas and remain a constant kerosene production was found promising. Biomass gasification is a mature technology and the capacity required in this study (100 ton/h) for gasification and gas cleaning downstream will not cause difficulties. The wood pellet market is developing fast and the Port of Rotterdam is an important transit location, making it an attractive location for biomass gasification. On the other hand, sustainability of the biomass can be questionable. The CO_2 captured by trees will eventually be released again when kerosene is consumed. Hence the biomass source is also important to determine the sustainability. But integrating biomass gasification in a system depending on intermittent electricity supply is a reliable alternative to maintain constant syngas and kerosene production.

  Capacity required for PEM electrolysis and DAC is technically and economically more difficult. Electrolysis stacks for large scale H_2 production need to overcome certain challenges, as described in the first sub question, before it is technically and economically attractive. DAC technology is not yet mature and only available for small scale applications. They contribute to a large fraction of CAPEX and OPEX, resulting in an average fuel price of 1.74-2.78€/kg. But expected technical and economical improvements in the coming decades will reduce the average fuel price to 1.49-2.78€/kg in 2050. Hence, the price gap between conventional kerosene and synthetic kerosene can be overcome, a requirement to make this project feasible. Expected increase of carbon taxes will also reduce the price gap. So the feasibility of this project will increase in time, when new technologies have become more mature and economically attractive.

6.1. Recommendations

- CO_2 capture can be done by several methods. This research study applies an amine-based method. Aspen Plus is an appropriate program to model DAC. Integrating the DAC plant will optimise and extent the model. Process fluctuations and consequently changing mass and energy balances give a more precise estimation.
- The hydrocracker within this system is modelled easy and does not take changing operating conditions and changing inlet flow compositions into account. Even as the DAC plant, optimising the hydrocracker will optimise the total system.
- More research on $CO_2 - H_2S$ removal, due to low relative volatility of CO_2 and H_2S at high CO_2 concentrations it is very difficult to separate the two components. On the other hand, DACs require also energy/electricity to obtain CO_2. Therefore further research is recommended to find out which method is more profitable. It will also reduce the costs for CO2 tax.
- Aspen Plus is a steady state analysis program. But renewable electricity comes with fluctuations on small timescales and therefore dynamic analyses will finally be necessary to examine the behavior on daily or even hourly basis.
- Ambitious plans for the coming decades are launched to build pipeline networks for CO_2 and H_2. Since these components form a key in the production process, these future plans can be promising [37]. Although the project loses some independence, reliability of the process can potentially be improved.
- Different configurations for the process can be examined to optimise system performance. At first, the hydrocracker is placed after the distillation phase. But another setup can be to place the hydrocracker before the distillation phase. By separating the heavy waxes on forehand and crack them, and subsequently mix with the lower hydrocarbons.

  Secondly, the product stream of the SMR contains a high amount of CO_2. This is unfavorable for the performance of the FT reactor. An alternative can be to redirect the stream to the H_2S/CO_2 removal process. CO_2 and other heavy compounds will be removed from the stream and a purer syngas stream arrives at the FT reactor. On the downside, capacity of the H_2S/CO_2 remover needs to increase seriously. This increases installation costs for the removal process and operating costs regarding DEA.
- Adding a dryer to make use of other sources of biomass as well. Pellets have low moisture content, but if the biomass source is taken broader there will be sources with higher moisture content whereby drying is required. CAPEX will increase.
- Bed materials can enhance the product gas quality. This research study uses quartz sand as bed material, which is inert. But other bed materials can potentially absorb CO_2, H_2S and NH_3 leading to higher quality product gas. In addition, gas cleaning downstream may become less complicated. On contrary, these bed materials require other process steps, increasing CAPEX and OPEX, before it can be recycled. Potentially the most attractive bed materials are dolomite $(CaMg(CO_2)_3)$, calcites $(CaCO_3)$, magnesites $(MgCO_3)$ and olivines $((Mg, Fe)_2SiO_4)$. They reach significant activity at high temperatures and are non-toxic [113]. Promising bed materials will face problems, some are not tested on large scale plants, and require thorough research but can potentially optimise the gasifier performance.

Bibliography

[1] Aardgas en elektriciteit, gemiddelde prijzen van eindverbruikers. https://opendata.cbs.nl/statline/#/CBS/nl/dataset/81309NED/table?fromstatweb. Accessed: 2021-07-5.

[2] Hoe gaat rotterdam de CO-2 uitstoot van de scheepvaart reduceren? https://www.duurzaambedrijfsleven.nl/logistiek/30021/co2-uitstoot-haven-rotterdam. Accessed: 2020-10-14.

[3] Phyllis classification. https://phyllis.nl/Browse/Standard/ECN-Phyllis. Accessed: 2021-01-21.

[4] Transport fuel prices and taxes in Europe. https://www.eea.europa.eu/data-and-maps/indicators/fuel-prices-and-taxes/assessment-4. Accessed: 2021-08-10.

[5] Fluid heat transfer coefficients - heat exchanger surface combinations. https://www.engineeringtoolbox.com/overall-heat-transfer-coefficients-d_284.html. Accessed: 2021-07-1.

[6] Wind energy in The Netherlands. https://community.ieawind.org/about/member-activities/netherlands. Accessed: 2021-01-11.

[7] Real-time dagelijkse productie van duurzame elektriciteit. https://energieopwek.nl/. Accessed: 2021-07-6.

[8] Sustainable aviation fuel market 2021 analyzed in a new research study|Gevo, World Energy, Eni, SkyNRG, Fulcrum Bioenergy. https://www.mccourier.com/sustainable-aviation-fuel-market-2021-analyzed-in-a-new-research-study\-gevo-world-energy-eni-skynrg-fulcrum-bioenergy/. Accessed: 2021-01-10.

[9] Rotterdam The Hague Innovation Airport. https://www.stichtingrhia.nl/. Accessed: 2020-10-8.

[10] L. Abdelouahed, O. Authier, G. Mauviel, J. Corriou, G. Verdier, and A. Dufour. Detailed modeling of biomass gasification in dual fluidized bed reactors under Aspen Plus. *Energy & fuels*, 26(6): 3840–3855, 2012.

[11] S.S. Ail and S. Dasappa. Biomass to liquid transportation fuel via Fischer–Tropsch synthesis–technology review and current scenario. *Renewable and sustainable energy reviews*, 58:267–286, 2016.

[12] M. Asadullah. Biomass gasification gas cleaning for downstream applications: A comparative critical review. *Renewable and sustainable energy reviews*, 40:118–132, 2014.

[13] H. Atashi and F. Rezaeian. Modelling and optimization of Fischer–Tropsch products through iron catalyst in fixed-bed reactor. *International Journal of Hydrogen Energy*, 42(23):15497–15506, 2017.

[14] M.H. Azami and M. Savill. Comparative study of alternative biofuels on aircraft engine performance. *Proceedings of the Institution of Mechanical Engineers, Part G: Journal of Aerospace Engineering*, 231(8):1509–1521, 2017.

[15] J. Bao, W. Lu, J. Zhao, and X.T. Bi. Greenhouses for CO2 sequestration from atmosphere. *Carbon Resources Conversion*, 1(2):183–190, 2018.

[16] A. Baroutaji, T. Wilberforce, M. Ramadan, and A.G. Olabi. Comprehensive investigation on hydrogen and fuel cell technology in the aviation and aerospace sectors. *Renewable and Sustainable Energy Reviews*, 106:31–40, 2019.

[17] D.A. Bell, B.F. Towler, and M. Fan. *Coal gasification and its applications*. William Andrew, 2010.

[18] J.C. Beltrán-Prieto and K. Kolomazník. Use of approximate methods to determine minimum reflux ratio in distillation process. In *MATEC Web of Conferences*, volume 292, page 01050. EDP Sciences, 2019.

[19] R.J. van Berge. Natural gas conversion IV. *Studies in Surface Science and Catalysis*, 107: 207–212, 1997.

[20] J.M. Bermúdez, E. Ruisánchez, A. Arenillas, A.H. Moreno, and J.A. Menéndez. New concept for energy storage: microwave-induced carbon gasification with CO2. *Energy conversion and management*, 78:559–564, 2014.

[21] H. Boerrigter, M. Bolhár-Nordenkampf, E.P. Deurwaarder, T. Eriksson, J.W. Könemann, R. Rauch, S.V.B. Van Paasen, and J. Palonen. OLGA optimum. *Energy research Centre of the Netherlands, ECN-E–06-048*, 2006.

[22] A. Bogaerts and E.C. Neyts. Plasma technology: an emerging technology for energy storage. *ACS Energy Letters*, 3(4):1013–1027, 2018.

[23] M. Boosten. Biomassa verbruik en beschikbaarheid in Nederland. *Retrieved from http://www.biowkk.eu/wp-content/uploads/2017/04/6.-Martijn-Boosten-Probos-Biomassaverbruik-en-beschikbaarheid-in-Nederland. pdf.*, pages 20–12, 2017.

[24] C. Breyer, M. Fasihi, and A. Aghahosseini. Carbon dioxide direct air capture for effective climate change mitigation based on renewable electricity: a new type of energy system sector coupling. *Mitigation and Adaptation Strategies for Global Change*, 25(1):43–65, 2020.

[25] K.M. Broer, P.J. Woolcock, P.A. Johnston, and R.C. Brown. Steam/oxygen gasification system for the production of clean syngas from switchgrass. *Fuel*, 140:282–292, 2015.

[26] F.J. Campanario and F.J. Gutiérrez Ortiz. Fischer-Tropsch biofuels production from syngas obtained by supercritical water reforming of the bio-oil aqueous phase. *Energy Conversion and Management*, 150:599–613, 2017.

[27] M. Carmo, D.L. Fritz, J. Mergel, and D. Stolten. A comprehensive review on PEM water electrolysis. *International journal of hydrogen energy*, 38(12):4901–4934, 2013.

[28] W. Chen, T. Lin, Y. Dai, Y. An, F. Yu, L. Zhong, S. Li, and Y. Sun. Recent advances in the investigation of nanoeffects of Fischer-Tropsch catalysts. *Catalysis Today*, 311:8–22, 2018.

[29] J. Chi and H. Yu. Water electrolysis based on renewable energy for hydrogen production. *Chinese Journal of Catalysis*, 39(3):390–394, 2018.

[30] D. Chiaramonti, M. Prussi, M. Buffi, and D. Tacconi. Sustainable bio kerosene: Process routes and industrial demonstration activities in aviation biofuels. *Applied Energy*, 136:767–774, 2014.

[31] P. Chiesa. Advanced technologies for syngas and hydrogen (H2) production from fossil-fuel feedstocks in power plants. In *Advanced power plant materials, design and technology*, pages 383–411. Elsevier, 2010.

[32] I. Dafnomilis, G. Lodewijks, M. Junginger, and D.L. Schott. Evaluation of wood pellet handling in import terminals. *Biomass and Bioenergy*, 117:10–23, 2018.

[33] D. Daggett, R. Hendricks, and R. Walther. Alternative fuels and their potential impact on aviation. *National Aeronautics and Space Administration,NASA/TM*, 214365.5(49), 2006.

[34] N. Danilovic, K.E. Ayers, C. Capuano, J.N. Renner, L. Wiles, and M. Pertoso. (Plenary) challenges in going from laboratory to megawatt scale PEM electrolysis. *ECS Transactions*, 75(14): 395, 2016.

[35] R.M. de Deugd, F. Kapteijn, and J.A. Moulijn. Trends in Fischer–Tropsch reactor technology—opportunities for structured reactors. *Topics in Catalysis*, 26(1-4):29–39, 2003.

[36] J.B. DeCoste, M.H. Weston, P.E. Fuller, T.M. Tovar, G.W. Peterson, M.D. LeVan, and O.K. Farha. Metal–organic frameworks for oxygen storage. *Angewandte Chemie*, 126(51):14316–14319, 2014.

[37] CE Delft. Waterstofroutes nederland, 2018.

[38] L. Devi, K.J. Ptasinski, and F.J.J.G. Janssen. A review of the primary measures for tar elimination in biomass gasification processes. *Biomass and bioenergy*, 24(2):125–140, 2003.

[39] R.A. Diantari and I. Pujotomo. Calculation of electrical energy with solar power plant design. In *2016 International Seminar on Intelligent Technology and Its Applications (ISITIA)*, pages 443–446. IEEE, 2016.

[40] V. Dieterich, A. Buttler, A. Hanel, H. Spliethoff, and S. Fendt. Power-to-liquid via synthesis of methanol, DME or Fischer–Tropsch-fuels: a review. *Energy & Environmental Science*, 13(10): 3207–3252, 2020.

[41] O.Y.H. Elsernagawy, A. Hoadley, J. Patel, T. Bhatelia, S. Lim, N. Haque, et al. Thermo-economic analysis of reverse water-gas shift process with different temperatures for green methanol production as a hydrogen carrier. *Journal of CO2 Utilization*, 41:101280, 2020.

[42] H. Er-Rbib, C. Bouallou, and F. Werkoff. Production of synthetic gasoline and diesel fuel from dry reforming of methane. *Energy Procedia*, 29:156–165, 2012.

[43] R.L. Espinoza, A.P. Steynberg, B. Jager, and A.C. Vosloo. Low temperature Fischer–Tropsch synthesis from a Sasol perspective. *Applied Catalysis A: General*, 186(1-2):13–26, 1999.

[44] M. Fasihi, D. Bogdanov, and C. Breyer. Techno-economic assessment of power-to-liquids (PtL) fuels production and global trading based on hybrid PV-wind power plants. *Energy Procedia*, 99 (243-268):10th, 2016.

[45] M. Fasihi, O. Efimova, and C. Breyer. Techno-economic assessment of CO2 direct air capture plants. *Journal of cleaner production*, 224:957–980, 2019.

[46] Q. Feng, G. Liu, B. Wei, Z. Zhang, H. Li, H. Wang, et al. A review of proton exchange membrane water electrolysis on degradation mechanisms and mitigation strategies. *Journal of Power Sources*, 366:33–55, 2017.

[47] J. Fernandez De La Fuente. Application of microwave plasma technology to convert CO2 into high value products. *PhD thesis*, TU Delft, 2017.

[48] A.M. González, E.E.S. Lora, J.C.E. Palacio, and O.A.A. del Olmo. Hydrogen production from oil sludge gasification/biomass mixtures and potential use in hydrotreatment processes. *International Journal of Hydrogen Energy*, 43(16):7808–7822, 2018.

[49] S.A. Grigoriev, V.N. Fateev, D.G. Bessarabov, and P. Millet. Current status, research trends, and challenges in water electrolysis science and technology. *International Journal of Hydrogen Energy*, 45(49):26036–26058, 2020.

[50] G.H. Guvelioglu, P. Higginbotham, J.E. Palamara, G. Arora, D.L. Mamorsh, and K.S. Fisher. H2S Removal from CO2 by Distillation. In *Laurance Reid Gas Conditioning Conference, Norman: Oklahoma*, 2015.

[51] M.J. Haas, A.J. McAloon, W.C. Yee, and T.A. Foglia. A process model to estimate biodiesel production costs. *Bioresource technology*, 97(4):671–678, 2006.

[52] C.N. Hamelinck and A.P.C. Faaij. Future prospects for production of methanol and hydrogen from biomass. *Journal of Power sources*, 111(1):1–22, 2002.

[53] J. Han, Y. Liang, J. Hu, L. Qin, J. Street, Y. Lu, and F. Yu. Modeling downdraft biomass gasification process by restricting chemical reaction equilibrium with Aspen Plus. *Energy conversion and management*, 153:641–648, 2017.

[54] H.H. Haugen, B. Halvorsen, and M.S. Eikeland. Simulation of gasification of livestock manure with Aspen Plus. Conference: Proceedings of the 56th Conference on Simulation and Modelling (SIMS 56), 2015.

[55] H. Hofbauer, R. Rauch, G. Löffler, S. Kaiser, E Fercher, and H. Tremmel. *Six years experience with the FICFB-gasification process*. na, 2002.

[56] Y. Hu, A. Tewari, L. Varga, H. Li, and J. Yan. System dynamics of oxyfuel power plants with liquid oxygen energy storage. *Energy Procedia*, 142:3727–3733, 2017.

[57] M. Hupa, O. Karlström, and E. Vainio. Biomass combustion technology development–it is all about chemical details. *Proceedings of the Combustion Institute*, 36(1):113–134, 2017.

[58] G. Iaquaniello, G. Centi, A. Salladini, and E. Palo. Methanol economy: environment, demand, and marketing with a focus on the waste-to-methanol process. In *Methanol*, pages 595–612. Elsevier, 2018.

[59] IRENA. Future of wind, Deployment, investment, technology, grid integration and socio-economic aspects. *International Renwable Energy Agency*, 2019.

[60] Y. Ishimoto, M. Sugiyama, E. Kato, R. Moriyama, K. Tsuzuki, and A. Kurosawa. Putting costs of direct air capture in context. 2017.

[61] S.S. Jagtap. Evaluation of blended Fischer-Tropsch jet fuel feedstocks for minimizing human and environmental health impacts of aviation. In *AIAA Propulsion and Energy 2019 Forum*, page 4412, 2019.

[62] O.O. James, B. Chowdhury, M.A. Mesubi, and S. Maity. Reflections on the chemistry of the Fischer–Tropsch synthesis. *RSc Advances*, 2(19):7347–7366, 2012.

[63] M. Junginger, A. Louwen, N.G. Tuya, D. de Jager, E. van Zuijlen, and M. Taylor. Offshore wind energy. In *Technological learning in the transition to a low-carbon energy system*, pages 103–117. Elsevier, 2020.

[64] A. de Klerk. *Fischer-Tropsch Refining*. John Wiley Sons, Inc., 2012.

[65] R. Koelemeijer, J. Ros, C. Brink, M. Hekkenberg, P. Koutstaal, and B. Daniëls. *Effect kabinetsvoorstel CO2-heffing industrie*. PBL Planbureau voor de Leefomgeving, 2019.

[66] K.S. Lackner. Capture of carbon dioxide from ambient air. *The European Physical Journal Special Topics*, 176(1):93–106, 2009.

[67] F. Lau and R. Carty. Development of the IGT RENUGAS process. In *Intersociety Energy Conversion Engineering Conference*, page 4008, 1994.

[68] D. Leckel. Hydrocracking of iron-catalyzed Fischer-Tropsch waxes. *Energy & fuels*, 19(5):1795–1803, 2005.

[69] N.H. Leibbrandt, A.O. Aboyade, J.H. Knoetze, and J.F. Görgens. Process efficiency of biofuel production via gasification and Fischer–Tropsch synthesis. *Fuel*, 109:484–492, 2013.

[70] J. Li, G. Yang, Y. Yoneyama, T. Vitidsant, and N. Tsubaki. Jet fuel synthesis via Fischer-Tropsch synthesis with varied 1-olefins as additives using Co/ZrO2–SiO2 bimodal catalyst. *Fuel*, 171: 159–166, 2016.

[71] Z. Li, T. Yang, S. Yuan, Y. Yin, E.J. Devid, Q. Huang, D. Auerbach, and A.W. Kleyn. Boudouard reaction driven by thermal plasma for efficient CO2 conversion and energy storage. *Journal of Energy Chemistry*, 45:128–134, 2020.

[72] G. Liu, B. Yan, and G. Chen. Technical review on jet fuel production. *Renewable and Sustainable Energy Reviews*, 25:59–70, 2013.

[73] L. Liu, S. Das, T. Chen, N. Dewangan, J. Ashok, S. Xi, A. Borgna, Z. Li, and S. Kawi. Low temperature catalytic reverse water-gas shift reaction over perovskite catalysts in DBD plasma. *Applied Catalysis B: Environmental*, 265:118573, 2020.

[74] R. Luque, A.R. de la Osa, J.M. Campelo, A.A. Romero, J.L. Valverde, and P. Sanchez. Design and development of catalysts for Biomass-To-Liquid-Fischer–Tropsch (BTL-FT) processes for biofuels production. *Energy & Environmental Science*, 5(1):5186–5202, 2012.

[75] G. Marsh. Biofuels: aviation alternative? *Renewable Energy Focus*, 9(4):48–51, 2008.

[76] X. Meng. Biomass gasification: the understanding of sulfur, tar, and char reaction in fluidized bed gasifiers. *PhD thesis*, TU Delft, 2012.

[77] D. Mignard. Correlating the chemical engineering plant cost index with macro-economic indicators. *Chemical Engineering Research and Design*, 92(2):285–294, 2014.

[78] S. Modekurti, J. Eslick, B. Omell, D. Bhattacharyya, D.C. Miller, and S.E. Zitney. Design, dynamic modeling, and control of a multistage CO2 compression system. *International Journal of Greenhouse Gas Control*, 62:31–45, 2017.

[79] M. Mofarahi, Y. Khojasteh, H. Khaledi, and A. Farahnak. Design of CO2 absorption plant for recovery of CO2 from flue gases of gas turbine. *Energy*, 33(8):1311–1319, 2008.

[80] I.L. Motta, N.T. Miranda, R. Maciel Filho, and M.R.W. Maciel. Sugarcane bagasse gasification: Simulation and analysis of different operating parameters, fluidizing media, and gasifier types. *Biomass and Bioenergy*, 122:433–445, 2019.

[81] S. Mudhasakul, H. Ku, and P.L. Douglas. A simulation model of a CO2 absorption process with methyldiethanolamine solvent and piperazine as an activator. *International Journal of Greenhouse Gas Control*, 15:134–141, 2013.

[82] F. Müller-Langer, N. Dögnitz, C. Marquardt, A. Zschocke, T. Schripp, K. Oehmichen, S. Majer, N. Bullerdiek, A. Halling, D. Posselt, et al. Multiblend JET A-1 in Practice: Results of an R&D Project on Synthetic Paraffinic Kerosenes. *Chemical Engineering & Technology*, 43(8):1514–1521, 2020.

[83] K. Myöhänen, J. Palonen, and T. Hyppänen. Modelling of indirect steam gasification in circulating fluidized bed reactors. *Fuel Processing Technology*, 171:10–19, 2018.

[84] Engineering National Academies of Sciences, Medicine, et al. *Commercial aircraft propulsion and energy systems research: reducing global carbon emissions*. National Academies Press, 2016.

[85] Z. Navas-Anguita, P.L. Cruz, M. Martin-Gamboa, D. Iribarren, and J. Dufour. Simulation and life cycle assessment of synthetic fuels produced via biogas dry reforming and Fischer-Tropsch synthesis. *Fuel*, 235:1492–1500, 2019.

[86] M.B. Nikoo and N. Mahinpey. Simulation of biomass gasification in fluidized bed reactor using ASPEN PLUS. *Biomass and bioenergy*, 32(12):1245–1254, 2008.

[87] L.P.R. Pala, Q. Wang, G. Kolb, and V. Hessel. Steam gasification of biomass with subsequent syngas adjustment using shift reaction for syngas production: An Aspen Plus model. *Renewable Energy*, 101:484–492, 2017.

[88] J.E. Park, S.Y. Kang, S.H. Oh, J.K. Kim, M.S. Lim, C. Ahn, Y. Cho, and Y. Sung. High-performance anion-exchange membrane water electrolysis. *Electrochimica Acta*, 295:99–106, 2019.

[89] A.P. Payan, M. Kirby, C.Y. Justin, and D.N. Mavris. Meeting emissions reduction targets: a probabilistic lifecycle assessment of the production of alternative jet fuels. In *AIAA/3AF aircraft noise and emissions reduction symposium*, page 3166, 2014.

[90] L. Peters, A. Hussain, M. Follmann, T. Melin, and M.B. Hägg. CO2 removal from natural gas by employing amine absorption and membrane technology—A technical and economical analysis. *Chemical Engineering Journal*, 172(2-3):952–960, 2011.

[91] I. Petersen and J. Werther. Experimental investigation and modeling of gasification of sewage sludge in the circulating fluidized bed. *Chemical Engineering and Processing: Process Intensification*, 44(7):717–736, 2005.

[92] J.A. Petri. Fluid catalytic cracking and hydrotreating processes for fabricating diesel fuel from waxes, March 12 2009. US Patent App. 11/899,693.

[93] M.J. Prins, K.J. Ptasinski, and F.J.J.G. Janssen. Exergetic optimisation of a production process of Fischer–Tropsch fuels from biomass. *Fuel Processing Technology*, 86(4):375–389, 2005.

[94] S. Proskurina, M. Junginger, J. Heinimö, B. Tekinel, and E. Vakkilainen. Global biomass trade for energy—Part 2: production and trade streams of wood pellets, liquid biofuels, charcoal, industrial roundwood and emerging energy biomass. *Biofuels, Bioproducts and Biorefining*, 13(2):371–387, 2019.

[95] M. Puig-Gamero, D.T. Pio, L.A.C. Tarelho, P. Sánchez, and L. Sanchez-Silva. Simulation of biomass gasification in bubbling fluidized bed reactor using Aspen Plus®. *Energy Conversion and Management*, 235:113981, 2021.

[96] J. Qiao, Y. Liu, and J. Zhang. *Electrochemical reduction of carbon dioxide: fundamentals and technologies*. CRC Press, 2016.

[97] I.K. Reksowadojo, L.H. Duong, and D.N.G. Pham. Review of typical biofuel for aviation alternative fuel purposes. *Ng. Pham*, 4:20–30, 2014.

[98] E. Rezaei and S. Dzuryk. Techno-economic comparison of reverse water gas shift reaction to steam and dry methane reforming reactions for syngas production. *Chemical engineering research and design*, 144:354–369, 2019.

[99] M.L.V. Rios, A.M. González, E.E.S. Lora, and O.A.A. del Olmo. Reduction of tar generated during biomass gasification: A review. *Biomass and bioenergy*, 108:345–370, 2018.

[100] A. Rödl, C. Wulf, and M. Kaltschmitt. Assessment of Selected Hydrogen Supply Chains—Factors Determining the Overall GHG Emissions. In *Hydrogen Supply Chains*, pages 81–109. Elsevier, 2018.

[101] A.K. Sahu, V. Raghavan, and B.V.S.S.S. Prasad. Numerical simulation of gas-solid flows in fluidized bed gasification reactor. *Advanced Powder Technology*, 30(12):3050–3066, 2019.

[102] B. Sajjadi, W. Chen, M. Fan, A. Rony, J. Saxe, J. Leszczynski, and T.K. Righetti. A techno-economic analysis of solar catalytic chemical looping biomass refinery for sustainable production of high purity hydrogen. *Energy Conversion and Management*, 243:114341, 2021.

[103] S. Samadi, S. Lechtenböhmer, C. Schneider, K. Arnold, M. Fischedick, D. Schüwer, and A. Pastowski. Decarbonization pathways for the industrial cluster of the port of rotterdam. Wuppertal Institute for Climate, Environment and Energy, 2016.

[104] M. Samorani. The wind farm layout optimization problem. In *Handbook of wind power systems*, pages 21–38. Springer, 2013.

[105] J. Sánchez, M.D. Curt, N. Robert, and J. Fernández. Biomass resources. In *The Role of Bioenergy in the Bioeconomy*, pages 25–111. Elsevier, 2019.

[106] M. Sánchez, E. Amores, D. Abad, L. Rodríguez, and C. Clemente-Jul. Aspen Plus model of an alkaline electrolysis system for hydrogen production. *International Journal of Hydrogen Energy*, 45(7):3916–3929, 2020.

[107] W.G.J.H.M. van Sark. Prijsontwikkeling hernieuwbare bronnen: zon-PV en off-shore wind. In *De Doorbraak van Duurzaam*, pages 104–110. 2014.

[108] S. Schemme, J.L. Breuer, M. Köller, S. Meschede, F. Walman, R.C. Samsun, R. Peters, and D. Stolten. H2-based synthetic fuels: a techno-economic comparison of alcohol, ether and hydrocarbon production. *International Journal of Hydrogen Energy*, 45(8):5395–5414, 2020.

[109] O. Schmidt, A. Gambhir, I. Staffell, A. Hawkes, J. Nelson, and S. Few. Future cost and performance of water electrolysis: An expert elicitation study. *International Journal of Hydrogen Energy*, 42(52):30470–30492, 2017.

[110] D. Selvatico, A. Lanzini, and M. Santarelli. Low temperature Fischer-Tropsch fuels from syngas: kinetic modeling and process simulation of different plant configurations. *Fuel*, 186:544–560, 2016.

[111] L. Shah, P. Thacker, M. Quintana, and R. Song. Fischer-Tropsch tail-gas utilization, May 1 2003. US Patent App. 10/001,820.

[112] X. Shen, Q. Meng, M. Dong, J. Xiang, S. Li, H. Liu, and B. Han. Low-Temperature Reverse Water–Gas Shift Process and Transformation of Renewable Carbon Resources to Value-Added Chemicals. *ChemSusChem*, 12(23):5149–5156, 2019.

[113] M. Siedlecki. On the gasification of biomass in a steam-oxygen blown CFB gasifier with the focus on gas quality upgrading: technology background, experiments and mathematical modeling. *PhD thesis*, TU Delft, 2011.

[114] V.S. Sikarwar, M. Zhao, P.S. Fennell, N. Shah, and E.J. Anthony. Progress in biofuel production from gasification. *Progress in Energy and Combustion Science*, 61:189–248, 2017.

[115] M. van der Sluys. Instraling door de zon in nederland. *Retrieved from http://han.vandersluys.nl/pub/PDFs/FactSheetHAN_InstralingZon.pdf*, 2020.

[116] B. Sridharan. System Study Towards the Integration of Indirect Biomass Gasification, Methanol and Power Production. *MSc thesis*, TU Delft, 2017.

[117] S. Srinivas, R.P. Field, and H.J. Herzog. Modeling tar handling options in biomass gasification. *Energy & Fuels*, 27(6):2859–2873, 2013.

[118] I. Staffell and S. Pfenninger. The increasing impact of weather on electricity supply and demand. *Energy*, 145:65–78, 2018.

[119] E. van Steen and M. Claeys. Fischer-Tropsch Catalysts for the Biomass-to-Liquid (BTL)-Process. *Chemical Engineering & Technology: Industrial Chemistry-Plant Equipment-Process Engineering-Biotechnology*, 31(5):655–666, 2008.

[120] R.N. Tennyson and R.P. Schaaf. Guidelines can help choose proper process for gas-treating plants. 1977.

[121] R. Terwel, J. Kerkhoven, and F.W. Saris. Carbon Neutral Aviation. *Europhysics News*, 50(5-6): 29–32, 2019.

[122] S. Thapa, N. Indrawan, P.R. Bhoi, A. Kumar, and R.L. Huhnke. Tar reduction in biomass syngas using heat exchanger and vegetable oil bubbler. *Energy*, 175:402–409, 2019.

[123] W.L. Theo, J.S. Lim, H. Hashim, A.A. Mustaffa, and W.S. Ho. Review of pre-combustion capture and ionic liquid in carbon capture and storage. *Applied energy*, 183:1633–1663, 2016.

[124] M.J.A. Tijmensen, A.P.C. Faaij, C.N. Hamelinck, and M.R.M. van Hardeveld. Exploration of the possibilities for production of Fischer-Tropsch liquids and power via biomass gasification. *Biomass and bioenergy*, 23(2):129–152, 2002.

[125] G. Towler and R. Sinnott. *Chemical engineering design: principles, practice and economics of plant and process design*. Elsevier, 2019.

[126] A.R. Trenka, C.M. Kinoshita, P.K. Takahashi, V.D. Phillips, C. Caldwell, R. Kwok, M. Onischak, and S.P. Babu. Demonstration plant for pressurized gasification of biomass feedstocks. Technical report, Institute of Gas Technology, Chicago, IL (United States), 1991.

[127] M.N. Uddin, K. Techato, J. Taweekun, M.D.M. Rahman, M.G. Rasul, T.M.I. Mahlia, and S.M. Ashrafur. An overview of recent developments in biomass pyrolysis technologies. *Energies*, 11 (11):3115, 2018.

[128] E. Uzunoglu and C.G. Soares. Hydrodynamic design of a free-float capable tension leg platform for a 10 MW wind turbine. *Ocean Engineering*, 197:106888, 2020.

[129] Z. Wang, C. Li, and Y. Yamauchi. Nanostructured nonprecious metal catalysts for electrochemical reduction of carbon dioxide. *Nano Today*, 11(3):373–391, 2016.

[130] H. Wei, W. Liu, X. Chen, Q. Yang, J. Li, and H. Chen. Renewable bio-jet fuel production for aviation: A review. *Fuel*, 254:115599, 2019.

[131] J. Xie, W. Zhong, B. Jin, Y. Shao, and Y. Huang. Eulerian–Lagrangian method for three-dimensional simulation of fluidized bed coal gasification. *Advanced Powder Technology*, 24(1): 382–392, 2013.

[132] Y.Y. Yahya and A. Gambardella. Power-to-Gas concepts integrated with syngas production through gasification of forest residues-Process modelling. *MSc thesis*, Chalmers University of Technology, 2017.

[133] L. Yang, L. Pastor-Pérez, S. Gu, A. Sepúlveda-Escribano, and T.R. Reina. Highly efficient Ni/CeO2-Al2O3 catalysts for CO2 upgrading via reverse water-gas shift: Effect of selected transition metal promoters. *Applied Catalysis B: Environmental*, 232:464–471, 2018.

[134] B. Zhang and J. Zhang. Rational design of Cu-based electrocatalysts for electrochemical reduction of carbon dioxide. *Journal of energy chemistry*, 26(6):1050–1066, 2017.

[135] X. Zhang, S.H. Chan, H.K. Ho, S. Tan, M. Li, G. Li, J. Li, and Z. Feng. Towards a smart energy network: The roles of fuel/electrolysis cells and technological perspectives. *International Journal of Hydrogen Energy*, 40(21):6866–6919, 2015.

[136] W. Zhou, B. Zhu, D. Chen, F. Zhao, and W. Fei. Technoeconomic assessment of China's indirect coal liquefaction projects with different CO2 capture alternatives. *Energy*, 36(11):6559–6566, 2011.

A

Relative solubility of syngas components for chilled methanol

Table A.1: Relative solubility of syngas components in methanol at $-25°C$ [17]

Component	Relative solubility
H_2	0.005
CO	0.02
CO_2	1^a
H_2S	7.06
Benzene	59.5
CH_4	0.05
C_2H_4	0.46
C_2H_6	0.42
C_3H_8	2.35

^{a} Basis of relative solubility

B

Schematic of complete Aspen Plus model

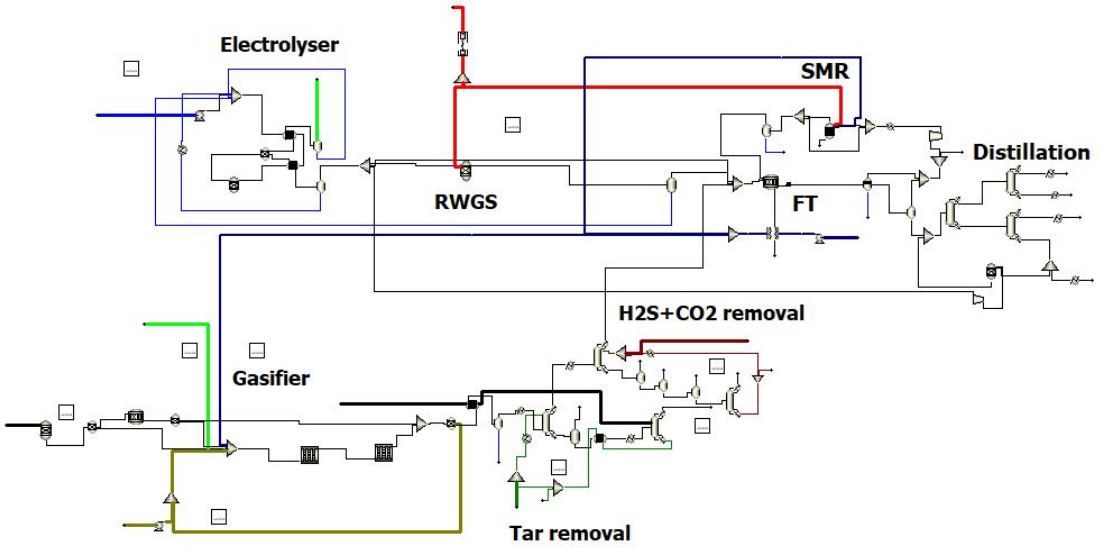

Figure B.1: Schematic of the process developed in Aspen Plus

C

Mass yields pyrolysis process

Table C.1: Mass yields for the pyrolysis process in the gasifier PYROL (T=1184K), according to $Y_i = aT^2 + bT + c$ [10]

Component	Mass yield[a] [%]
CH_4	7.20
H_2	1.35
CO	37.75
CO_2	10.46
C_2H_4	3.33
C_2H_6	0.04
C_6H_6	2.43
C_7H_8	2.95
C_6H_6O	0
$C_{10}H_8$	0.41
H_2O	24.02
$Char$	10.08

[a] Mass yields are normalized to include char and moisture content

D

Validation steam-to-biomass ratio on dry basis

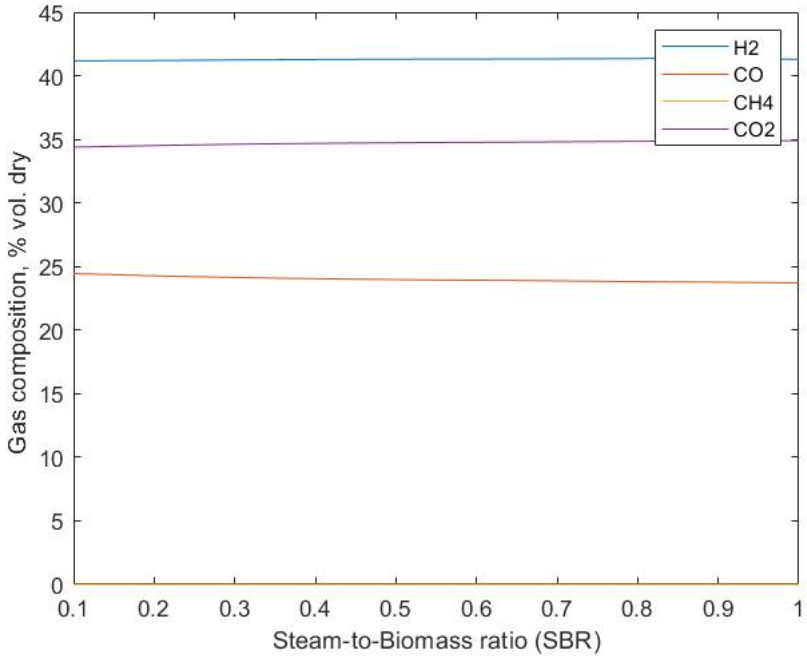

Figure D.1: Product gas composition on dry basis for the Aspen Plus model with varying SBR (T=$900°C$, P=25 bar, ER=0.38)

E

H_2S/CO_2 removal using amine absorption (DEA)

Sulfur removal can take place by high and low temperature technologies. Physical and chemical absorption, commonly with metal oxide as sorbent, are high temperature technologies. But these technologies operate at temperatures of at least $400°C$, which makes it very energy intensive. Amine based absorption is usually applied as low temperature technology. Amines can be subdivided into primary, secondary and tertiary amines. The secondary amine, diethanolamine (DEA), is less reactive for H_2S and CO_2 than the primary monoethanolamine (MEA) [90]. Lower reactivity reduces the energy requirements for regeneration and hence the processing costs. For this reason the low temperature technology chemical absorption will be applied, which is an industrially applied method [90].

The most suitable property method for CO_2 absorption is Electrolyte Non-Random Two-Liquid activity coefficient (ELECNRTL). It offers the most versatile properties for aqueous and mixed solvent systems. Missing binary interaction parameters are predicted from UNIFAC model [81].

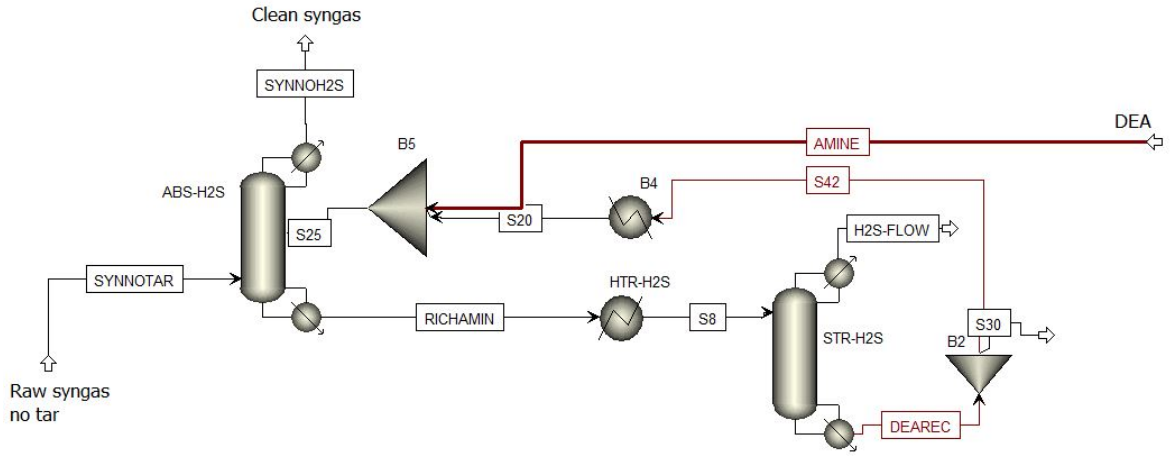

Figure E.1: Schematic of H_2S and CO_2 removal process developed in Aspen Plus

Schematic H_2S/CO_2 removal
The configuration of the H_2S removal is comparable to the tar removal process and based on a the study of Peters et al. [90]. Two columns, ABS-H2S and STR-H2S, represent the absorber and stripper section respectively as shown in Figure E.1. Raw syngas is fed at the bottom of the first column while DEA enters on the top stage (Figure E.2). A high operating pressure of 50 bar is maintained to achieve

optimal CO_2 and H_2S separation. Amine/raw syngas ratio is found to be 4.5:1 mass. % by iteration for optimal performance of the absorber. At this point, H_2S content is just below $0.1mg/Nm^3$. Validation for obtaining this fraction can be found in Chapter 3.3.3. Further downstream this fraction will decrease because the sweet syngas is mixed with syngas from the electrolyzer and RWGS which does not contain H_2S.

Table E.1: Mole fractions of the present components before and after the absorber

	Sweet syngas	Rich syngas solution
H_2O	0.02	0
CO_2	0.38	0.01
H_2	0.41	0.70
CO	0.19	0.29
H_2S	1729 mg/Nm^3	0.08 mg/Nm^3
NH_3	5954 mg/Nm^3	1e-3 mg/Nm^3
Temperature [$^\circ C$]	85	37
Pressure [bar]	25	53

A pump decreases the pressure of the rich amine solution to 2.5 bar, which is equal to the operating pressure of the stripper. A heater HTR-H2S decreases the flow pressure to 2.5 bar with a temperature of $63^\circ C$. The operating conditions of the stripper, as well as the absorber, are shown in Table E.2. Approximately 99% of DEA leaves in the bottom stream and will be recycled. A purge stream will avoid accumulation of unfavorable components, resulting in total DEA losses within the cycle of 4-5%. Additional unit operations for the top flow after the stripper can increase recycle efficiency, but will also increase energy demand and costs.

Table E.2: Column specifications for H_2S/CO_2 removal process

	Absorber	Stripper
Number of stages	10	10
Pressure [bar]	50	2.5
Condenser	No	No
Reboiler	No	Yes (Kettle)
Boilup ratio (mass)		1.33

E.1. Validation amine scrubber

Removal of H_2S and CO_2 takes place in a similar way as tar removal. An absorber absorbs the H_2S and CO_2 by the amine DEA. Main focus of this removal process is to decrease H_2S ratio below $0.1mg/Nm^3$ (Table 2.8). With this, a large fraction of CO_2 is also removed. The study of Peters et al. [90] concluded that amine absorption can reach $< 0.5\%$ CO_2 in the sweet gas stream.

Results of the H_2S and CO_2 removal can be found in Figure E.3 and Figure E.4. The absorber shows similar behavior as the tar removal process. Increasing the number of stages or pressure will increase H_2S removal and curves get closer when pressure further increases. Preferred H_2S concentration of $0.1mg/Nm^3$ is not reached within 12 stages for 30 and 40 bar. This requirement on the other hand is reached for an absorber with 10 stages or higher for 50 and 60 bar. Therefore an absorber with 10 stages and 50 bar is applied to this model. A similar trend is observed for CO_2 removal, where >99.5% of the inlet CO_2 is removed for this absorber (Appendix F.1).

Increasing the DEA/raw syngas ratio has a positive effect on the removal efficiency, as observed in other studies [79] [90]. H_2S content below $0.1mg/Nm^3$ is reached for DEA/raw syngas ratio from 4.5. At this point >99% of CO_2 is removed from the raw syngas stream as well.

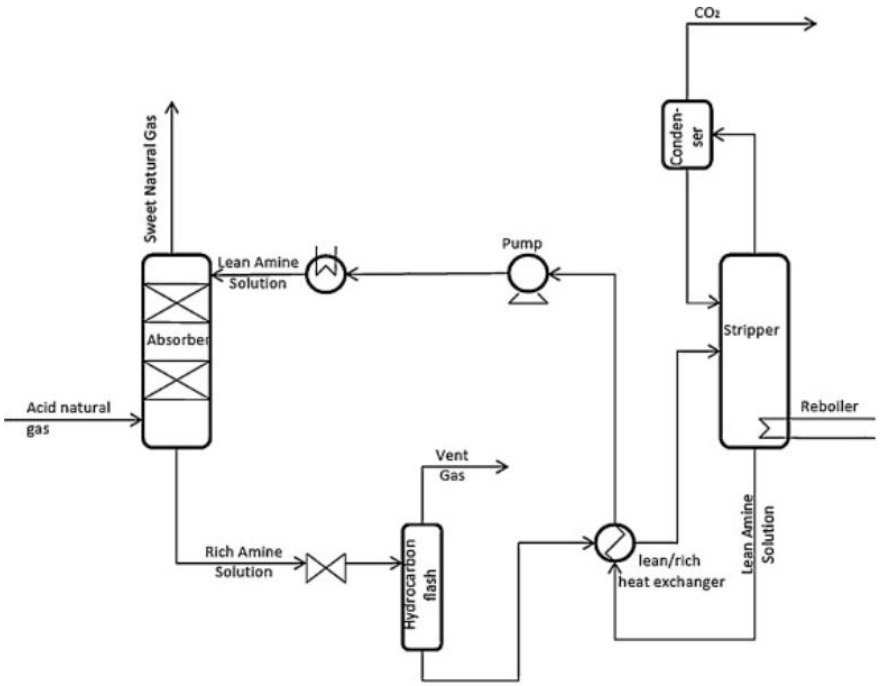

Figure E.2: Overview of the H_2S/CO_2 absorption process [90]

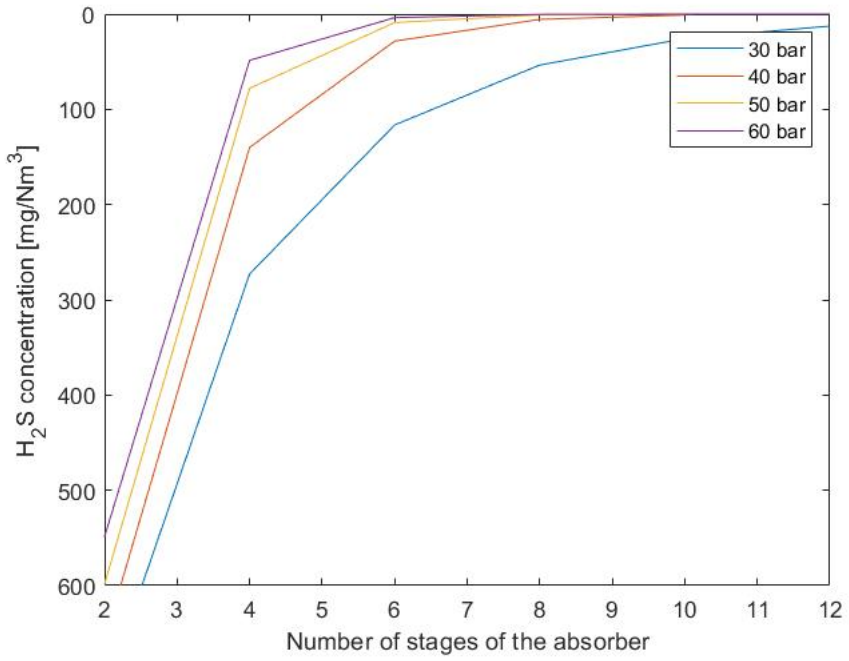

Figure E.3: Sensitivity analysis for pressure and number of stages for the absorber on the H_2S concentration. The inlet methanol flow is fixed at 4.3 $kg_{DEA}/kg_{raw\ syngas}$.

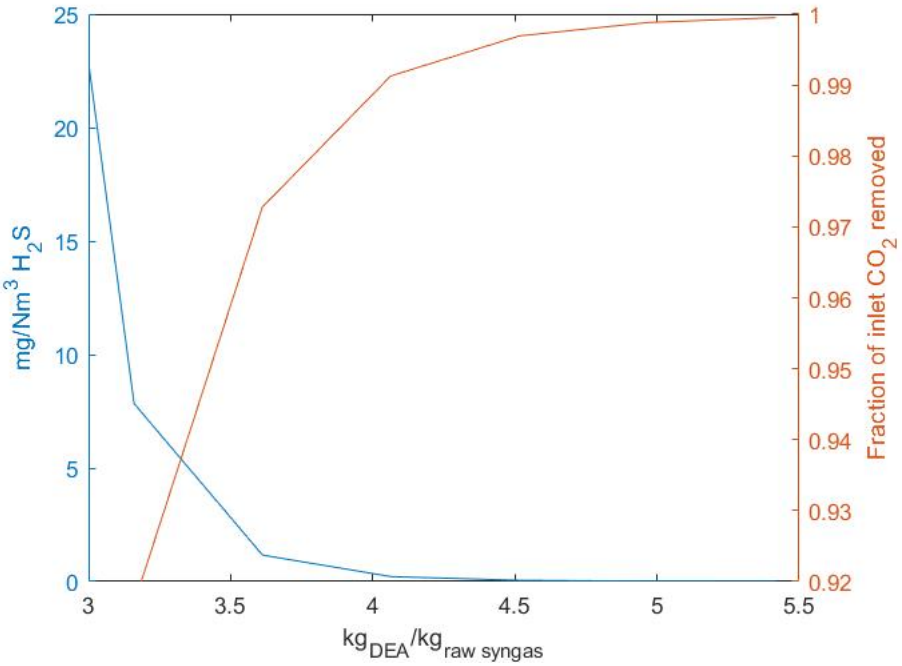

Figure E.4: DEA required to remove H_2S and CO_2 from raw syngas. Absorber has 12 stages operating at 36 bar. Raw syngas inlet conditions: $85^{\circ}C$, 25 bar. DEA inlet stream: $56^{\circ}C$ and 1 bar.

F

Validation H_2S/CO_2 removal for CO_2

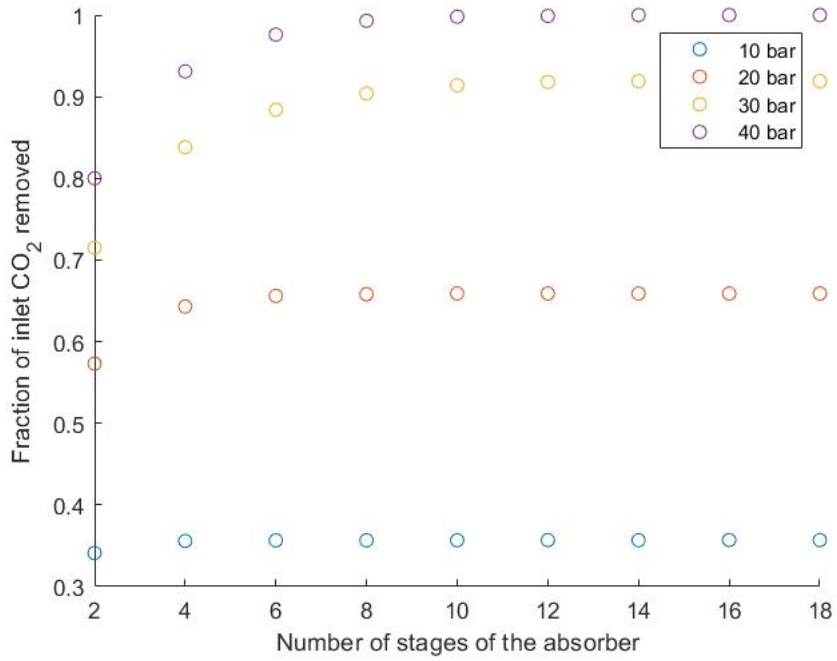

Figure F.1: Fraction of inlet CO_2 removed in absorber by different number of stages (P=10 bar, $kg_{MeOH}/kg_{raw\ syngas}$=2.5)

G

Scenario results (extended)

G.1. Scenario results

Table G.1: Results for scenario 1

Gasification		**DAC and WE**	
Biomass input [ton/h]	43.04	H_2O input [ton/h]	34.74
Dynamic load	40-45%	CO_2 input RWGS [ton/h]	36.70
		CO_2 input SMR [ton/h]	0
SBR ratio	0.8	Air input DAC [ton/h]	1194
Steam input [ton/h]	34.43		
		WE dynamic load	100%
ER ratio	0.42		
Oxygen input [ton/h]	18.29	Produced H_2 [ton/h]	5.35
		Produced oxygen [ton/h]	42.43
Aspen Plus model			
reactor dimensions		Electricity	
Length [m]	7.32	PEM [MW]	319.2
Diameter [m]	2.71	DAC [MW]	11.4
		Pumps/Compressors [MW]	10.2
		Total [MW]	**340.8**
Gas cleaning		**FT reactor**	
Tar removal		$H_2 : CO$ ratio FT reactor	2.06:1
Oil [ton/h]	9.68	Syngas fraction gasification [%]	34.0
		Syngas fraction WE [%]	66.0
H_2S/CO_2 removal			
Methanol [ton/h]	19.83		
Efficiencies		**Distillation**	
$\eta_{energy,kerosene}$	13.10 %	Kerosene [ton/h]	5.90
$\eta_{energy,fuels}$	34.79 %	Gasoline [ton/h]	4.41
$ton_{CO_2}/ton_{kerosene}$	6.27	Diesel [ton/h]	2.52
ton_{CO_2}/ton_{fuel}	2.36	Wax [ton/h]	2.85

Table G.2: Results for scenario 2

Gasification		**DAC and WE**	
Biomass input [ton/h]	98.51	H_2O input [ton/h]	12.37
Dynamic load	100%	CO_2 input RWGS [ton/h]	11.06
		CO_2 input SMR [ton/h]	1.50
SBR ratio	0.8	Air input DAC [ton/h]	392.47
Steam input [ton/h]	78.81		
		WE dynamic load	30%
ER ratio	0.40		
Oxygen input [ton/h]	39.60	Produced H_2 [ton/h]	1.82
		Produced oxygen [ton/h]	14.46
Aspen Plus model			
reactor dimensions		Electricity	
Length [m]	7.32	PEM [MW]	111.4
Diameter [m]	4.10	DAC [MW]	3.8
		Pumps/Compressors [MW]	7.5
		Total [MW]	**122.7**
Gas cleaning		**FT reactor**	
Tar removal		$H_2 : CO$ ratio FT reactor	2.04:1
Oil [ton/h]	5.27	Syngas fraction gasification [%]	83.0
		Syngas fraction WE [%]	17.0
H_2S/CO_2 removal			
Methanol [ton/h]	28.71		
Efficiencies		**Distillation**	
$\eta_{energy,kerosene}$	12.51 %	Kerosene [ton/h]	6.32
$\eta_{energy,fuels}$	32.84 %	Gasoline [ton/h]	4.53
$ton_{CO_2}/ton_{kerosene}$	11.39	Diesel [ton/h]	2.70
ton_{CO_2}/ton_{fuel}	3.17	Wax [ton/h]	3.05

G.2. Oxygen storage

To determine the required oxygen storage, an analysis is done on monthly and daily basis. $energieopwek.nl$ [7] monitors all types of renewable power every ten minutes. Table G.4 shows the results of the monthly analysis. For each month the solar and combined offshore and onshore wind power is retrieved in 2020.

Required oxygen is based on the two scenarios assuming a wind/solar ratio of 1/1. From the data it can be concluded that May produces the most renewable power while January the least. Resulting in May be equivalent to scenario 1, while the other months are scaled between scenario 1 and 2. Since monthly power production is an average over the days, oxygen production and consumption for both scenarios is moderated with 25% as shown in Table G.3.

Table G.3: Oxygen production and consumption for scenario 1 and 2 for calculating required oxygen storage on monthly basis

	Oxygen Produced [ton/h]	Oxygen Consumed [ton/h]
Scenario 1	35.44	23.62
Scenario 2	21.45	34.27

From Table G.4 it can be concluded that there is a shortage of oxygen in January and December, while the other months result in overproduction. On a yearly basis more oxygen is produced than consumed, with an average of 3.4 ton/h. But the underproduction in two months indicate that oxygen storage is not only required on daily basis but also on monthly basis. Hence an analysis is done for days in December where renewable electricity production is low.

Table G.5 shows the results of a day in December with barely renewable electricity production. Assumed is that the peak moment (14:00) represents for 80% scenario 2. A shortage of 460 ton is

reached, which is equivalent to approximately $350m^3$ when stored as liquid oxygen (LOX). But periods of low electricity production can hold for multiple days, hence a bigger storage is required than calculated for this day only. Liquid oxygen, especially large storage, comes with certain risks. Severe conditions such as low temperature and high pressure require special attention regarding safety. Small storage tanks are widely available, but do not satisfy the calculated storage for this research study. Bigger LOX storage tanks are more scarce, but Hu et al. [56] reported a LOX storage tank of $2500m^3$. To meet the storage for this research problem covering multiple days of oxygen shortcomings, storage tanks similar to [56] will be necessary.

Table G.4: Oxygen storage calculation, based on data from $energieopwek.nl$ [7]

2020	Wind [MW]		Solar [MW]		0.5*wind+0.5*solar	Scenario 1	Scenario 2	Produced [ton/h]	Consumed [ton/h]	Net [ton/h]
January	1950	72.4	208	11.2	41.8	0.39	0.61	26.8	30.2	-3.3
February	2694	100	382	20.6	60.3	0.64	0.36	30.5	27.4	3.1
March	1963	72.9	980	53	62.9	0.68	0.32	31.0	27.0	4.0
April	1192	44.2	1580	85.4	64.8	0.71	0.29	31.3	26.7	4.6
May	1156	42.9	1850	100	71.5	1.00	0.00	35.4	23.6	11.8
June	1152	42.8	1670	90.3	66.5	0.73	0.27	31.7	26.5	5.2
July	1209	44.9	1550	83.8	64.3	0.70	0.30	31.2	26.8	4.4
August	1311	48.7	1530	82.7	65.7	0.72	0.28	31.5	26.6	4.9
September	1437	53.3	1190	64.3	58.8	0.62	0.38	30.2	27.6	2.5
October	2630	97.6	559	30.2	63.9	0.69	0.31	31.2	26.9	4.3
November	2290	85.0	422	22.8	53.9	0.55	0.45	29.2	28.4	0.8
December	2210	82.0	227	12.3	47.2	0.46	0.54	27.9	29.4	-1.5

Table G.5: Oxygen shortage calculation on daily basis [7]

Time $[h]$	Scenario 1	Scenario 2	Oxygen produced [ton]	Oxygen consumed [ton]	Net [ton]
0:00	0.04	0.96	18.1	38.7	-20.6
1:00	0.04	0.96	18.1	38.7	-20.6
2:00	0.04	0.96	18.1	38.7	-20.6
3:00	0.04	0.96	18.1	38.7	-20.6
4:00	0.04	0.96	18.1	38.7	-20.6
5:00	0.04	0.96	18.1	38.7	-20.6
6:00	0.04	0.96	18.1	38.7	-20.6
7:00	0.05	0.95	18.2	38.6	-20.4
8:00	0.05	0.95	18.4	38.5	-20.1
9:00	0.07	0.93	18.8	38.1	-19.3
10:00	0.12	0.88	20.0	37.1	-17.1
11:00	0.15	0.85	20.9	36.4	-15.5
12:00	0.17	0.83	21.4	35.9	-14.5
13:00	0.20	0.80	22.0	35.4	-13.4
14:00	0.20	0.80	22.1	35.3	-13.2
15:00	0.20	0.80	22.0	35.4	-13.4
16:00	0.18	0.82	21.5	35.8	-14.3
17:00	0.13	0.87	20.3	36.8	-16.5
18:00	0.09	0.91	19.4	37.6	-18.3
19:00	0.06	0.94	18.5	38.4	-19.9
20:00	0.05	0.95	18.2	38.6	-20.5
21:00	0.04	0.96	18.1	38.7	-20.6
22:00	0.04	0.96	18.1	38.7	-20.6
23:00	0.04	0.96	18.1	38.7	-20.6
24:00	0.04	0.96	18.1	38.7	-20.6
				Total [ton]	-462.5